ANALYTICAL MODIFICATION OF THE V-NOTCHED RAIL SHEAR TEST APPARATUS FOR DYNAMIC TESTING

A Thesis By

Vinila Rao Tatipalli

Bachelor of Technology, Jawaharlal Nehru Technological University, India, 2008

Submitted to the Department of Aerospace Engineering
and the faculty of the Graduate School of
Wichita State University
in partial fulfillment of
the requirements for the degree of
Master of Science

May 2014

ANALYTICAL MODIFICATION OF THE V-NOTCHED RAIL SHEAR TEST APPARATUS FOR DYNAMIC TESTING

The following faculty members have examined the final copy of this thesis for form and content, and recommend that it be accepted in partial fulfillment of the requirement for the degree of Master of Science, with a major in Aerospace Engineering.

_____
Suresh Raju, Committee Chair

_____
Gerardo Olivares, Committee Member

_____
Ramazan Asmatulu, Committee Member

DEDICATION

To my parents, my sisters, and my fiancé

ACKNOWLEDGEMENTS

I would like to sincerely express my gratitude to my advisor Dr. Suresh Raju for supporting and encouraging me throughout. He has been a great inspiration ever since I knew him. He has been very kind, supportive and always available whenever I needed help. He helped me understand minor things with huge patience. His expertise in wide range of areas helped me learn a lot. I thank him wholeheartedly for all the support, help and inspiration he has provided.

I would like to thank my parents, my sisters and my fiancé for being with me every moment of my life, in good and bad times, for believing in me and providing enormous support and encouragement. It is because of them I stand strong, healthy and confident. I cannot express how important their support is in my life.

I would like to thank Dr. Gerardo Olivares for being so kind, helpful and encouraging while working at NIAR. I cannot thank him enough for providing access to all the facilities and tools which helped me gain knowledge and experience utterly useful in the existing market. I would also like to thank Mr. Juan Felipe for his extreme patience, support and help. It is because of him I gained the opportunity to explore various tools and update my knowledge. I absolutely thank everyone in the computational mechanics lab at NIAR for helping me so much. I would also like to thank Dr. Gerardo Olivares and Dr. Ramazan Asmatulu for their valuable time and help in reviewing my thesis and making valued suggestions.

Finally, I would like to thank all those people who encouraged and helped me complete my thesis work. It is because of my family and people I worked with, I stand in this position, successful and living my dream!

ABSTRACT

Dynamic testing is required in structural engineering applications to characterize material properties over a wide range of strain rates and temperatures. One of the major concerns to obtain accurate data during dynamic testing is the oscillations in the test apparatus. If the frequencies of the system were increased to a point where the acceptable bandwidth of measured signal is within the first natural frequency, accuracy of the measured data could be improved by minimizing the effects of fixture vibrations. Since frequency is directly proportional to stiffness and inversely proportional to mass, this work presents several cases where structural modifications were applied to the test fixture based on the stiffness and mass to increase the bandwidth.

V-notched Rail Shear test apparatus is widely used for characterizing laminated composite materials because of its advantages over other shear test methods. Present work uses numerical modeling of test apparatus as it gives a flexibility to modify any component and to isolate the source of vibrations. With a series of structural modifications to the test fixture which are primarily based on either changing its stiffness or mass, the apparatus is analyzed for a range of loading rates. The results are later analyzed in the frequency domain and an increase in the bandwidth is observed. As discussed, significant increment was observed in one of the methods presented in this work which deals with a reduction in mass of the apparatus by half. An analysis to check the effect of fixture bending on the specimen loading was carried out and it was observed that the specimen was undergoing a combined loading effect at very high loading rates. This suggests the physical limitation of the test apparatus. Also, a simple demonstration of variations encountered in the test data, as a result of filtering data using low-pass and band-stop filters is also presented in this work.

TABLE OF CONTENTS

LIST OF TABLES

LIST OF FIGURES

LIST OF FIGURES (continued)

LIST OF FIGURES (continued)

LIST OF FIGURES (continued)

LIST OF FIGURES (continued)

Figure Page

LIST OF FIGURES (continued)

CHAPTER 1

INTRODUCTION

Dynamic testing is important in many engineering structural applications since various components involved must be designed to function over a broad range of strain rates and temperatures. The materials should be characterized at the strain rates and temperatures of the intended application. As a result of increasing demand for improved manufacturing techniques and safety in structures, measuring accurate and reliable material properties at high strain rates is necessary. The primary concern here would be the oscillations and the stress waves within the testing apparatus at high speeds as this will impair the load cell reading, thereby making the data obtained more difficult to interpret.

Some of the standardized shear test methods reported in literature are the Iosipescu shear test (ASTM D5379) [1], the two-rail shear test (ASTM D4255/D4255M) [2], and the V-notched rail shear test (ASTM D7078/D7078M) [3]. Data gathered from such test methods had been used to obtain nominal *quasi-static* properties which are utilized in the design of structural members such as found in the aircraft industry. V-notched rail shear test method illustrated in Figure 1, incorporates the best features of Iosipescu and two-rail shear tests. When the assembly is loaded in tension using a mechanical testing machine, the relative displacement between the two fixture halves introduces shear forces in the specimen. Failure occurs across the notched specimen due to the developed stresses. The notches are intended to enforce failure across the gage region. As a result, the average shear stress is increased in the reduced width of the specimen. Also, the shear specimen in this test standard provides a larger gage section and enhanced loading capability compared to other test methods. Experimentally, the test apparatus consists of two fixture halves where one is connected to the load cell and another to an actuator, as shown in

Figure 1. The tensile mode of loading lends itself to high speed testing from a safety point of view as the two halves of the test fixture are moving away from each other. Experimental work carried out using V-notched rail shear test apparatus to study the effects of strain rate on the in-plane shear behavior of reinforced composite materials have shown a varying trend in material strength at higher stroke rates [4]. It was observed that characterizing the behavior of composite materials using dynamic testing is not an easy task due to the vibrations encountered by the system [5]. Because of the vibrational and wave propagation effects in the system at high stroke rates, the stress-strain behavior of the materials have shown a drastic change.

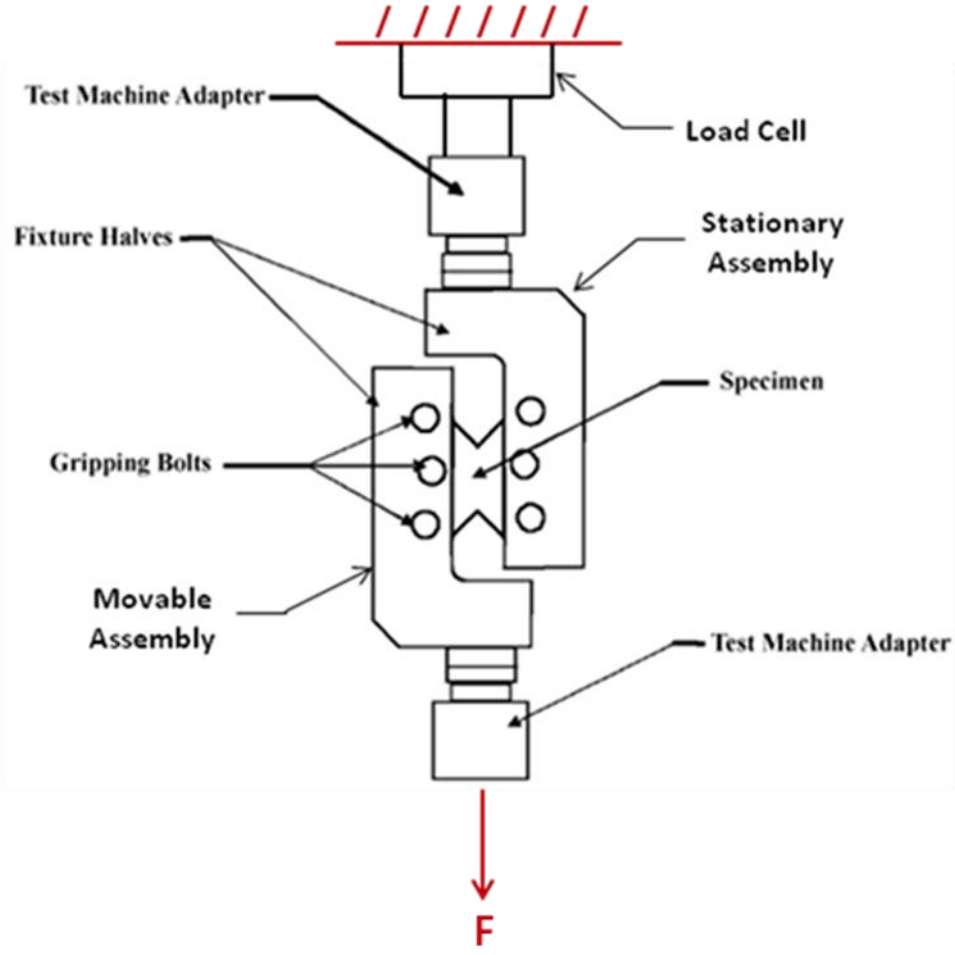

Figure 1. Assembled standard V-notched rail shear apparatus [6]

Consider a single degree-of-freedom (SDOF) spring-mass system where the excitation force is applied to the mass as shown in Figure 2. The system response may be expressed in terms of fraction of the applied force amplitude that is transmitted through the system to the support. If the amplitude of the applied force is F (excitation) and the force transmitted is P, the ratio P/F is known as transmissibility (T). This SDOF is a simple approximation of the test apparatus such that the spring represents the load cell stiffness and the mass represents the test apparatus. Maximum force amplification (transmissibility) occurs at resonance when the ratio of the excitation frequency to the natural frequency is equal to 1. As shown in Figure 3, it can be noted that transmissibility is flattened as damping is increased. Upon analyzing the problem statement, the fixture vibrational effects on the test data could be minimized if the resonance frequency is increased such that the acceptable bandwidth of the measured data is well below the resonant frequency of the test apparatus. This can be achieved by increasing the frequencies of the test apparatus. Since the frequency is defined as "(stiffness (k)/mass (m))$^{1/2}$", either increasing stiffness or decreasing mass would help in increasing the frequencies of the apparatus.

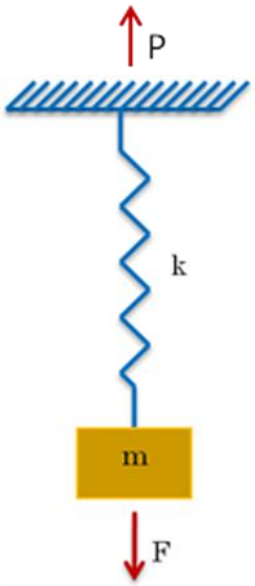

Figure 2. SDOF system – Forced vibration without damping

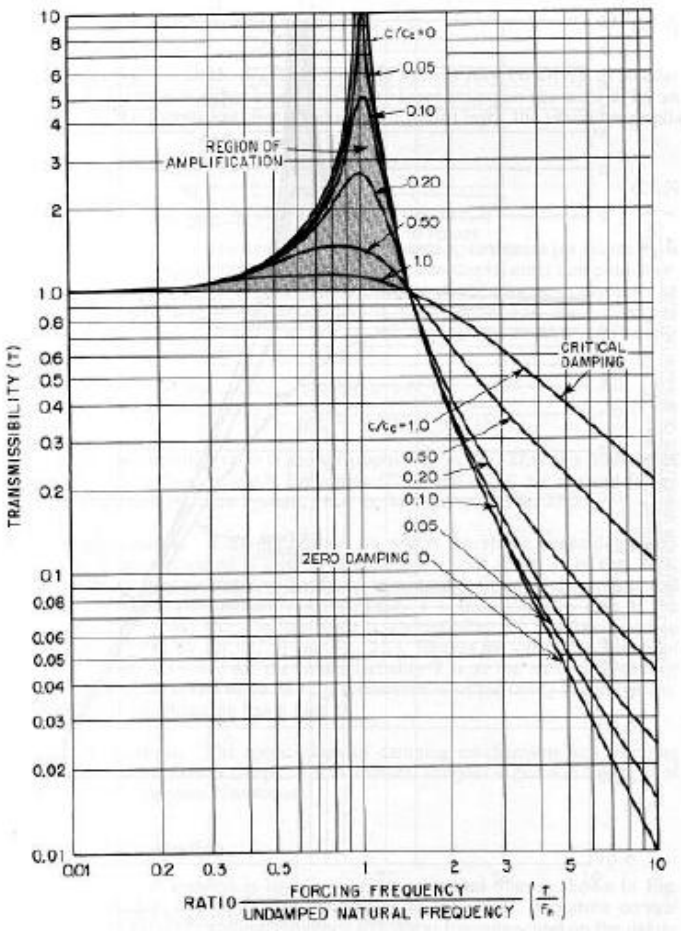

Figure 3. Displacement transmissibility for a damped single degree of freedom system [7]

The test method used for the experimental work mentioned above has been chosen for the current research i.e. the V-notched rail shear test apparatus [6]. With a series of structural modifications to the fixture halves shown in Figure 1, the frequencies of the test apparatus were increased, so that the peak frequencies fall beyond the bandwidth of the measured data (excitation) at different test speeds. These modifications (numerical) were made to primarily affect the mass and stiffness of the fixture halves. Several cases are presented in this work along with their results compared to the standard model. This report presents an evaluation of the forces extracted from the load cell and the minimum section of the V-notched coupon, analyzed in the frequency domain.

The primary factors in the present work that affect the transmissibility are the mass of the fixtures, eccentricity of loading and the load cell itself. An effort to have the measured signal within the first bandwidth is the primary focus of the present work. This helps in reducing vibrations within the useful range of the data. The analyses presented in this report also facilitate in identifying the physical limitation of the test fixture. Figure 4 shows a free-body diagram of the test apparatus with standard fixtures, indicating the loading directions. Force history results are compared between the specimen and the load cell for the following scenarios:

- Assembly with standard fixtures vs. Assembly with modified fixtures
- Steel fixtures vs. Aluminum fixtures
- Comparison in time and frequency domains

Also, this work briefly presents the inconsistencies in the results after filtering data, using low-pass and band-stop filters. Filtered and unfiltered data were compared while highlighting the variations observed.

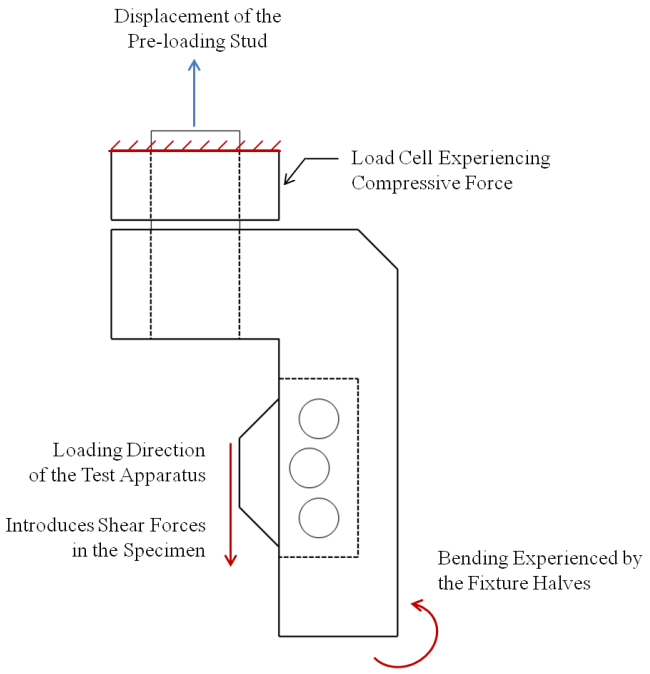

Figure 4. Free-body diagram of the standard test apparatus

CHAPTER 2

LITERATURE REVIEW

2.1 V-Notched Rail Shear Test

Adams, et al., [8] developed the V-notched rail shear test method (Figure 5) which is used to measure shear modulus and shear strength of materials especially continuous fiber reinforced composites. Shear testing is mainly preferred to measure in-plane shear properties of various materials.

Prior to the development of V-notched rail shear method, the most widely used method was Iosipescu shear test (Figure 6) which also used a V-notched coupon. It was first developed by Iosipescu [1] and was later applied to unidirectional composites by Adams and Walrath [9]. The major limitation of this method was the smaller gage section of the specimen which is not suitable for certain composites which requires a larger gage section to facilitate the larger reinforcement architecture (unit cell). Also the concentrated loadings on the specimen edges caused the risk of edge crushing. Another major limitation was the compression-mode-loading of the Iosipescu test fixture which is not suitable for high speed testing as there will be a risk of damaging the test fixture. The test method which was also commonly used earlier was the two-rail shear test (Figure 7) [2] which addressed the limitations of Iosipescu method. In this test method, load is applied through the specimen faces. This was the major limitation of this test as six holes had to be machined to accommodate the gripping bolts, which is a time consuming and costly processes. Because of this, shear properties generated using this method was questionable due to the stress concentrations developed in the specimen. Later this method was modified by Hussain and Adams [10] by using roughened grips, thereby eliminating the need of holes in the

specimen. Also, the heavy mass of the fixture makes it unsuitable for the present work as some of the structural modifications are purely based on reducing the mass of the fixture.

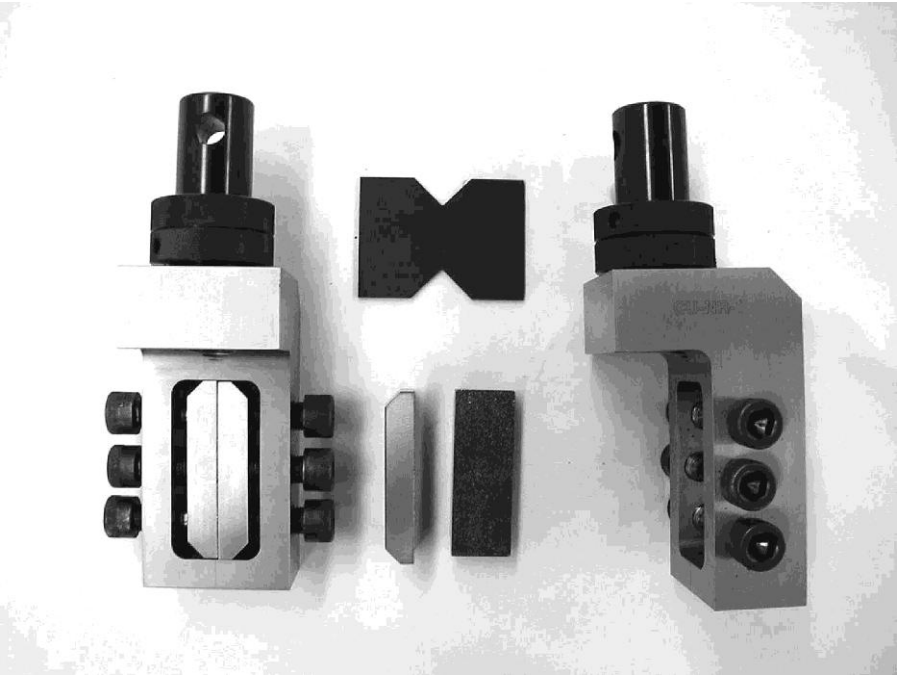

Figure 5. Partially assembled V-notched rail shear test fixture [11]

Figure 6. Iosipescu shear test fixture [12]

Figure 7. Two-rail shear test fixture [12]

Based on the limitations of test standards described above, V-notched rail shear test has been developed which includes the attractive features of both two-rail shear test and Iosipescu test methods. V-notched rail shear test fixture was based on the two-rail shear test fixture. This test standard was developed to allow the shear testing of many materials which include multidirectional and textile composite laminates, and also for determining the lamina shear properties of composite materials. Daniel Adams [6] concluded that uniform states of shear stresses were produced at the gage section of the coupon due to the incorporation of V-notch configuration of Iosipescu shear test method. Also, stress concentrations that occur adjacent to the rails in an unnotched specimen used in two-rail shear test were reduced due to the usage of effective V-notched specimen. One of the major limitations of Iosipescu shear test of having smaller gage section in the specimen was addressed by scaling the V-notched specimen by a factor of three, thereby allowing shear testing of coarser textile composites which requires a larger gage section. With composites, not only the V-notched rail shear test method produces acceptable gage section failures for a variety of multidirectional laminates, it also provides excellent gripping for the specimen [6].

2.2 Literature Review

Raju, et al., [4] have experimentally characterized the in-plane shear properties of fiber reinforced composite materials such as Newport NB321/3k70 plain weave carbon fabric/epoxy and NB321/7781 fiberglass/epoxy, Cytec PWC/T300/3KNT and Fibercote 3KPW/E365 under medium strain rates. The V-notched rail shear apparatus was used to study the effects of strain rate on the in-plane shear strengths and failure modes. Testing was conducted under tension loading mode which was preferred over compression loading at nominal stroke rates ranging between 2.5 x 10^{-5} and 2.54 m/s. It was observed that the shape of the stress-strain curves were similar up to stroke rates of 2.54 m/s. A trend of increasing stress levels were observed with the stroke rate at a given strain level and a reduction in stiffness was also observed with increasing stroke rates. Failure mode was observed to change from a shear mode across the minimum section (Figure 8) to a complex failure mode away from the minimum section (Figure 9 and Figure 10). The three coupons shown in each figure represent the failure modes at 100 in/sec, 250 in/sec and 500 in/sec. Also, stress-strain behavior was observed to change drastically at a stroke rate of 2.54 m/s, indicating wave propagation effects.

Figure 8. Failure modes across the minimum section of the coupon Cytec PWC/T300/3KNT at different stroke rates [5]

Figure 9. Complex failure modes across the sections of the coupon Newport PWCF at different stroke rates [5]

Figure 10. Complex failure modes across the sections of the coupon Newport SWGF at different stroke rates [5]

Leeuwen, et al., [13] have evaluated various shear test methodologies in order to explore the potential differences that were seen in the results. Since appropriate shear characteristics are very important for accurate simulations, different methods of obtaining shear properties were compared for fiber reinforced plastics. This study was carried out based on the requirements of blade designers as the loading is dominated by shear in some parts of the blade. Comparison was made among +/- 45^0 tension test, 10^0 off-axis tension test, Iosipescu and V-notched rail shear test methods. Shear moduli from these tests were comparable whereas ultimate shear strengths varied more among one another showing more pronounced differences. It was observed that the stitching configuration and orientation of the fibers influenced the results of Iosipescu and V-notched rail tests.

Jen, et al., [14] have designed a new shear test fixture with the Iosipescu specimen geometry. The new fixture includes four pairs of shafts to eliminate any misalignment of the fixture halves during testing. The objective of the design is to determine if shear strength tests on Sitka spruce specimens generate reliable data for shear modulus and shear strength for wood and other materials. The research also focused on controlling the twisting of two halves of the fixture and to eliminate any transverse normal strains in the specimen caused by the fixture design. A trial and error approach was followed in designing the fixture. This improved test fixture was observed to be appropriate for studying shear properties of solid wood, plastics, metals and other materials.

Hussain and Adams [15] measured the unidirectional in-plane shear properties of epoxy materials using Wyoming-modified two-rail shear test fixture. The tests were conducted on unidirectional and cross-ply specimens of carbon/epoxy and glass/epoxy materials. Specimens with trapezoidal and rectangular geometries along with tabs and various aspect ratios were considered. It was observed that 90^0 specimen failed prematurely in the grip section due to local stress concentrations near the corners of the gage section. It was reported that this specimen is too fragile for testing. Cross-ply specimens seem to fail in shear and produce reasonably good results. An alternative approach was suggested in the present study which is to machine the specimen gage section to be thinner. Tabbing the gripped sections and thereby making them stiffer minimizes premature failures. An un-tabbed cross-ply laminate for rectangular specimen was recommended for use with the fixture. Bonded and integral tab specimens of 0^0 orientations gave comparable results.

Garcia, et al., [16] presented investigations of stress distributions both experimentally and analytically occurring in a rail shear test. Various effects of non-uniform stresses on ultimate

strength and shear modulus due to rail flexibility, thermal expansion and specimen aspect ratio were shown. Graphite-polyimide laminates were studied and tested at room temperature. In order to explore the influence of thermal loadings and geometric parameters on the magnitude and distribution of in-plane normal and shear stresses, a two-dimensional finite-element model was used. It was observed that the direction of loading has little effect and aspect ratio of the specimen has major effect on the stress distributions within the specimen. 0^0 oriented specimens exhibited very high normal stresses perpendicular to the filaments and tapering the rails resulted in an increase in the magnitude of the normal stresses. Better stiffness and strength data were obtained in the bonded rail-test configuration due to proper gripping of the specimen than the bolted configuration. For elevated-temperature tests, bolted-rail test technique was used which indicated that an accurate measure of the initial shear modulus can be obtained.

Lee and Munro [17] examined the commonly used in-plane shear test methods for advanced composite materials and using a decision analysis technique, three test methods were identified as most promising. The shear test methods available provide either qualitative or quantitative data. Qualitative methods usually provide comparative values of shear modulus and shear strength while quantitative methods determine the complete shear stress/strain response of composite materials. In order to obtain accurate shear stress/strain response, the test section should be one of the maximum shear stress regions of the specimen. Decision analysis technique is very useful for evaluating a large number of solutions against a large number of criteria. In this study, nine major in-plane shear test methods were evaluated with respect to eleven criteria. Every method is rated on a relative basis depending upon how important authors considered each criterion.

2.3 Literature Research on Related Areas

Lamancusa [7] studied about the vibrations and its possible solutions that could cause machinery failure. A vibration problem could be described as an internally generated mechanical or fluid disturbance (source), airborne or structural medium through which the disturbance is transmitted to the receiver (path) and a responding system, usually having many natural frequencies (receiver). Solution to any vibration problem involves experimental characterization of system parameters, modeling system dynamics using simple lumped model, identifying natural frequencies and their coincidence with excitation frequencies and calculating system response if the excitation frequencies and forces are known. The basic principle to minimize the transmission of vibrations from source to receiver is to make the natural frequency of a machine on its foundation as far below the excitation frequency as possible. Natural frequencies of a system or a receiver should be avoided to coincide with excitation frequencies. It could be achieved either by adding stiffeners (raising natural frequency) or by adding mass (lowering natural frequency). Transmissibility is defined as the force transmitted to the input force. When the excitation frequency is as high above the natural frequency as possible, maximum vibration isolation or minimum transmissibility occurs.

Andrew and Michael [18] described vibration control methods for industrial equipment. Reducing force of excitation inputs due to misalignment or unbalance would decrease the vibration response of the system. Constant excitation force can be reduced by adding mass. Amplification due to resonance can be reduced by tuning (changing) the natural frequency of the system. Applying damping to the system was observed to help in reducing vibrations which converts the mechanical energy into heat.

2.4 Objective

The objective of the present investigation is to numerically evaluate the V-notch rail shear apparatus for its effectiveness in testing materials at elevated test speeds. The numerical modeling will be conducted using LS-DYNA [19]. The numerical models will be employed to obtain a measure of the force transmitted through the load cell when the test fixture is loaded at different test speeds. In addition, the test fixture geometry will be modified to increase its bending stiffness with the aim of increasing the first resonant frequency. The effects of increasing stiffness and reducing mass will be studied. In addition, the effects of low-pass and band-stop filtering of load signals as measured by the load cell (numerical) will be analyzed. This was done to highlight the fact that the filtering techniques may not fix the issues related to test fixture vibrations.

CHAPTER 3

DESCRIPTION OF THE TEST APPARATUS

3.1 Standard Fixture

The present work is based on V-notched rail shear test [6]. The standard fixture and the coupon dimensions are shown in Figure 11 and Figure 12 respectively. As shown, the test apparatus consists of two fixture halves, four gripping plates and twelve gripping bolts. The specimen with symmetrically located V-notches is carefully clamped between the gripping plates, which helps in providing a uniform clamping pressure. The gripping plates also add to the bending stiffness of the test fixture, while the gripping bolts are used to apply the clamping force. This allows the specimen notches to align along the line of applied load. The test assembly is extended by a testing machine while monitoring load from the load cell mounted on top of one of the fixture.

When the test apparatus is loaded in tension using a mechanical testing machine, the relative displacement of the two fixture halves introduces shear forces in the specimen. Failure occurs across the notched specimen due to the developed stresses. Shear strain distribution is influenced by the notches in the central region of the coupon producing more uniform outcome than one without notches. As a result, the average shear stress is increased in the reduced width of the specimen. This test method incorporates the best features of Iosipescu and two-rail shear tests. Also, the shear specimen in this test standard provides a larger gage section and enhanced loading capability compared to other test methods [6].

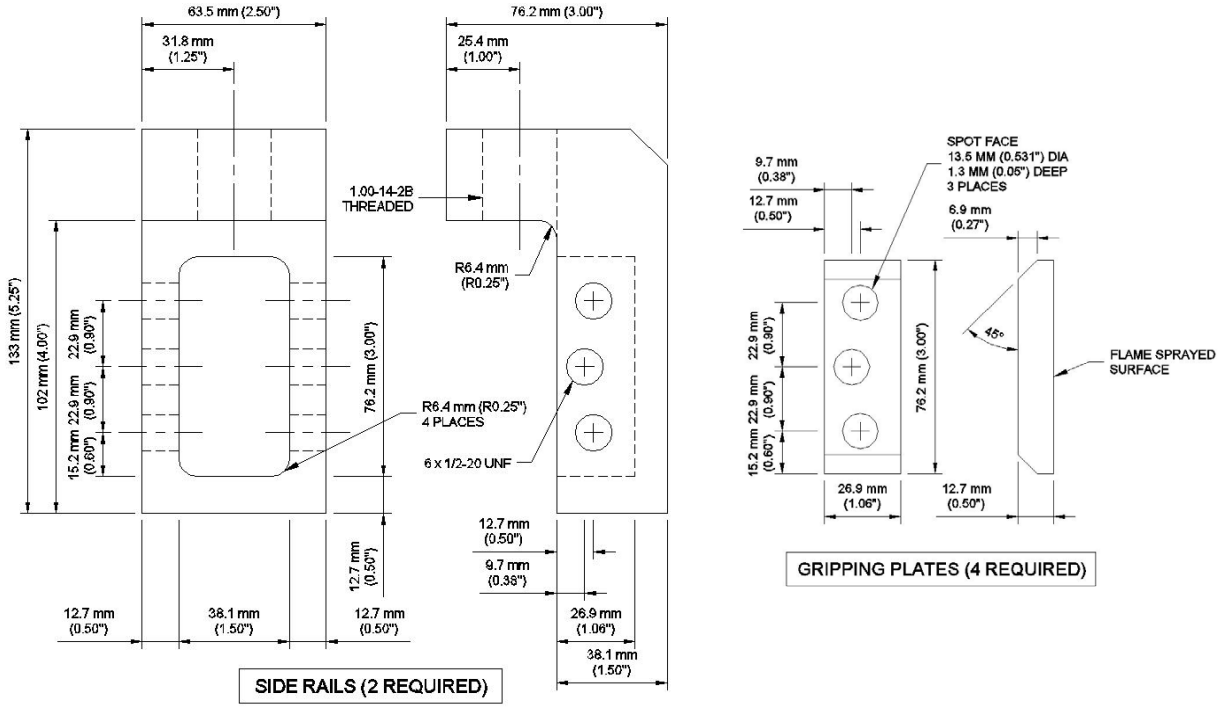

Figure 11. Dimensions of V-notched rail shear test fixture per ASTM D7078/D7078M [11]

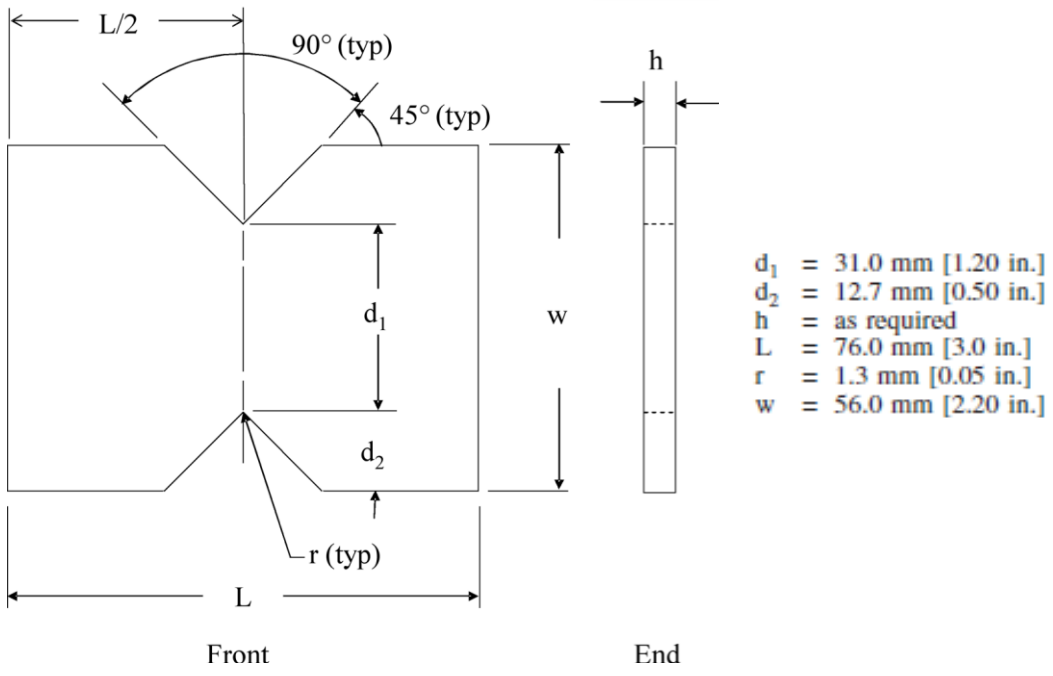

Figure 12. V-notched rail shear test specimen per ASTM D7078/D7078M [6]

3.2 Modified Fixture

In an effort to reduce mass and increase the stiffness, structural modifications were incorporated to the fixture half of the standard assembly. The structural changes discussed in this section are the initial changes applied to the apparatus. The modifications shown in Figure 13 are the only changes made to the assembly i.e. only the fixture halves were modified. Webbings are added to increase the bending stiffness of the fixture and a description on quantifying stiffness is presented in Chapter 4. Material in three different locations was chamfered, shown in Figure 13, as it only adds up to the overall mass. Both standard and modified assemblies were loaded similarly. The results are compared and discussed in later chapters. Details of the numerical model are explained in Chapter 4. Figure 14 illustrates a comparison of the standard and the modified fixtures.

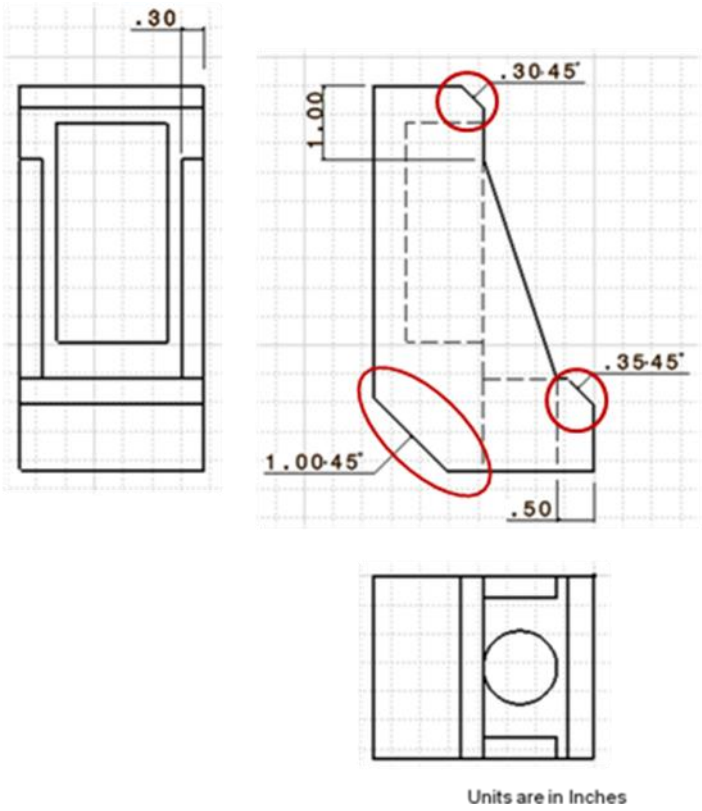

Figure 13. Modifications made to the standard fixture half

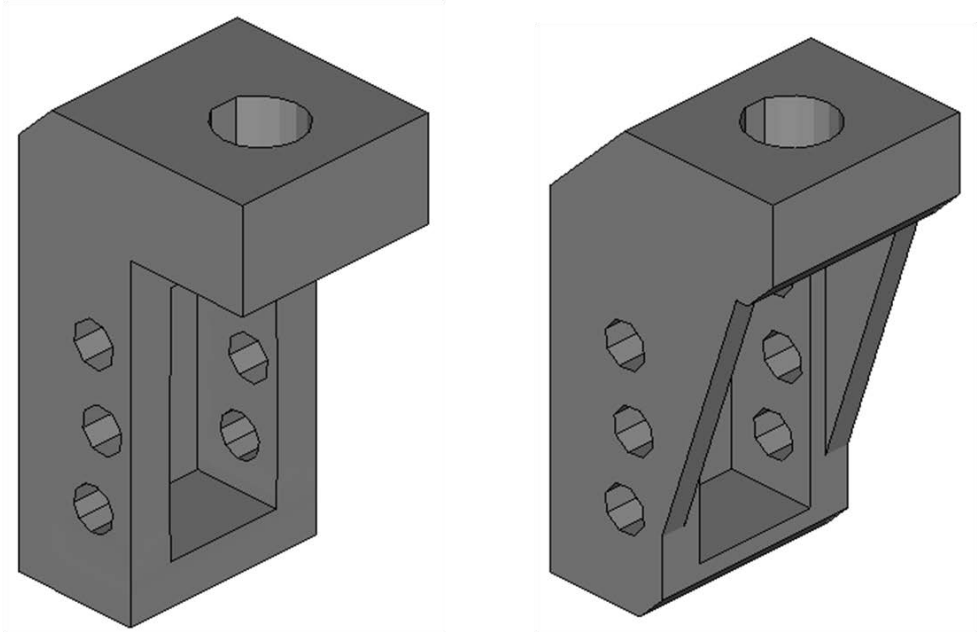

Figure 14. Comparison of standard and modified fixtures

Throughout this report, test apparatus with standard fixtures will be referred as ‘Standard Assembly’ while the test apparatus with modified fixtures (discussed in this section), will be referred as ‘Modified Assembly’. The fixture halves of both assemblies are analyzed for Stainless Steel and Aluminum materials to interpret the effect of mass on the frequencies as aluminum has approximately three time lower mass compared to steel (discussed in detail in Chapter 4).

Table 1 documents the mass of the fixture halves for both steel and aluminum materials. As shown, the modified fixtures have slightly lowered mass compared to the standard fixtures. Comparison of the natural frequencies of both test assemblies is presented in Section 4.3.

TABLE 1

MASS OF THE FIXTURE HALVES

	VOLUME (mm^3)	DENSITY ($tonne/mm^3$)	MASS	
			(tonne)	(lb)
Standard Fixture	291719	7.860E-09 (Steel)	2.29E-03	5
Modified Fixture	285479		2.24E-03	4.93
Standard Fixture	291719	2.796E-09 (Aluminum)	8.15E-04	1.8
Modified Fixture	285479		7.98E-04	1.76

CHAPTER 4

FINITE ELEMENT MODELING

4.1 Meshing

Finite element modeling is a technique of subdividing a model into smaller components of simple geometry called finite elements [20]. It can also be described as a numerical technique for obtaining approximate solutions of the partial differential equations. All simulations discussed in this document were preprocessed using CATIA V5 [21] and HyperMesh v11.0 [20], processed using LS-DYNA V971 [19], and post processed using LS-PrePost 2.1 [19] and HyperGraph v11.0 [20].

Primary components of the assembly such as the fixture half, gripping plates and gripping bolts were modeled as per the standard dimensions in CATIA V5 prior to finite element modeling. Each part is modeled independently and then assembled together. Simple geometries such as the loading stud, specimen and the load cell were modeled directly in the preprocessor HyperMesh. Figure 15 shows one of the two identical assemblies used in the test set up which consists of the following components: Fixture Half (x1), Gripping Plate (x2) and Gripping Bolt (x6). The standard fixture was later replaced with the modified version for further analyses. CATIA model of the modified fixture is shown in Figure 16. These 3-D models were then imported to HyperMesh for discretization.

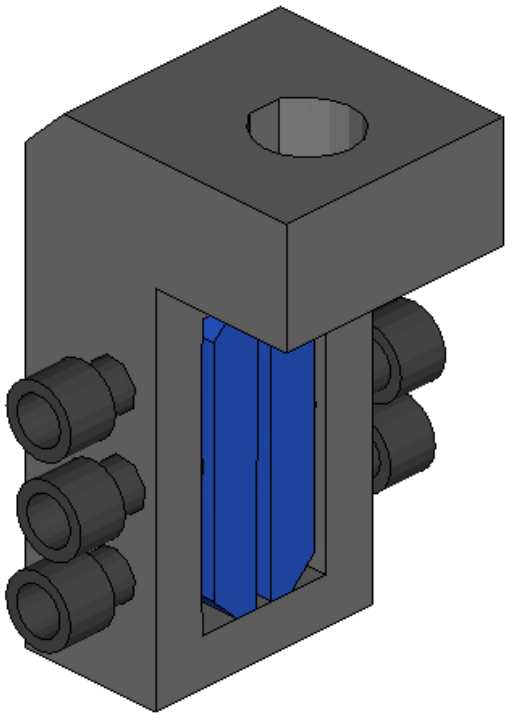

Figure 15. CATIA model – Standard shear fixture assembly

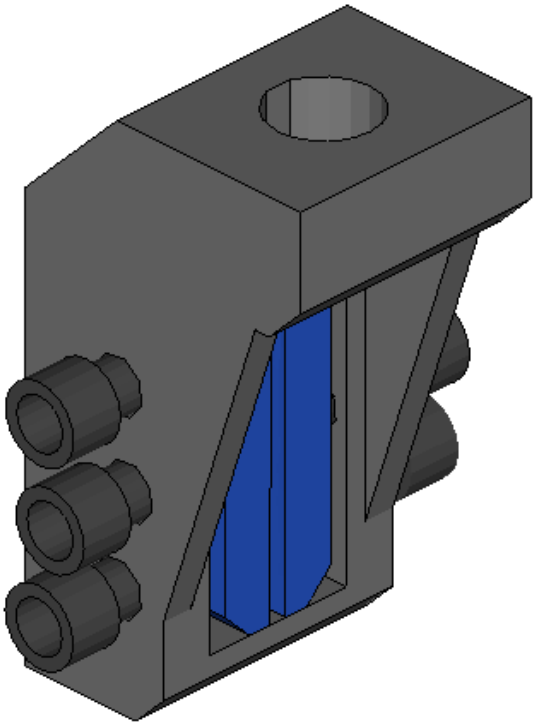

Figure 16. CATIA model – Modified shear fixture assembly

All components are modeled using solid elements, a combination of hex (8-noded) and penta (6-noded) elements. Number of elements in each component of a particular type is specified in Table 2. The fixture half and the loading stud were re-meshed for the modified assembly. Various parameters involved such as geometry cleanup, element quality etc. were checked to ensure quality of the elements. After meshing, all components are replicated to desired number and assembled together making sure to have no penetrations. Finite element models of the standard and the modified assemblies are shown in Figure 17 and Figure 18 respectively. Constant stress solid element (ELFORM=1), an LS-DYNA default solid element formulation and hourglass control type 6 (IHQ=6) are chosen for the present work. These are explained in Appendix of this report. Figure 19 shows an exploded view of the standard assembly presenting various parts. Except for the fixture halves, the assembly would be the same for any modified fixtures which are replaced accordingly.

The simulation time in LS-DYNA is controlled by the time step which is directly proportional to the mesh size. If the element size is very small, time step will also be very small and the simulation time might be unreasonably long. Element size cannot be very large either because it will not be able to capture the geometry details and solution accuracy. In this work, the smallest element size is contained by the gripping plates. In order to have practical time step and avoid long simulation time, the gripping plates were modeled as rigid bodies (explained further in later sections).

TABLE 2

DETAILS OF DISCRETIZATION

PART	ELEMENTS			MAX. ELEMENT SIZE (mm)	MIN. ELEMENT SIZE (mm)
	Penta	Hex	Total		
Fixture Half - Standard	94	3678	3772	6.5	2
Loading Stud - Standard	68	357	425	6	3.5
Preload Stud - Standard	52	273	325	6	3.5
Fixture Half - Modified	198	3228	3426	7.5	1.5
Loading Stud - Modified	60	1180	1240	5.5	2
Preload Stud - Modified	45	885	930	5.5	2
Test Coupon	12	228	240	5	3
Gripping Plate	292	6205	6497	3	1
Gripping Bolt	84	1452	1536	3	1.5
Load Cell	0	465	465	5	2.5

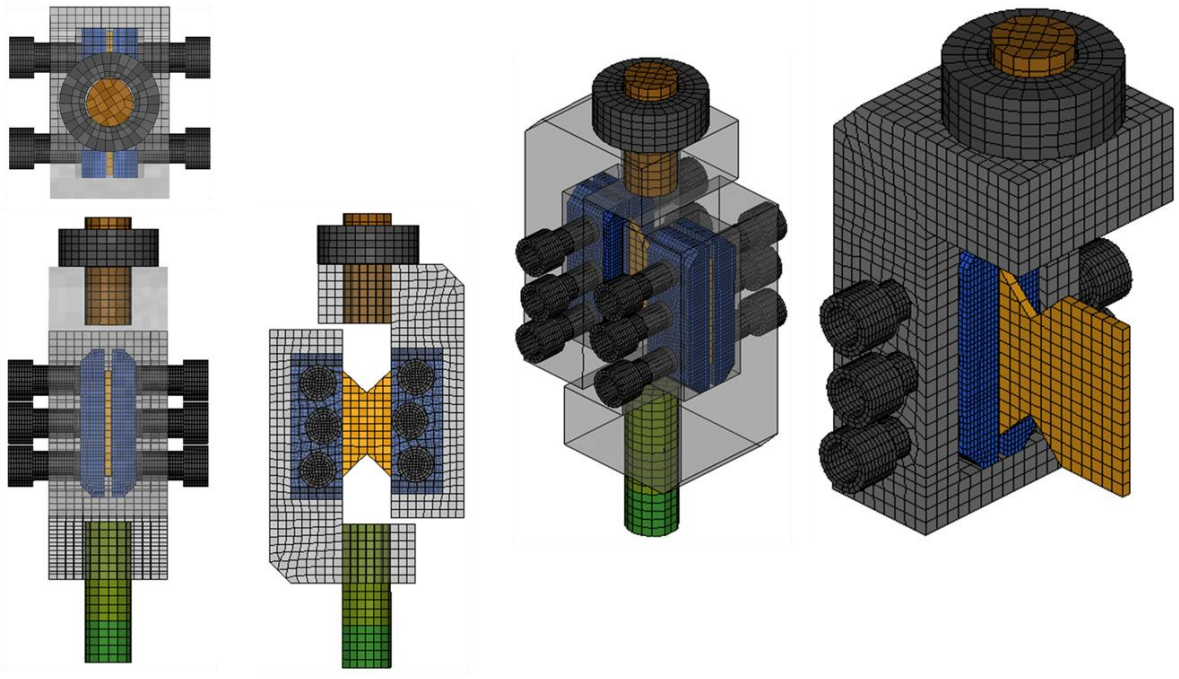

Figure 17. Finite element model of the Standard Test Assembly

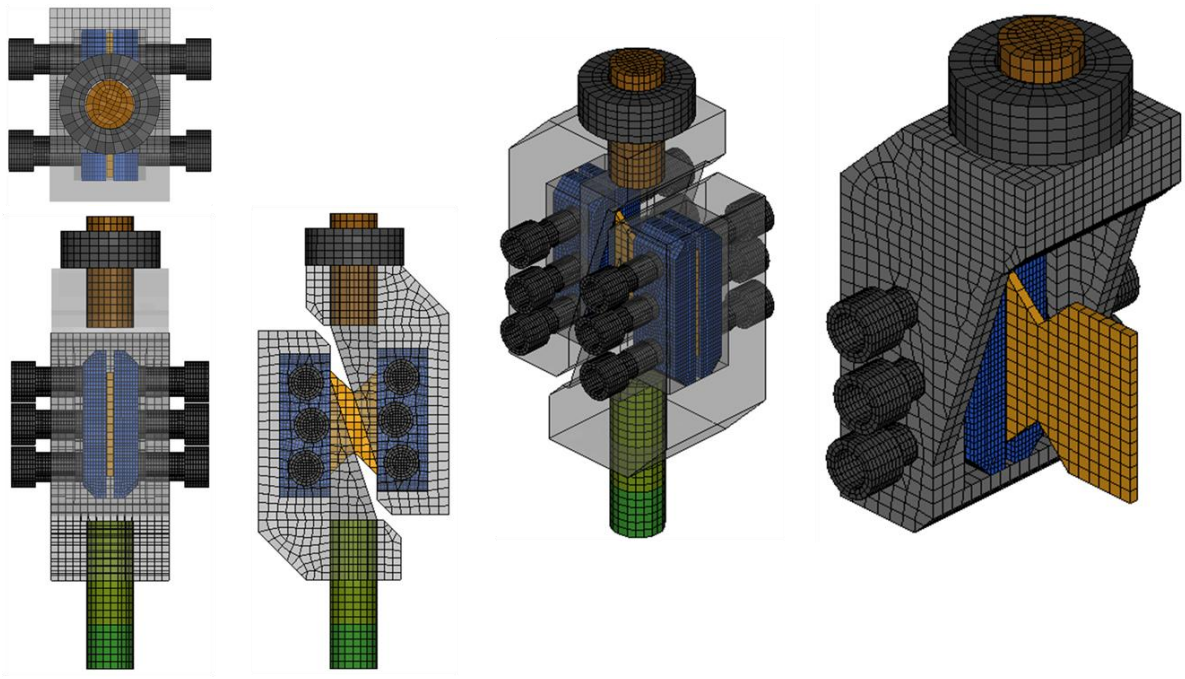

Figure 18. Finite element model of the Modified Test Assembly

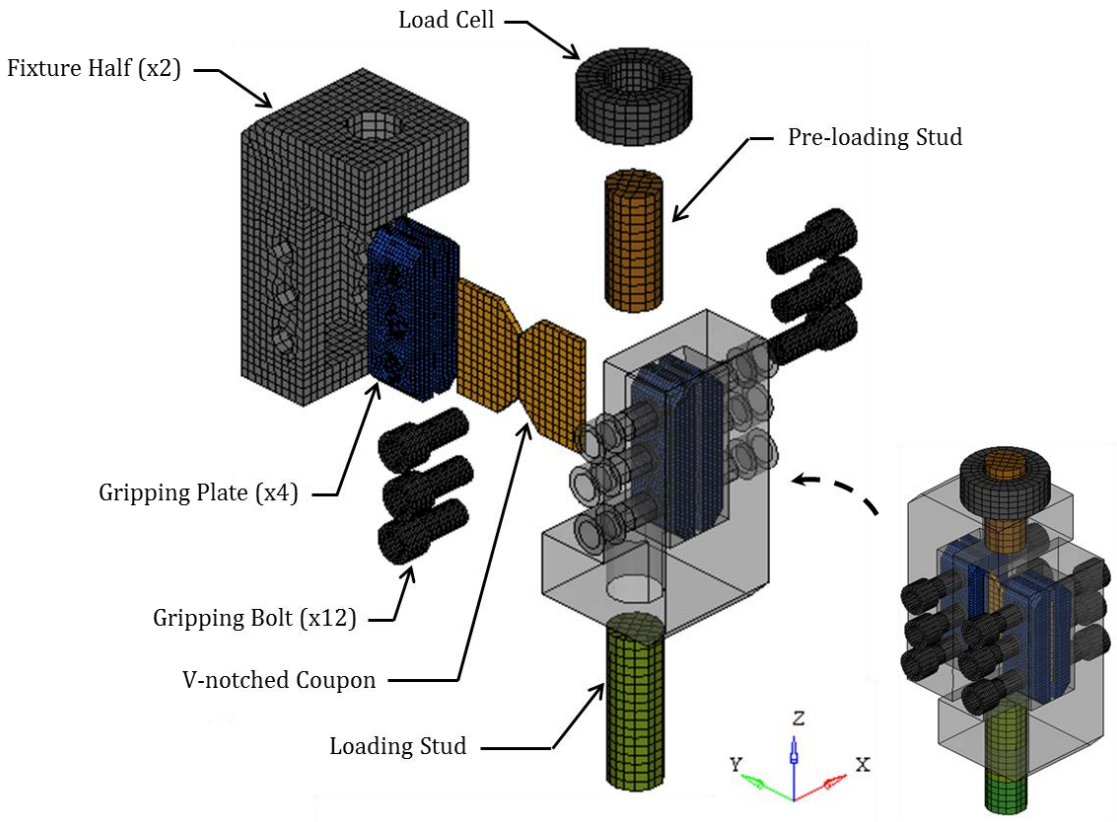

Figure 19. Identifying various components of the assembly

4.2 Materials

Aluminum 7075-T6 and 17-4 PH Stainless Steel are the two primary materials used for the model. Material properties summarized in Table 3 are obtained from MMPDS-5 [22]. Aluminum is used for the coupon while all other components are modeled as stainless steel parts. Except for the gripping plates, which are modeled as rigid bodies, all components are modeled as deformable bodies in order to gain computational efficiency as explained in Section 4.1. An analysis carried out with deformable and rigid gripping plates had shown no significant difference in the results. Therefore, gripping plates have been modeled as rigid bodies throughout this work. Figure 20 shows materials used for various parts while Figure 21 shows rigid and deformable bodies.

Fixture halves of the standard and the modified assemblies are analyzed for stainless steel as well as aluminum materials. Primary intension of analyzing the assemblies with aluminum fixtures is to observe the effect of mass on the frequency content of the system, since mass of aluminum is nearly three times lower than that of steel (Table 1).

TABLE 3

MATERIAL PROPERTIES

MATERIAL	DENSITY [ρ]	YOUNG'S MODULUS [E]	POISSON'S RATIO [υ]
Stainless Steel 17-4 PH	7.860E-09	196000	0.26
Aluminum 7075-T6	2.796E-09	74750	0.33

[mm, tonne/mm^3, sec, N, N/mm^2]

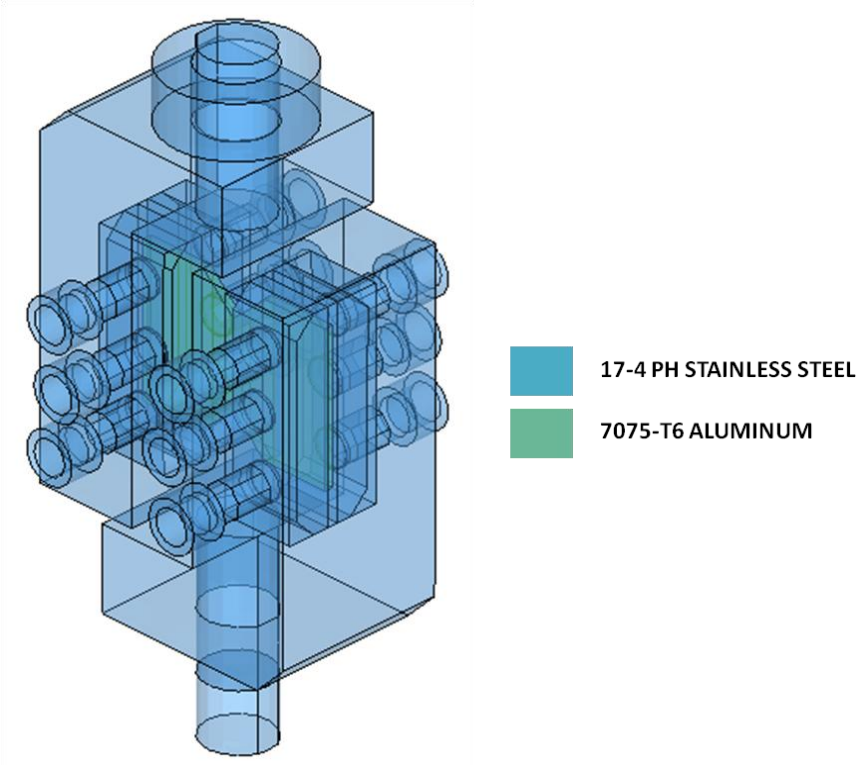

Figure 20. Identifying the material of various components

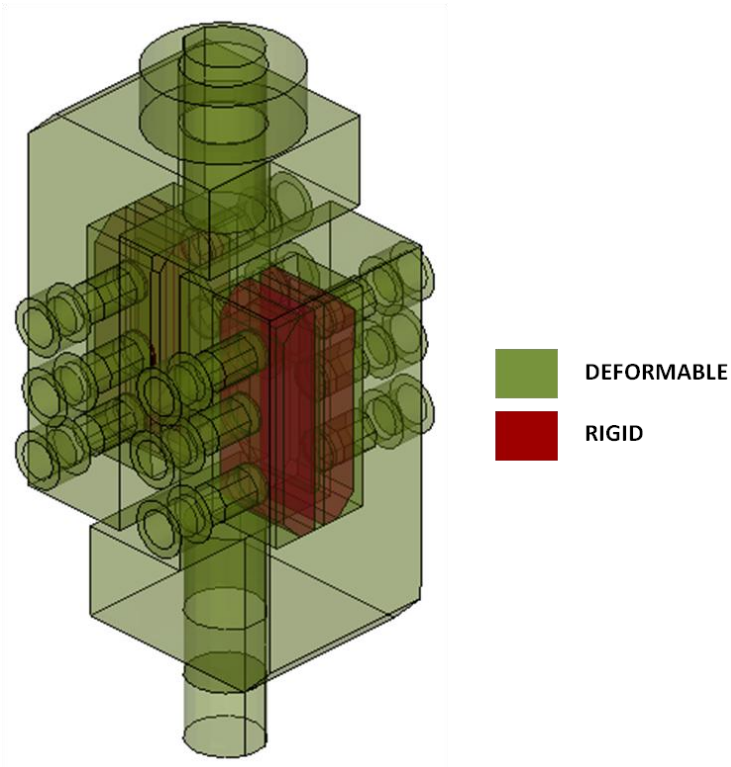

Figure 21. Assembly showing deformable and rigid bodies

Material cards are defined in HyperMesh, which allows creating various cards compatible with LS-DYNA. Material card MAT_1 (*MAT_ELASTIC) was used to model deformable bodies while MAT_20 (*MAT_RIGID) for rigid bodies.

Test specimen in this work is modeled with a single layer of solid elements across the thickness. The present work, which is based on entirely numerical approach, is an initial attempt to understand the various parameters affecting the frequencies. Effect of mesh sensitivity on the results is not included in the scope of this work. However, effect of change in mesh such as using shell elements or more than one solid element across the thickness for the coupon is recommended for future studies. Therefore the present work uses a specimen made of aluminum material (an isotropic material) to have more control over modeling failure unlike a composite material, where modeling failure is much more complicated.

The minimum section elements in the specimen are modeled to behave as a brittle material and fail at a pre-defined failure strain. A thin layer of solid elements are modeled in the minimum section of V-notched coupon. These elements are defined using MAT_13 (*MAT_ISOTROPIC_ELASTIC_FAILURE) with the properties of aluminum used to model the coupon. Figure 22 shows the elements in the minimum section. Properties defined in MAT_13 are given in Table 4. The elements defined in MAT_13 are modeled with lower yield strength compared to the yield strength of the aluminum used. Failure occurs when the effective plastic strain reaches the failure strain (EPF) parameter defined in the material card. At this time the deviatoric stresses are set to zero and the element loses its ability to carry tension [19].

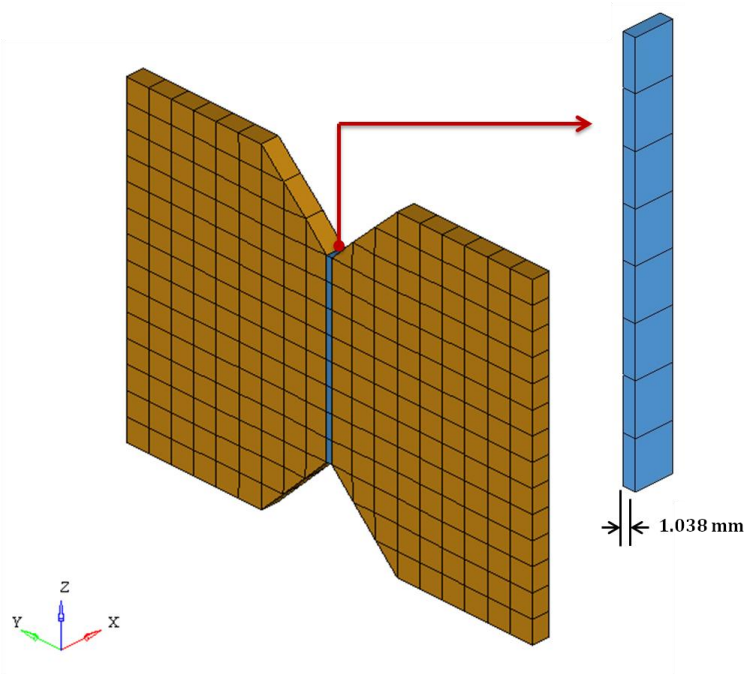

Figure 22. Elements in the minimum section of V-notched coupon

TABLE 4

MAT_13 MATERIAL CARD

DENSITY [ρ]	SHEAR MODULUS [G]	YIELD STRESS [SIGY]
2.796E-09	26890	345
PLASTIC HARDENING MODULUS [ETAN]	PLASTIC FAILURE STRAIN [EPF]	ELEMENT EROSION OPTION [REM]
31300	0.01	0

[mm, tonne/mm^3, sec, N, N/mm^2]

4.3 Stiffness and Natural Frequencies

In order to quantify stiffness, the assembly shown in Figure 23 was loaded through the specimen, as represented. Displacement along the loading direction and the load from a section across the fixture half were extracted. Figure 24 presents the load versus displacement curves for the standard and modified assemblies with steel and aluminum fixtures. As shown, the modified

fixtures with steel material was interpreted to be 67% stiffer compared to the standard steel fixture.

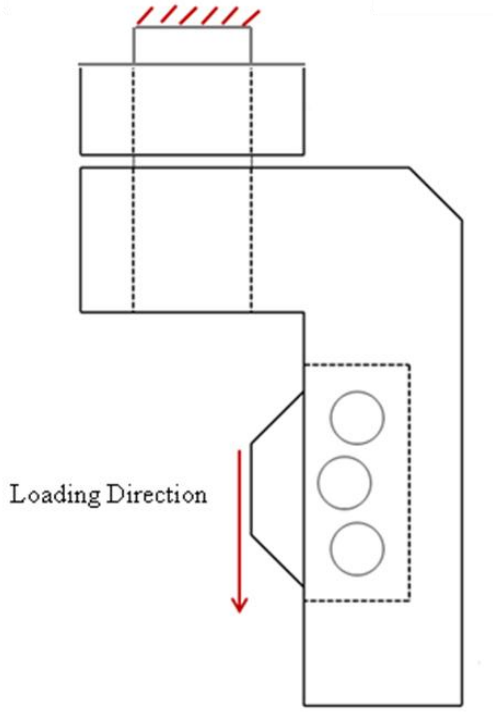

Figure 23. Boundary conditions – Quantifying stiffness

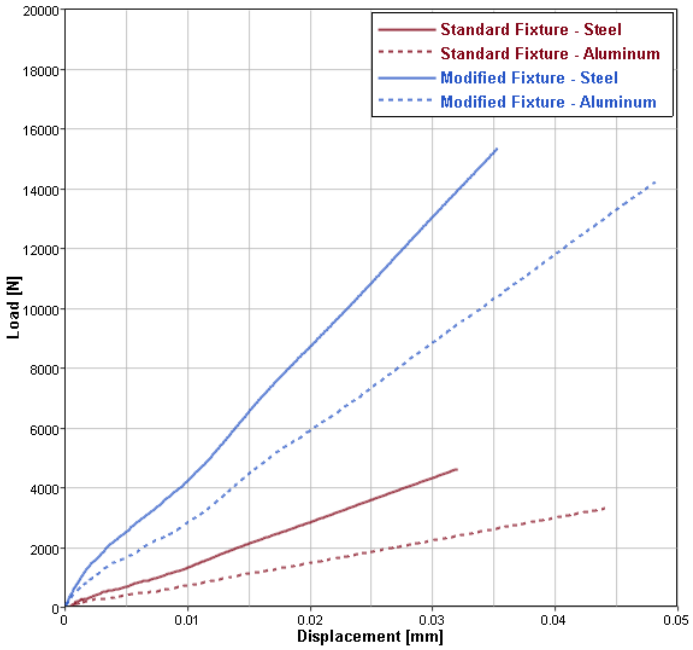

Figure 24. Fixture halves – Variation in stiffness

In LS-DYNA, with the help of implicit analysis, first modes of natural frequencies were estimated for the standard & modified test apparatus with steel and aluminum fixtures. The results are documented in Table 5 below:

TABLE 5

NATURAL FREQUENCIES

NATURAL FREQUENCY (Radians)			
STANDARD MODEL (Steel Fixtures)	MODIFIED MODEL (Steel Fixtures)	STANDARD MODEL (Aluminum Fixtures)	MODIFIED MODEL (Aluminum Fixtures)
44.213	77.131	76.217	114.917

4.4 Contacts and Constraints

Various types of contacts and constraint modeling options are available in LS-DYNA suitable for different jobs. The cards used for the current model are given below between two components at a time:

- Fixture Half to Load Cell: CONTACT_AUTOMATIC_SURFACE_TO_SURFACE
- Fixture Half (surface) to Bolts (nodes): CONTACT_TIED_NODES_TO_SURFACE
- Gripping Plate (part Id) to Bolts (nodes): CONTRAINED_EXTRA_NODES_SET
- Gripping Plate (part Id) to Coupon (nodes): CONTRAINED_EXTRA_NODES_SET
- Fixture Half and Stud: SHARE NODES

Nodes common to the fixture half and the stud are merged. The contacts and constraint options discussed above are graphically shown in Figure 25. Automatic contact types in LS-DYNA checks for penetrations between master and slave parts. It will make one attempt to eliminate any detected penetrations which will not necessarily be removed, leading to nonphysical behavior [19]. In order to avoid this, penetrations between the parts are checked and

removed. Since the gripping plates are modeled as rigid bodies, any contact to them would be constraining the nodes to the part. The slave nodes in tied contact types are constrained to move with master surface. In tied contacts, the rotational degrees of freedom of the slave nodes are constrained and preferably a body with coarser mesh is chosen as the master component.

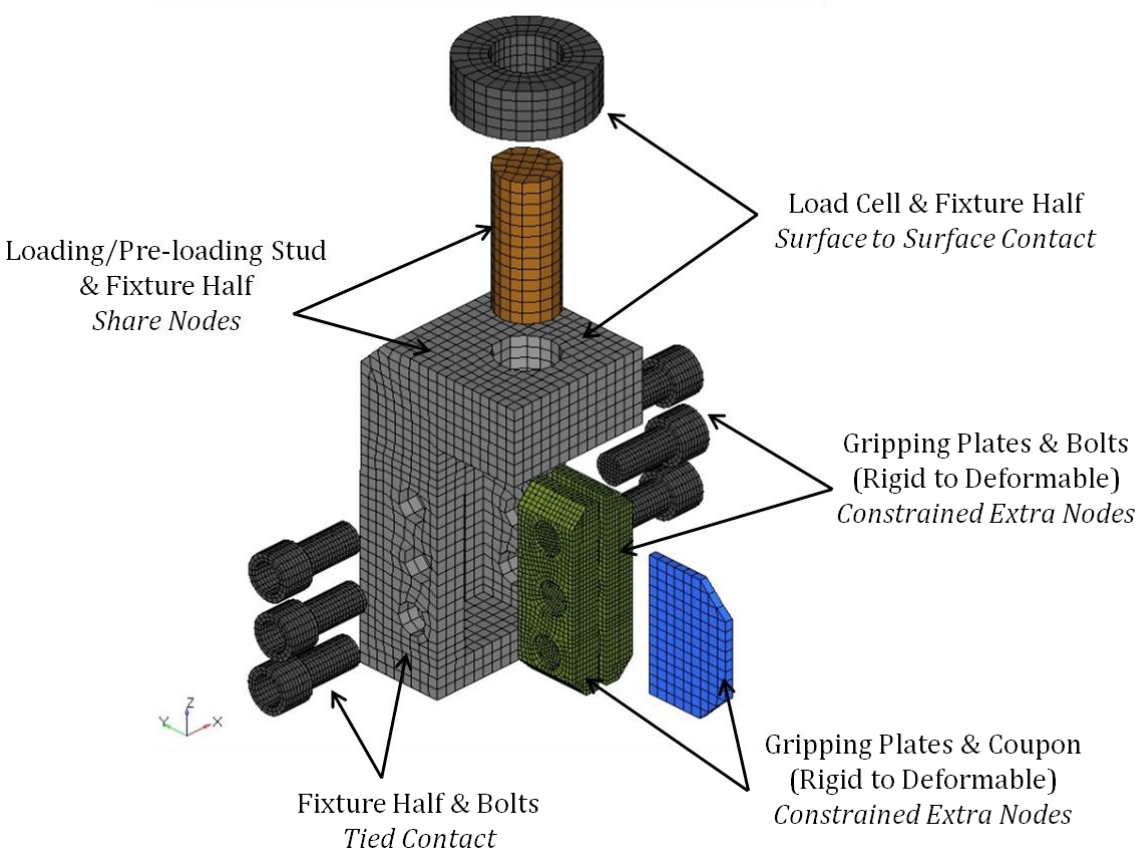

Figure 25. Contacts and constraints between various parts of the test apparatus

4.5 Boundary Conditions

Tensile loading in global z-direction was applied to the model to produce shear stresses in the gage section of the specimen by relatively displacing the fixture halves. A set of nodes on the top stud were displaced in the positive global z-direction using LS-DYNA card BOUNDARY_PRESCRIBED_MOTION_SET in order to pre-load the load cell. To constrain nodes in translational and rotational degrees of freedom, LS_DYNA card

BOUNDARY_SPC_SET was used wherever required. A set of nodes on the bottom loading stud were constrained in all degrees of freedom except the translational z-direction so that it is pulled only in one direction by avoiding deformation in other directions. The nodes on the top surface of the load cell are constrained in translational z-direction and a couple of nodes on the same surface are constrained in translational y-direction in order to constrain rotational degrees of freedom of the load cell. The nodes on the bottom loading stud were displaced in negative global z-direction using a displacement curve corresponding to a particular displacement rate. Figure 26 shows the boundary conditions discussed above on the test apparatus with modified fixtures. These conditions are consistent for all models that are discussed in this report.

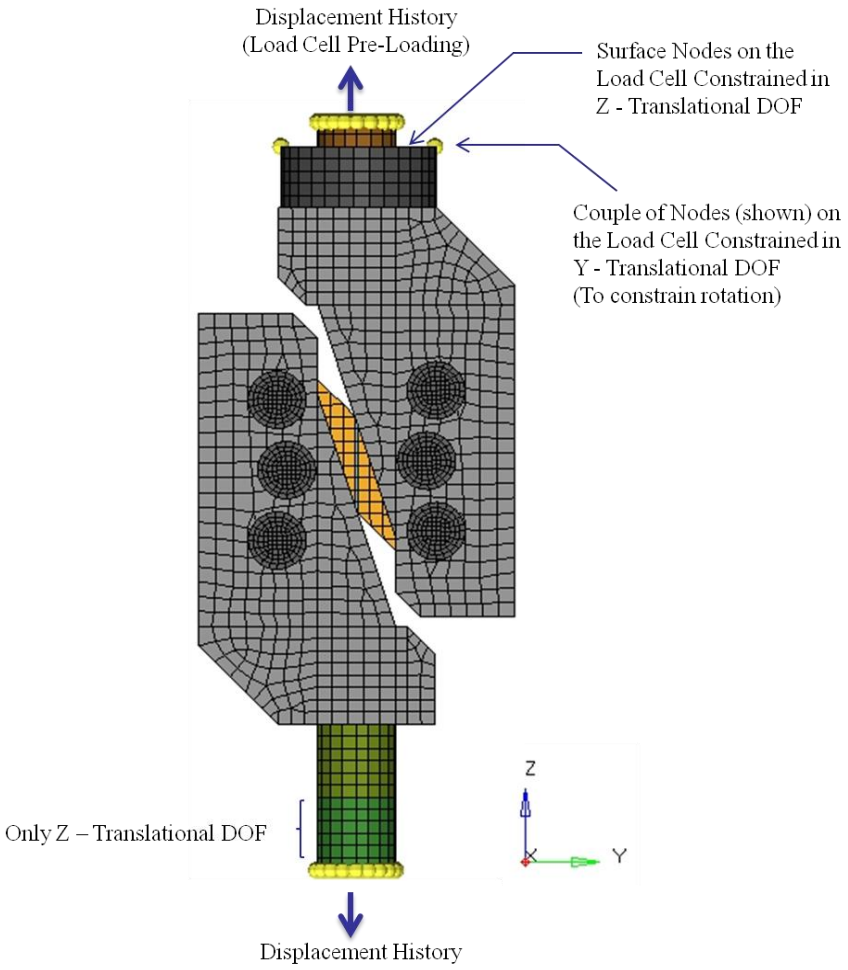

Figure 26. Boundary conditions

4.6 Cross-section Planes and Control Cards

In order to extract results, various cross-section planes are defined which outputs the requested data such as the stresses, strains, forces etc. Data is primarily compared between the load cell and the minimum section. Location of these two cross-section planes is shown in Figure 27. LS-DYNA card used to define these planes is DATABASE_CROSS_SECTION_SET which uses elements and nodes to define a plane. As shown, the set of elements chosen to define a plane on the load cell do not include elements from the pre-loading stud, which pass through the plane. The load cell is pre-loaded prior to loading the model. The stresses from the pre-loaded load cell are then initialized while loading the model at various displacement stroke rates (explained in detail in Section 4.7 and Section 4.8). This is done using the control cards available in LS-DYNA.

The desired output is requested through the control card DATABASE_OPTION where the files are created during the analysis. Forces are requested through the parameter 'SECFORC' while stresses and strains through 'ELOUT'. Parameters like the termination time, sampling rate, time step, and damping are also defined using the control cards. Termination time is varied depending on the rate at which the model is loaded and so is the sampling rate. With an increase in the stroke rate, sampling rate is reduced in order to capture data more accurately. Also, hourglass and element formulation, explained in the Appendix, are defined using control and property cards respectively.

The value defined for damping in LS-DYNA is equal to twice the lowest mode of natural frequency. And as a result of pre-loading the model in a separate analysis, huge excitation was observed in the transition period from pre-load to transient analysis. Because of this reason higher damping value of 2000 has been used in this work. However, as discussed

earlier, further investigations on mesh sensitivity and damping are included in the future research. The time step and sampling rate defined in this work at all rates are documented in Table 6 below.

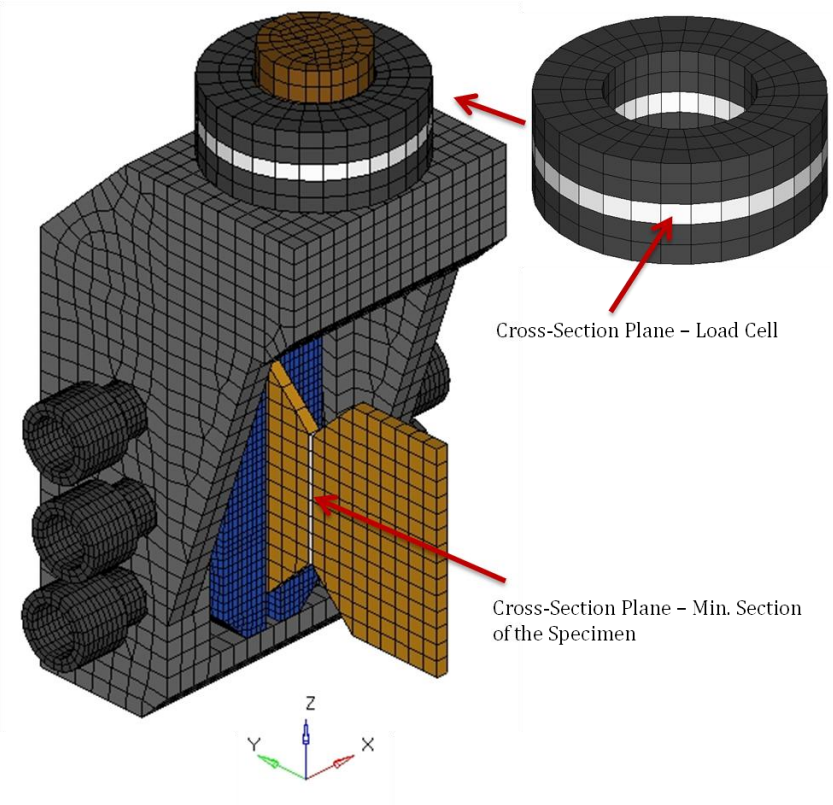

Figure 27. Location of cross-section planes – Load cell and specimen

TABLE 6

TIME STEP AND SAMPLING RATE

	STROKE RATE 1 in/sec	STROKE RATE 10 in/sec	STROKE RATE 100 in/sec	STROKE RATE 200 in/sec
Time Step	1.58253E-07			
Sampling Rate	1.0E-05	1.0E-05	1.0E-06	1.0E-07

4.7 Pre-loading Load Cell

Load cell pre-loading is done in a separate analysis prior to loading the test apparatus and the assembly includes only the components shown in Figure 28 which shows the model with standard fixture. While loading the model at different stroke rates, load cell stresses were initialized and the analysis was restarted with the pre-loaded load cell. Restart analysis in LS-DYNA used the following input cards:

- STRESS_INITIALIZATION: This card allows stresses from the selected parts to be initialized upon restart [19]. Therefore from the 'd3dump' file of the pre-load analysis, stresses from the load cell and the pre-loading stud are initialized in the restart input deck.
- CHANGE_CONTACT_SMALL_PENETRATION: This card checks for the penetrations in the restart input deck in order to avoid them during the restart analysis [19].
- CHANGE_VELOCITY: This card allows changing the velocities of certain nodes to be zero in the restart analysis which helps in avoiding initial displacements in the model [19].

Load cell is pre-loaded by displacing the top stud in the direction shown (Figure 28) i.e. global z-direction. The top stud is pulled to a desired distance per one millisecond (which is estimated based on several iterations made to achieve the desired load in the load cell) and kept constant through the rest of the analysis. Figure 28 also shows the coordinates of the displacement history used to pre-load the load cell. It shows the apparatus with standard steel fixture but the pre-load analysis was carried out separately for all assembles i.e. standard and modified assemblies with steel and aluminum fixtures. Figure 29 shows the contour of compressive z-stresses in the load cell. Pre-load force history is plotted and shown in Figure 30. As shown, the load cell is pre-loaded to see about 90 kN.

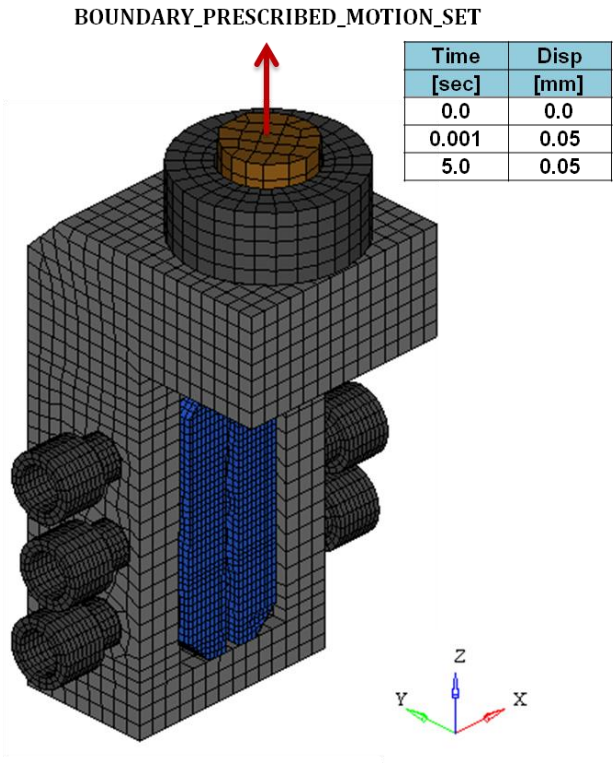

Figure 28. Model used to pre-load load cell

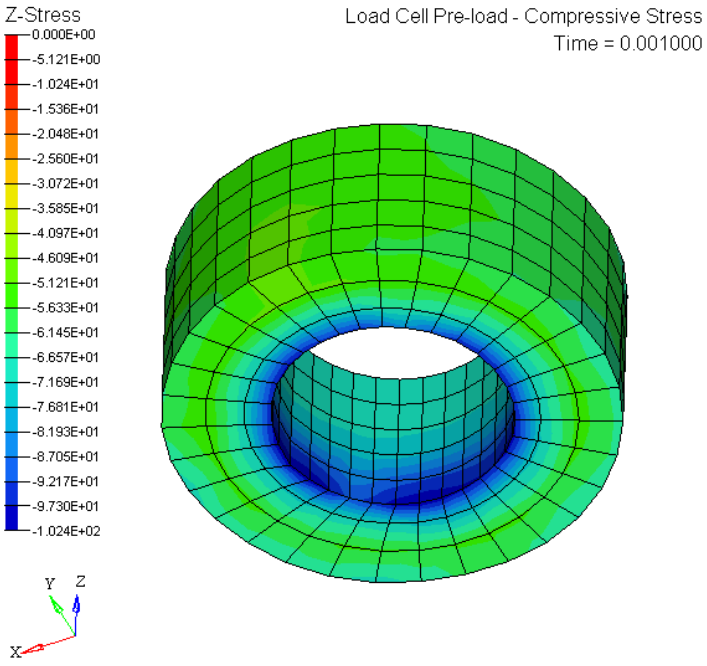

Figure 29. Compressive stress in the load cell - Preload

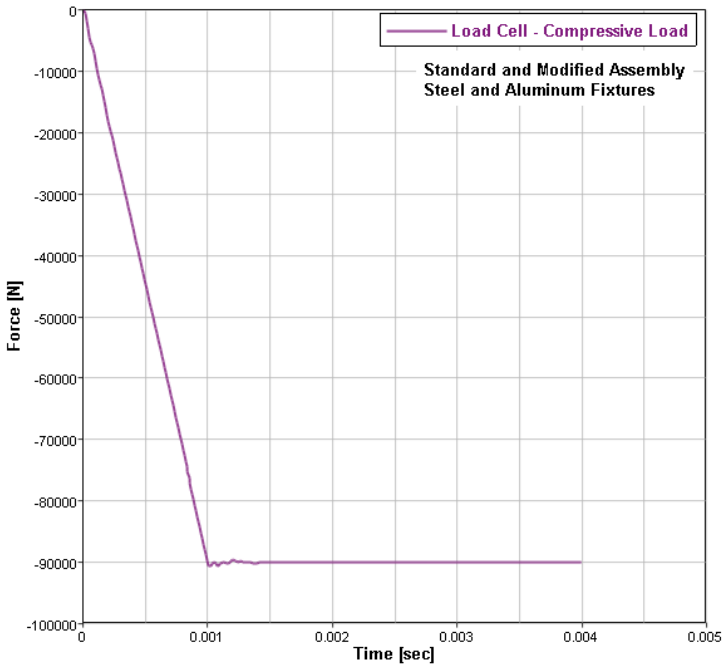

Figure 30. Pre-load force in the load cell

4.8 Analysis of Standard and Modified Fixtures

During pre-loading, the top stud is given a displacement in the positive z-direction which introduces a compressive load of approximately 90 kN in the load cell. Stresses from the pre-load analyses are initialized while loading the model at different stroke rates as explained in the previous section. The stud in the pre-load analyses is pulled using a displacement history but the analysis is terminated at 0.004 sec. Transient analysis is initiated right from the termination time of the pre-load analyses as shown in Figure 31.

During the initial phase, the system was excited as any system given an initial input of energy (either in the form of initial displacement or initial velocity) and released is subjected to free vibrations under right conditions. As explained in Section 4.6, damping is applied to the system in order to let the initial vibrations die out before the actual loading begins. This value is

estimated based on the results of several simulations carried out to observe the desired initial damping in the system.

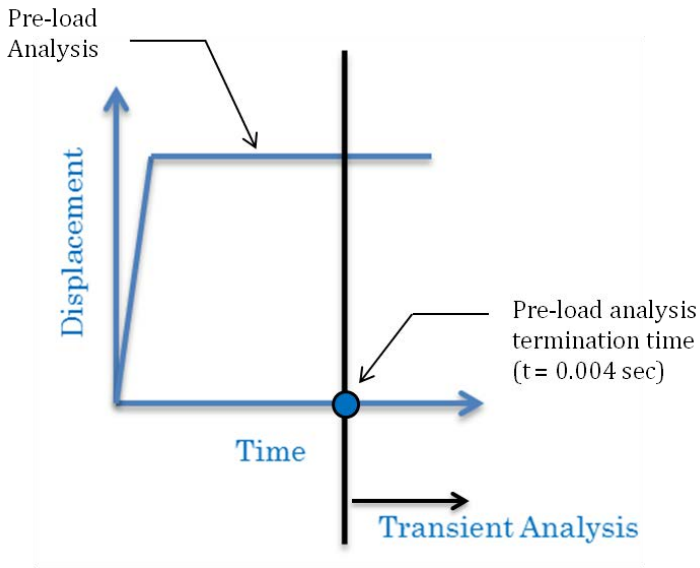

Figure 31. Nature of the preload curve and initiation of transient analysis

In order to model failure, the elements in the minimum section of the specimen are defined using the material card MAT_13 of LS-DYNA where the elements fail when they reach the plastic strain value defined in the card. Using a displacement history (Figure 32) corresponding to a particular stroke rate, the nodes on the bottom stud are displaced in the negative global z-direction as explained in Section 4.5. The model is loaded with a constant displacement stroke rate at 1 in/sec, 10 in/sec, 100 in/sec and 200 in/sec.

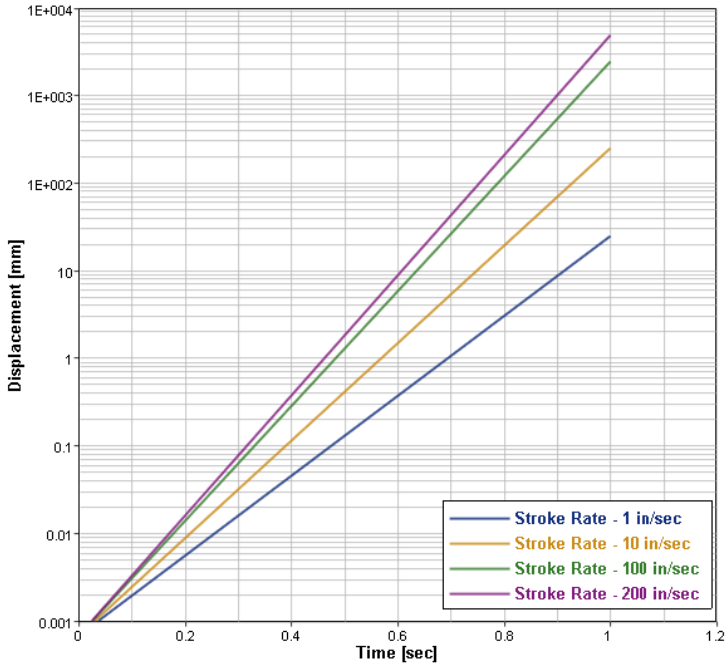

Figure 32. Displacement history at different stroke rates applied to load the model

The load seen in the load cell and the minimum section are compared. For a better comparison of the results between the pre-loaded load cell and the minimum section of the specimen, the pre-load in the load cell is removed from the data (for graphical representation purpose only) and compared with the load seen in the minimum section. Since some of the force is shunted through the stud, the load cell force is observed to be lower compared to the specimen. A correction factor is estimated for models with aluminum and steel fixtures for standard and modified versions by loading at quasi-static rate (0.01 in/sec). This factor is later applied to the load cell data. The estimated load cell correction factors are given below:

- Assembly with Standard steel fixtures - 1.575
- Assembly with Standard aluminum fixtures - 1.75
- Assembly with Modified steel fixtures - 1.4735
- Assembly with Modified aluminum fixtures – 1.5935

These correction factors are applied to the load cell data and the comparisons presented in Chapter 5 shows the corrected load cell data. Zero-padding is applied to the data in order to have a higher resolution FFT as explained in Appendix of this report.

CHAPTER 5

RESULTS AND DISCUSSION

5.1 Discussion of Results - Standard and Modified Fixtures

Upon loading the test apparatus in tension, the specimen failed as per the criteria defined in MAT_13 of the minimum section elements. Once the specimen failed, the assembly was excited and the vibrations in the system were captured by the load cell results indicated by the oscillations observed after the first pulse in time domain results. At lower rates such as 1 in/sec (Figure 33) and 10 in/sec (Figure 34), a perfect load ramp was observed in the results until the specimen failed followed by the excitation of the system. As the stroke rate increased, the load at which the specimen failed decreased. Also, starting from 100 in/sec, a time shift (phase shift) in the load cell results was observed compared to the specimen results (Figure 35). Until the frequency with first peak amplification has been encountered (highlighted in every plot with a green dot), the variation in the load cell and the minimum section results indicated a good correlation while observing increasing differences at higher rates. Zero padding has been applied to the time domain results in order to obtain a smoother looking curve in the frequency domain, for a better interpretation of the results by increasing the number of frequency bins.

Figure 33 through Figure 36 show a comparison of the corrected load cell and the minimum section data (at 1, 10, 100 & 200 in/sec) in time domain and frequency domain for the standard assembly with stainless steel fixtures. Up until 1 kHz, frequencies and amplitude of the load cell and the minimum section results coincided at 1 in/sec and 10 in/sec while variations were observed starting from 100 in/sec. These differences at higher rates in the initial phase were interpreted to be due to the zero padding applied to the time domain results.

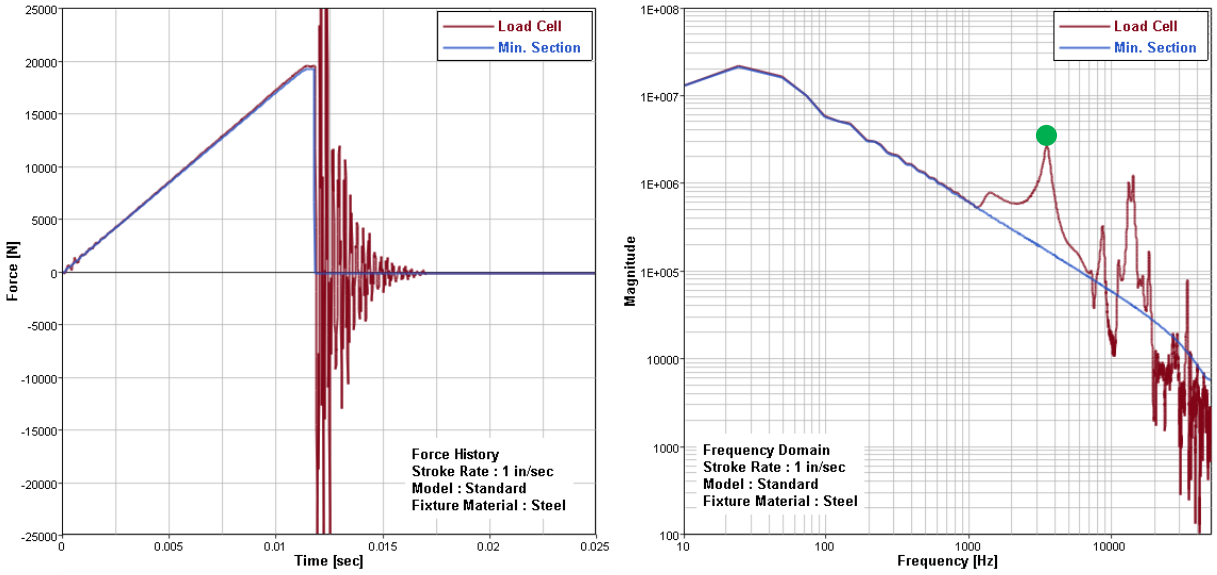

Figure 33. Time and frequency domain results comparison for standard model with stainless steel fixtures at stroke rate 1 in/sec

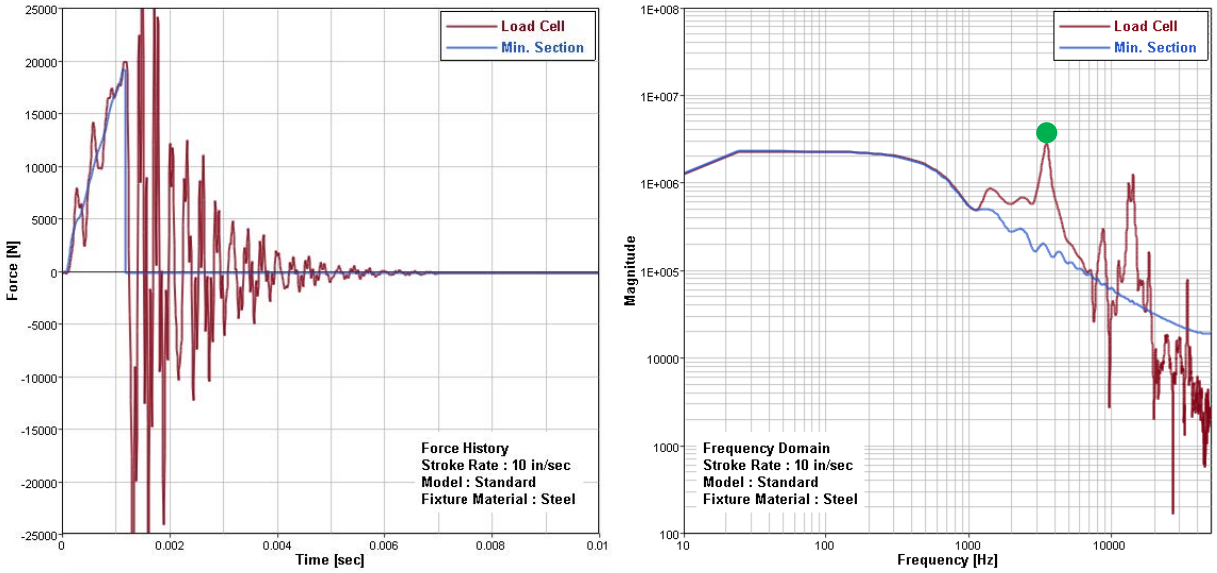

Figure 34. Time and frequency domain results comparison for standard model with stainless steel fixtures at stroke rate 10 in/sec

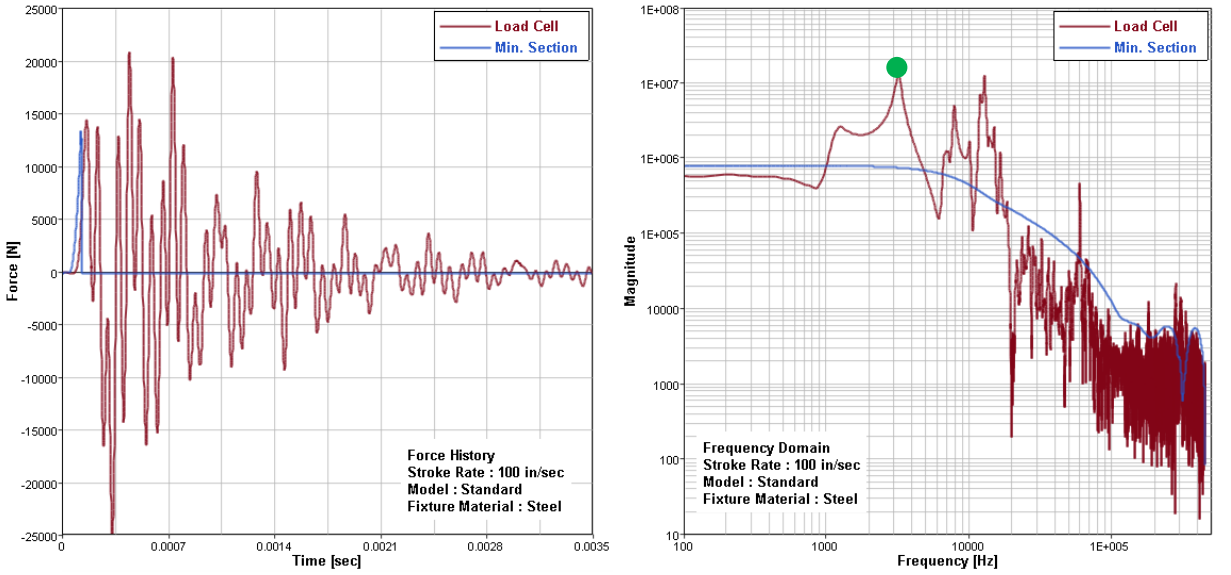

Figure 35. Time and frequency domain results comparison for standard model with stainless steel fixtures at stroke rate 100 in/sec

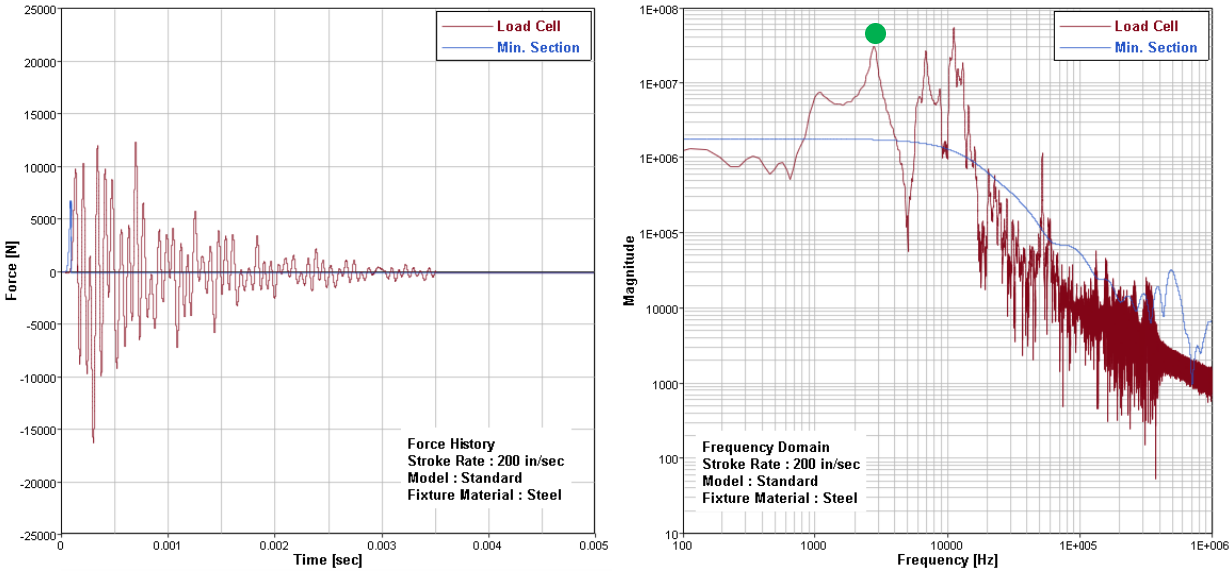

Figure 36. Time and frequency domain results comparison for standard model with stainless steel fixtures at stroke rate 200 in/sec

Figure 37 through Figure 40 present the results for the standard assembly with aluminum fixtures. As explained earlier, as a result of applying zero padding, variations in the initial phase were observed at higher rates.

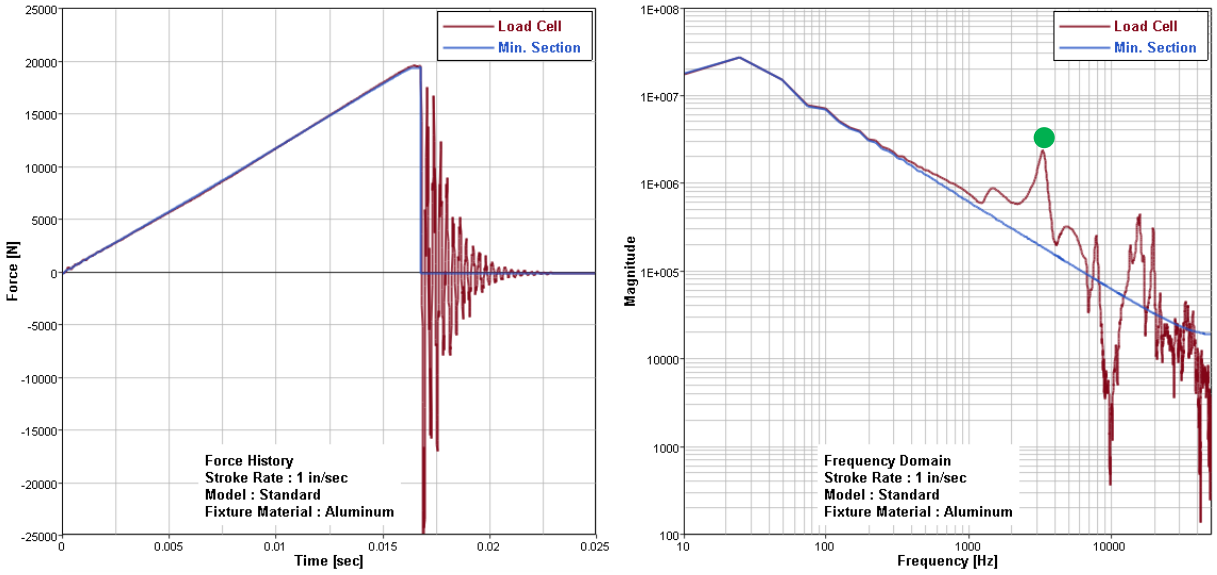

Figure 37. Time and frequency domain results comparison for standard model with aluminum fixtures at stroke rate 1 in/sec

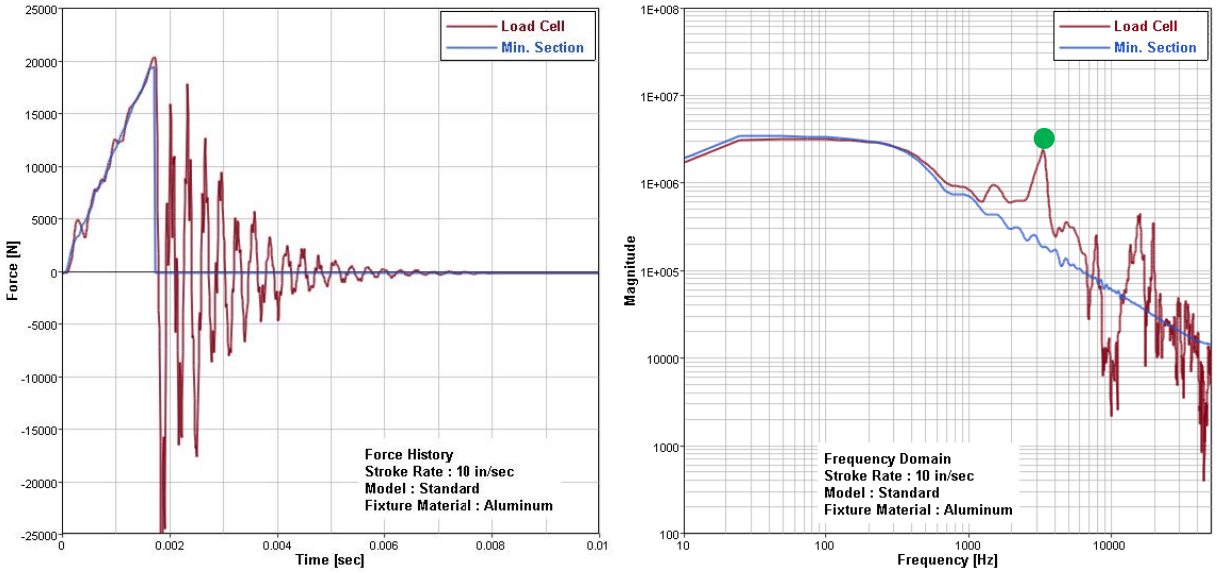

Figure 38. Time and frequency domain results comparison for standard model with aluminum fixtures at stroke rate 10 in/sec

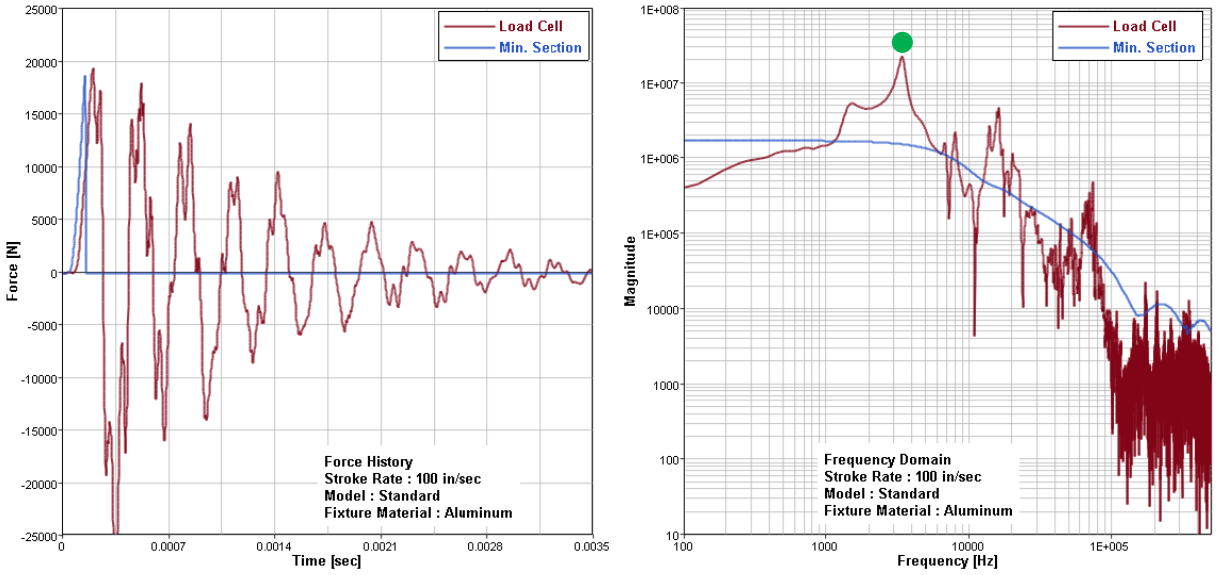

Figure 39. Time and frequency domain results comparison for standard model with aluminum fixtures at stroke rate 100 in/sec

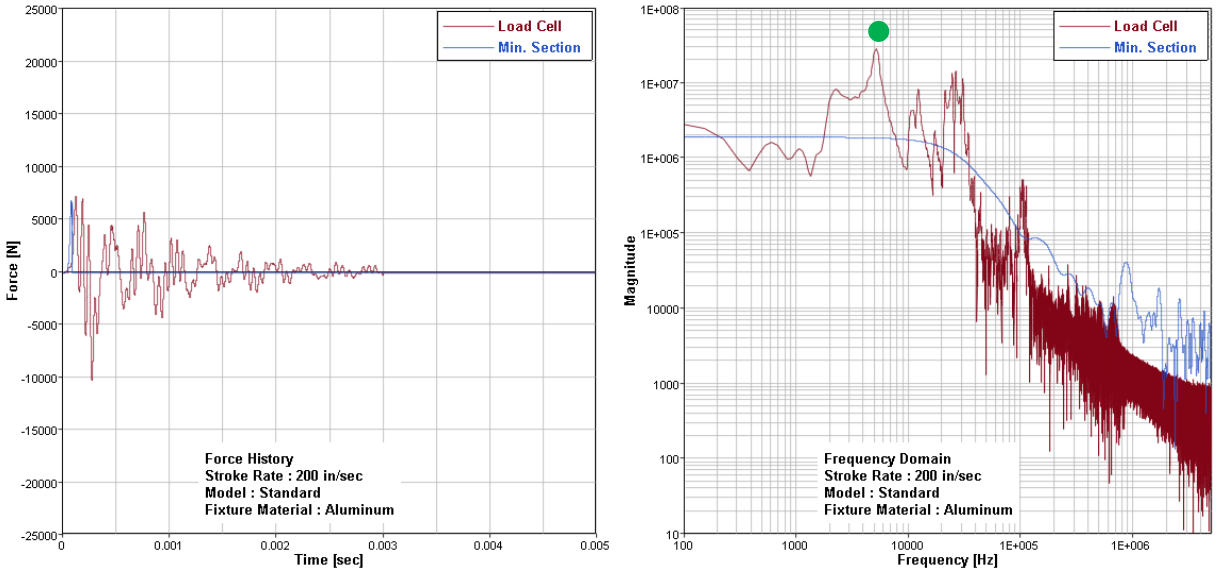

Figure 40. Time and frequency domain results comparison for standard model with aluminum fixtures at stroke rate 200 in/sec

Figure 41 through Figure 44 show a comparison of the corrected load cell and the minimum section data (at 1, 10, 100 & 200 in/sec) in time domain and frequency domain for the modified assembly with stainless steel fixtures. Similar explanation, as that of the standard

assembly, applies to the modified assembly as well but due to the increased fixture stiffness as a result of the added webbings, initial phase variation at 100 in/sec has reduced considerably while at 200 in/sec no significant change was observed. Also, a significant increment in the first band width has been observed with the modified fixtures compared to the standard.

Figure 45 through Figure 48 present the results for the modified assembly with aluminum fixtures. No significant change or improved correlation was observed in the initial phase with aluminum fixtures though a significant increment in the first band width was observed compared to the results with standard aluminum fixtures.

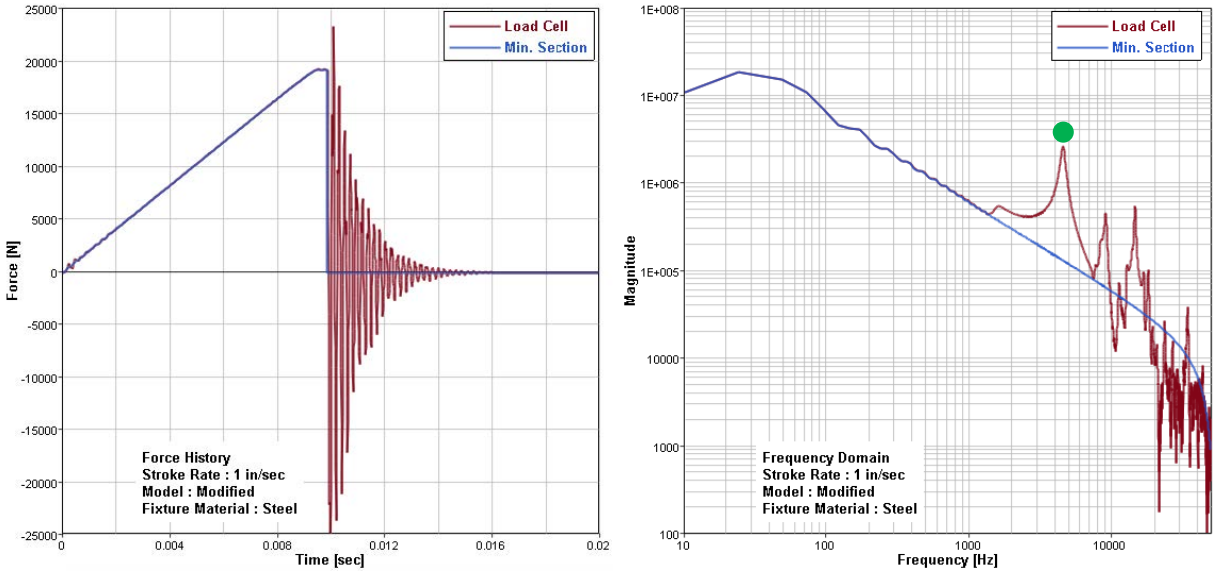

Figure 41. Time and frequency domain results comparison for modified model with stainless steel fixtures at stroke rate 1 in/sec

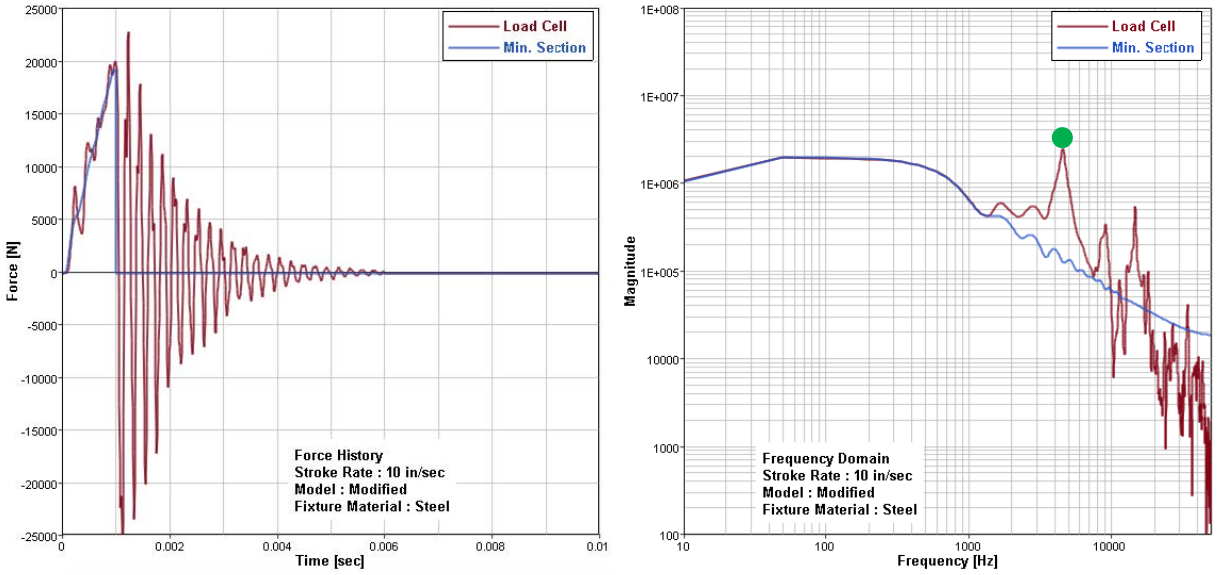

Figure 42. Time and frequency domain results comparison for modified model with stainless steel fixtures at stroke rate 10 in/sec

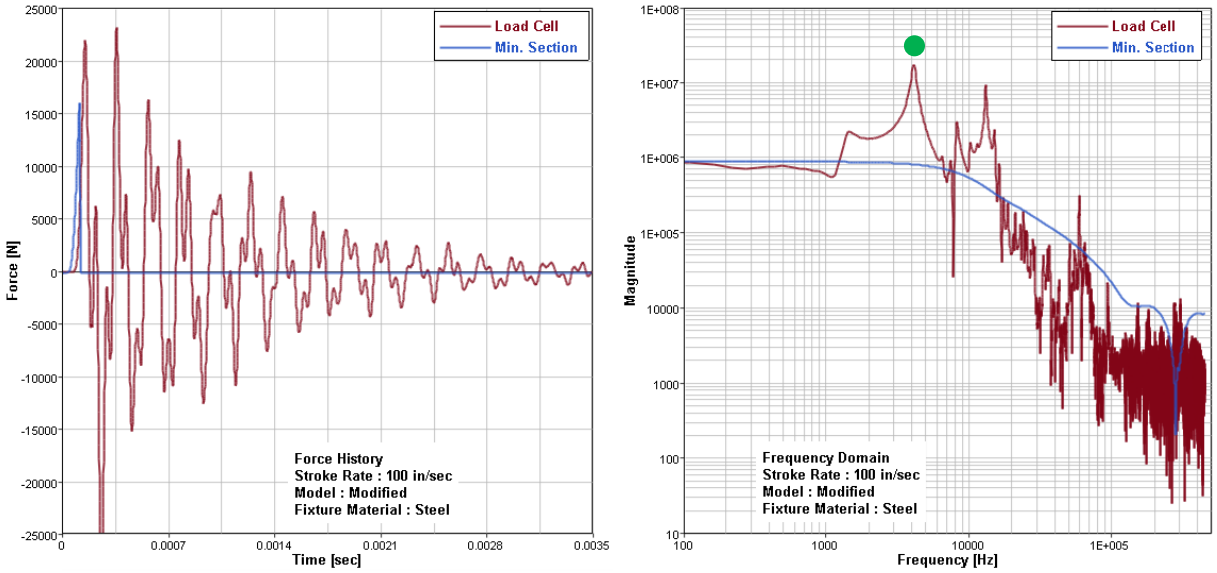

Figure 43. Time and frequency domain results comparison for modified model with stainless steel fixtures at stroke rate 100 in/sec

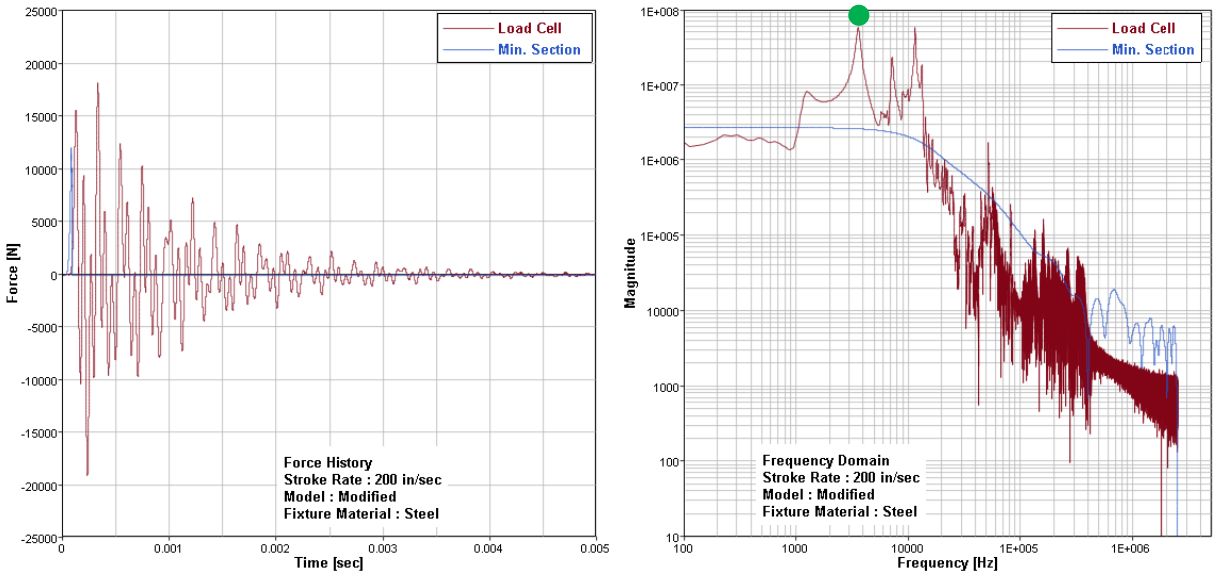

Figure 44. Time and frequency domain results comparison for modified model with stainless steel fixtures at stroke rate 200 in/sec

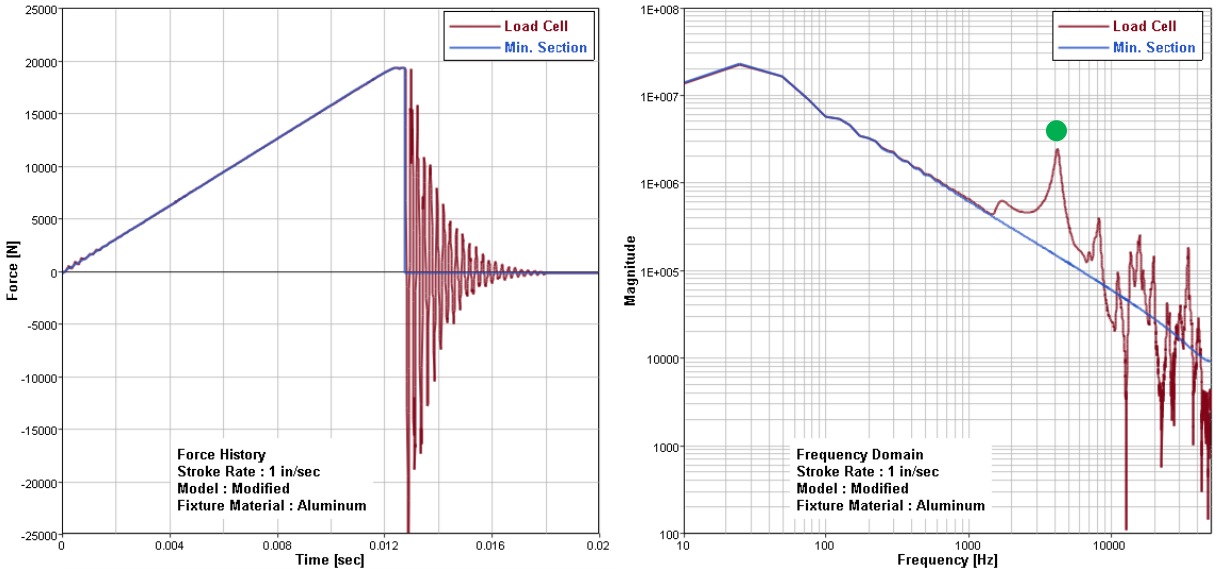

Figure 45. Time and frequency domain results comparison for modified model with aluminum fixtures at stroke rate 1 in/sec

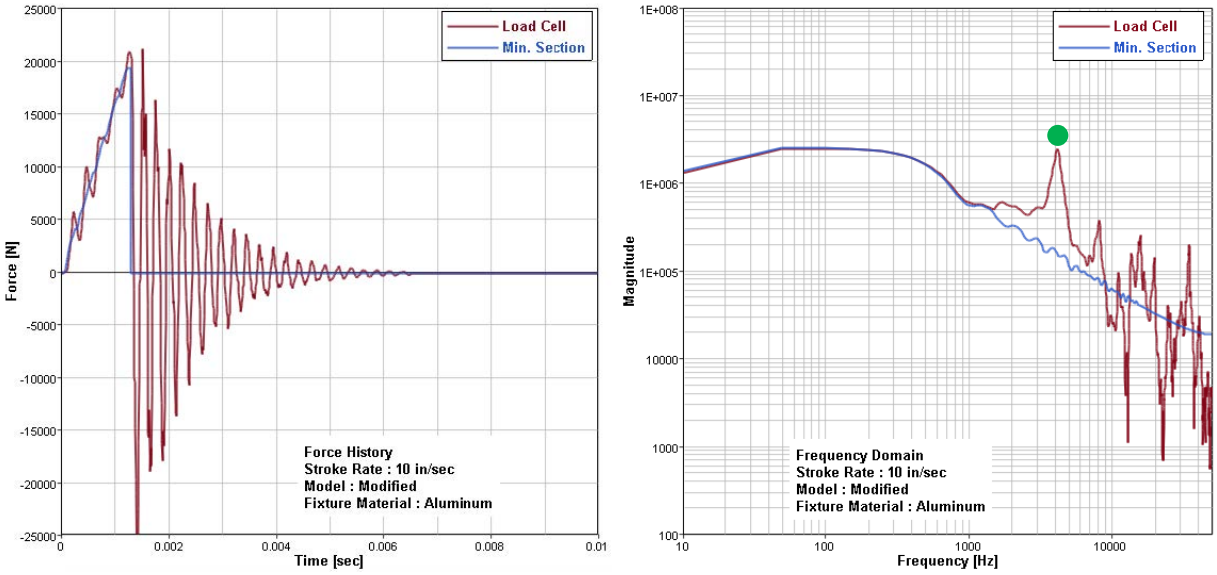

Figure 46. Time and frequency domain results comparison for modified model with aluminum fixtures at stroke rate 10 in/sec

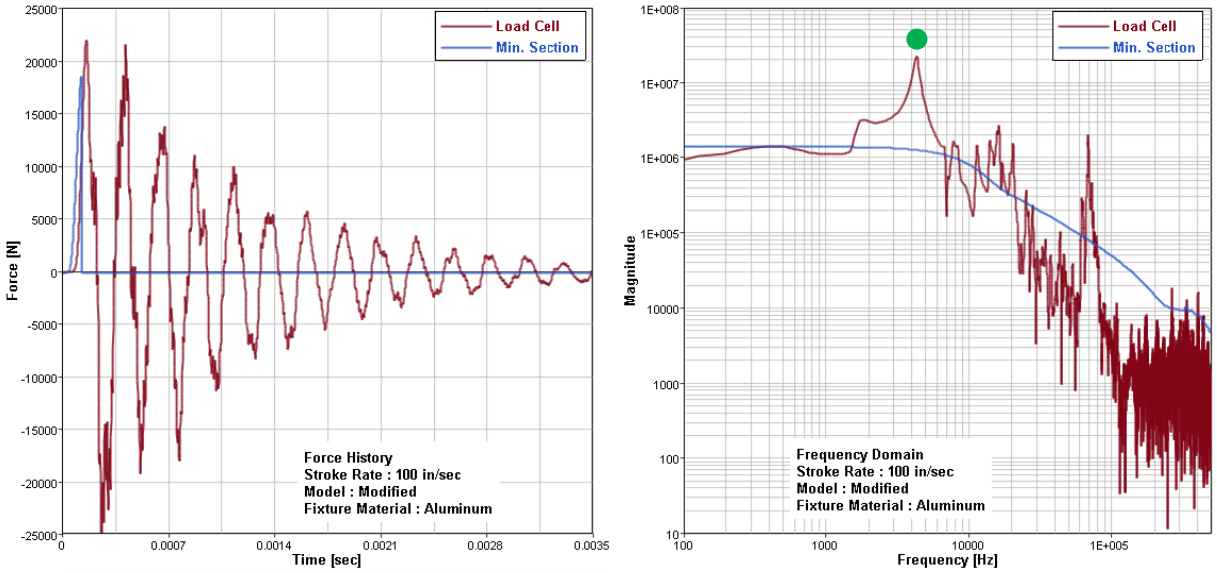

Figure 47. Time and frequency domain results comparison for modified model with aluminum fixtures at stroke rate 100 in/sec

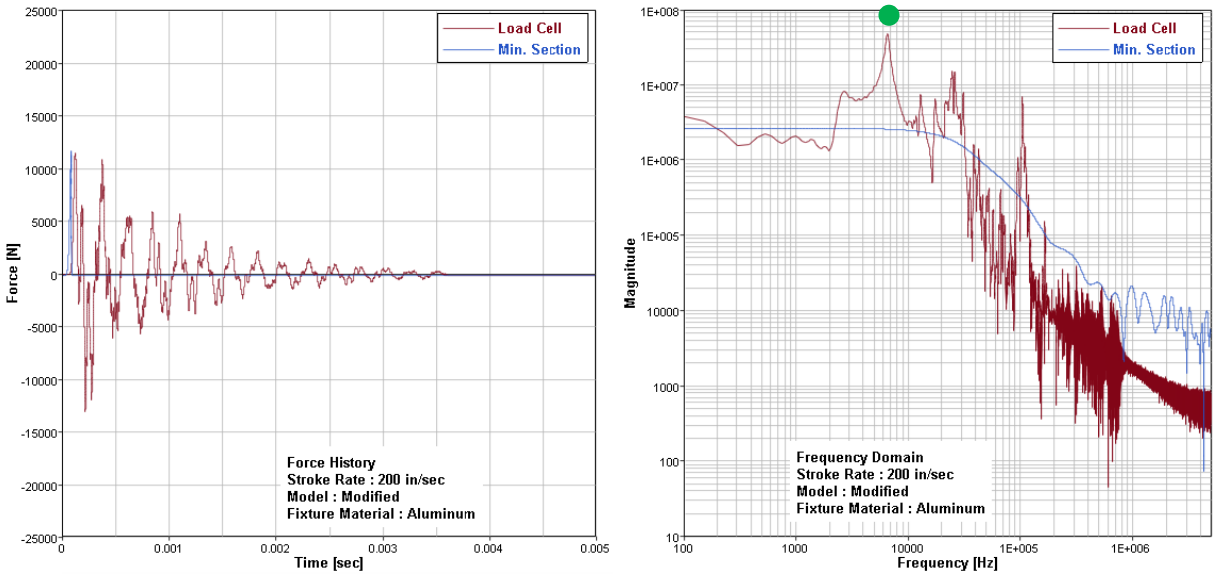

Figure 48. Time and frequency domain results comparison for modified model with aluminum fixtures at stroke rate 200 in/sec

Upon analyzing the data, the first frequency with peak amplification observed at all stroke rates for both standard and the modified models, represented by a green dot in every plot, are recognized in Table 7.

TABLE 7

FREQUENCY AT FIRST PEAK AMPLIFICATION

	FREQUENCY (Hz)			
STROKE RATE (in/sec)	STANDARD MODEL (Steel Fixtures)	MODIFIED MODEL (Steel Fixtures)	STANDARD MODEL (Aluminum Fixtures)	MODIFIED MODEL (Aluminum Fixtures)
1	3539.86	4565.20	3304.54	4192.33
10	3515.45	4589.61	3304.54	4143.01
100	3218.54	4123.48	3400.75	4322.45
200	2781.47	3619.73	5206.11	6584.19

An increment of 1 kHz was observed from the standard assembly to the modified assembly, which are presented through transmissibility plots from Figure 49 through Figure 56, for both steel and aluminum fixtures.

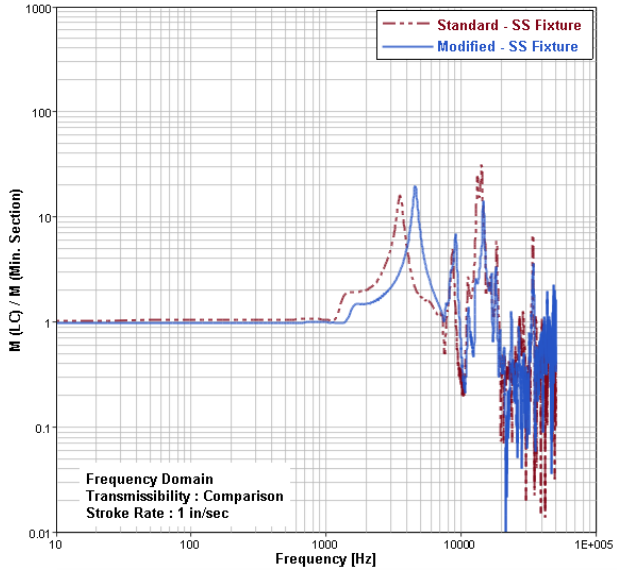

Figure 49. Transmissibility comparison of standard and modified assemblies with steel fixtures at stroke rate 1 in/sec

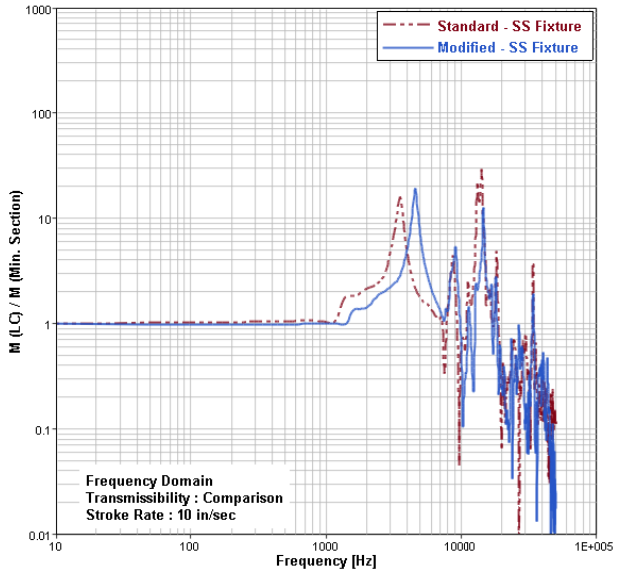

Figure 50. Transmissibility comparison of standard and modified assemblies with steel fixtures at stroke rate 10 in/sec

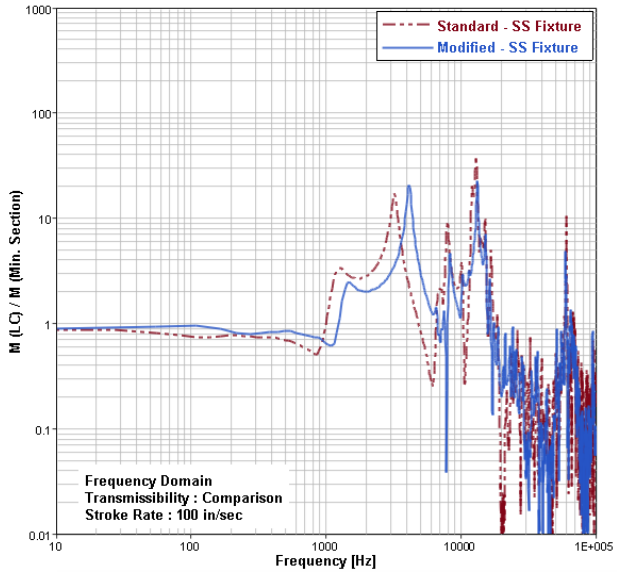

Figure 51. Transmissibility comparison of standard and modified assemblies with steel fixtures at stroke rate 100 in/sec

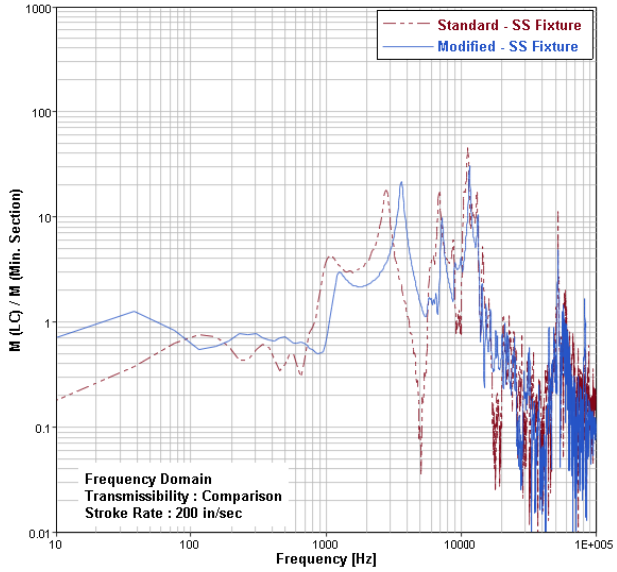

Figure 52. Transmissibility comparison of standard and modified assemblies with steel fixtures at stroke rate 200 in/sec

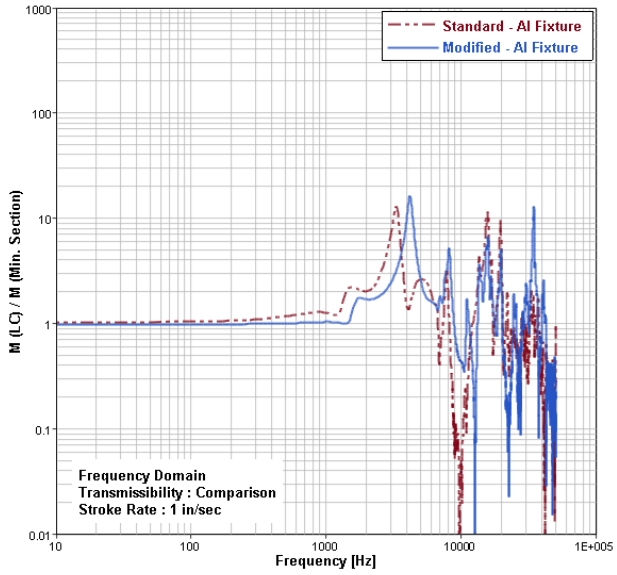

Figure 53. Transmissibility comparison of standard and modified assemblies with aluminum fixtures at stroke rate 1 in/sec

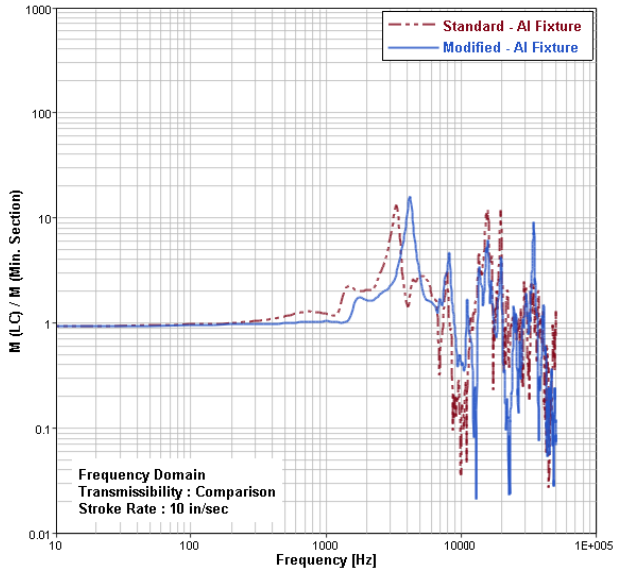

Figure 54. Transmissibility comparison of standard and modified assemblies with aluminum fixtures at stroke rate 10 in/sec

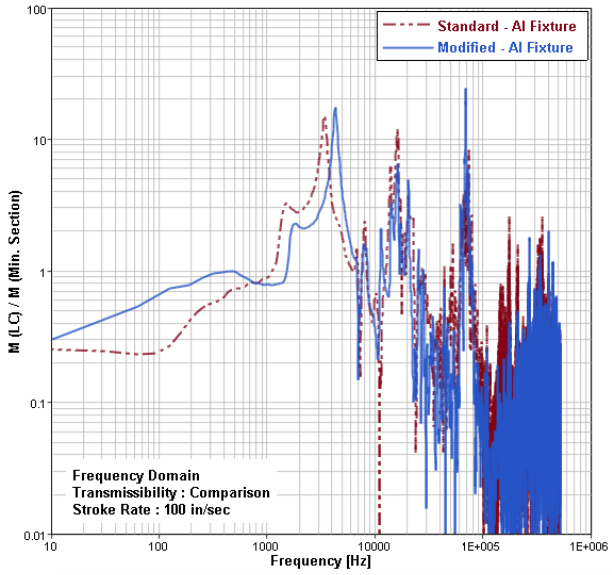

Figure 55. Transmissibility comparison of standard and modified assemblies with aluminum fixtures at stroke rate 100 in/sec

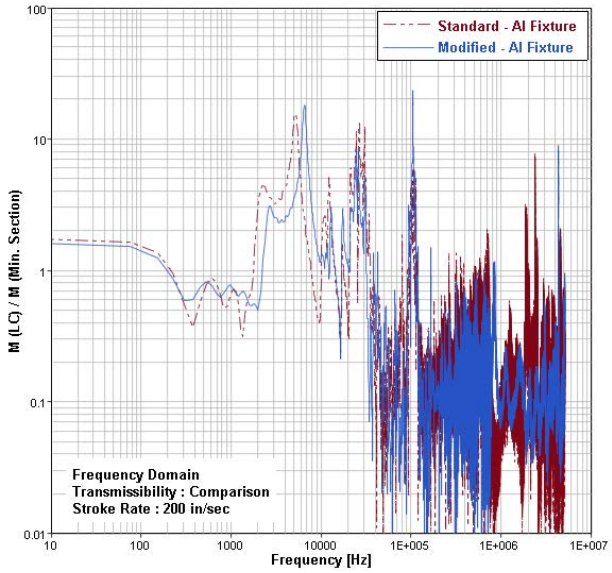

Figure 56. Transmissibility comparison of standard and modified assemblies with aluminum fixtures at stroke rate 200 in/sec

It can be observed that the initial phase differences are higher for the assembly with aluminum fixtures compared to that of steel fixtures, which increased as the displacement rate increased. The results with modified fixtures show a significant increment in the first band width.

Various other trials made in an effort to have much higher increment in the band width are presented later in this section. Therefore the initial modification to the fixture half, which increased its stiffness by 67% due to the added webbings, has increased the first band width while increasing the initial peak frequency by 1 kHz.

Shear stress versus shear stain results from an element in the minimum section of the specimen are extracted and presented below. The curve representing this data is named as 'Min. Section'. Experimentally, the load cell does not record strain data but measures the force seen by the specimen; therefore force from the load cell was divided with the minimum section cross-section area and plotted against the shear strain results mentioned above i.e. from the specimen minimum section element. The curve representing this data is named as 'Load Cell – Force'. These results are plotted at all stroke rates for standard and modified assemblies with steel and aluminum fixtures.

Figure 57 through Figure 64 presents shear stress versus shear strain results for the modified and the standard assemblies at all displacement rates ranging from 1 in/sec to 200 in/sec. It can be observed that as the rate increased, huge variation has been encountered in the comparison of the load cell and the specimen results. This variation was observed to be consistent with both standard and the modified assemblies though increasing the stability or decreasing the mass of the fixtures did not affect the variation observed in the results as the stroke rate increased.

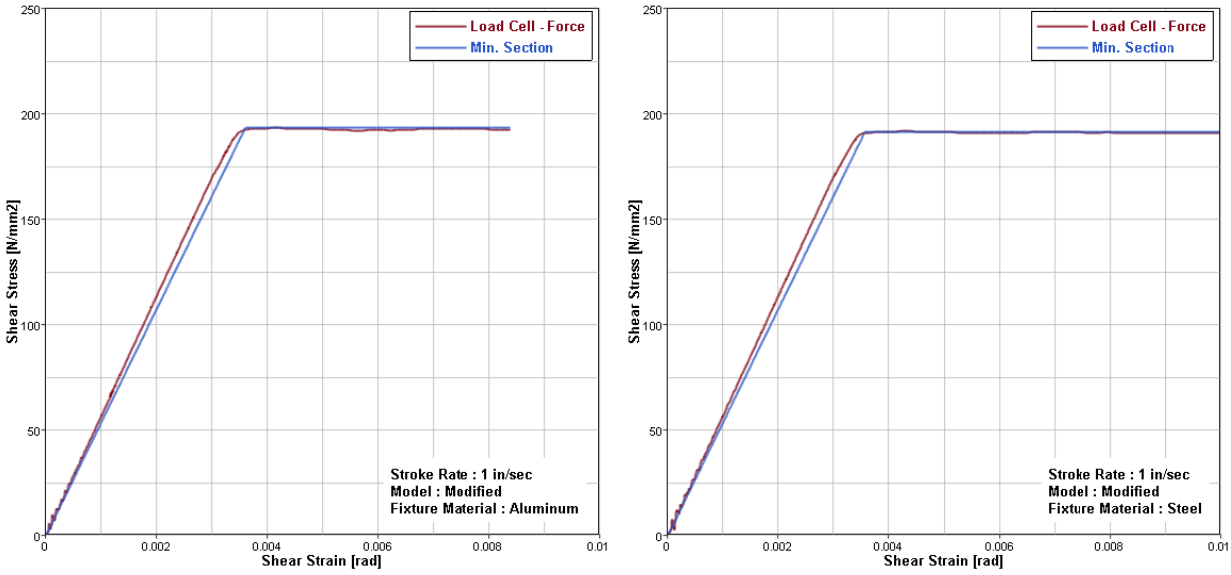

Figure 57. Shear stress vs. shear strain results for modified assembly with aluminum and steel fixtures at 1 in/sec

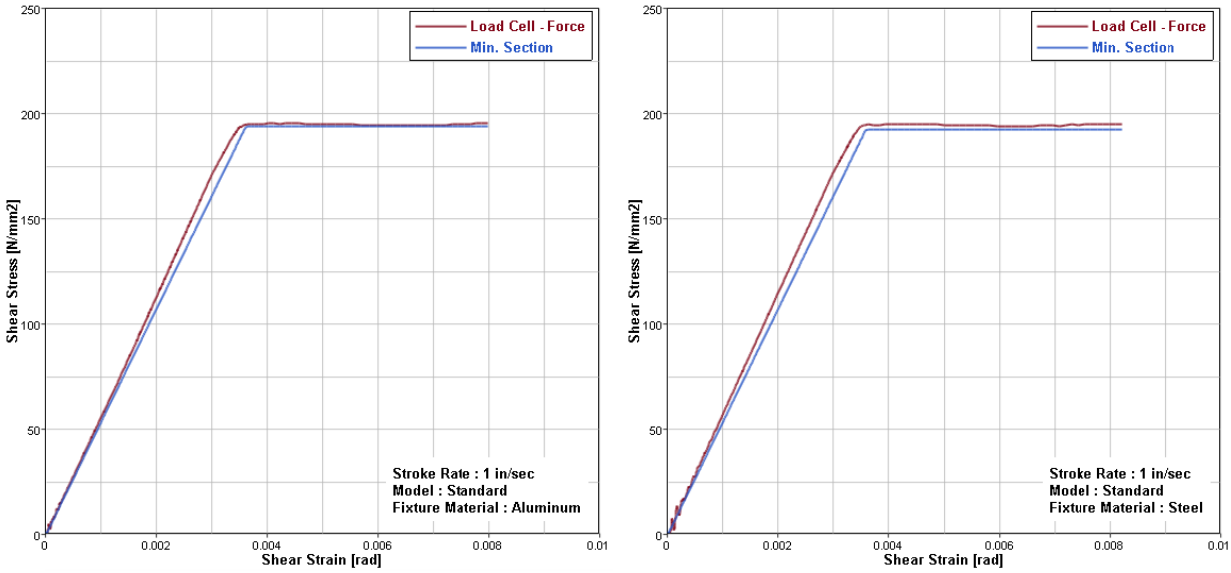

Figure 58. Shear stress vs. shear strain results for standard assembly with aluminum and steel fixtures at 1 in/sec

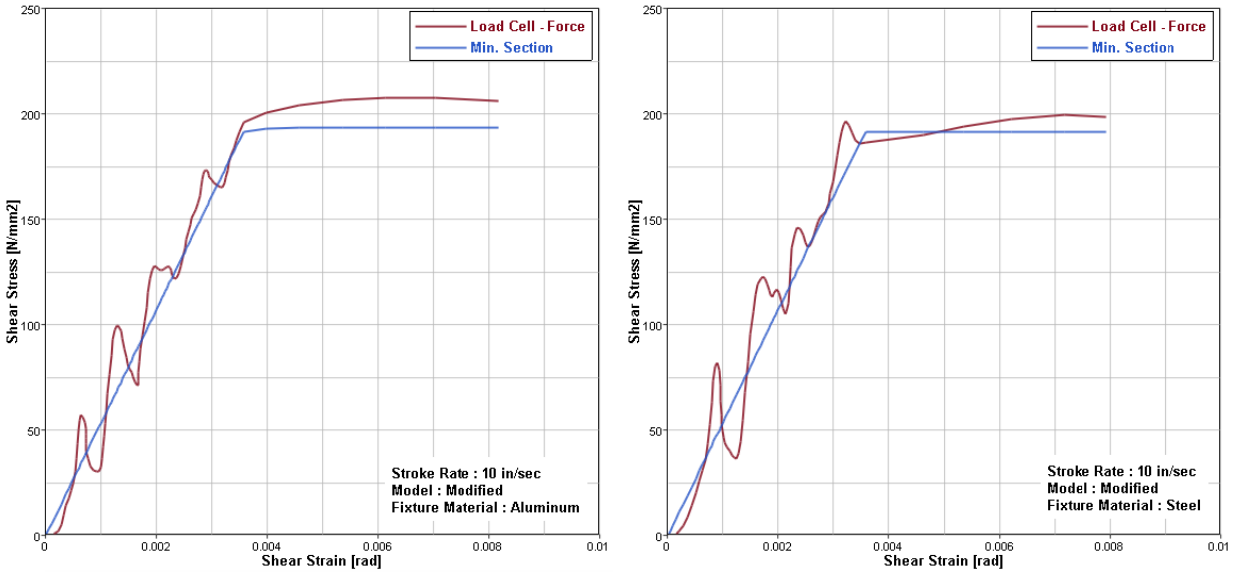

Figure 59. Shear stress vs. shear strain results for modified assembly with aluminum and steel fixtures at 10 in/sec

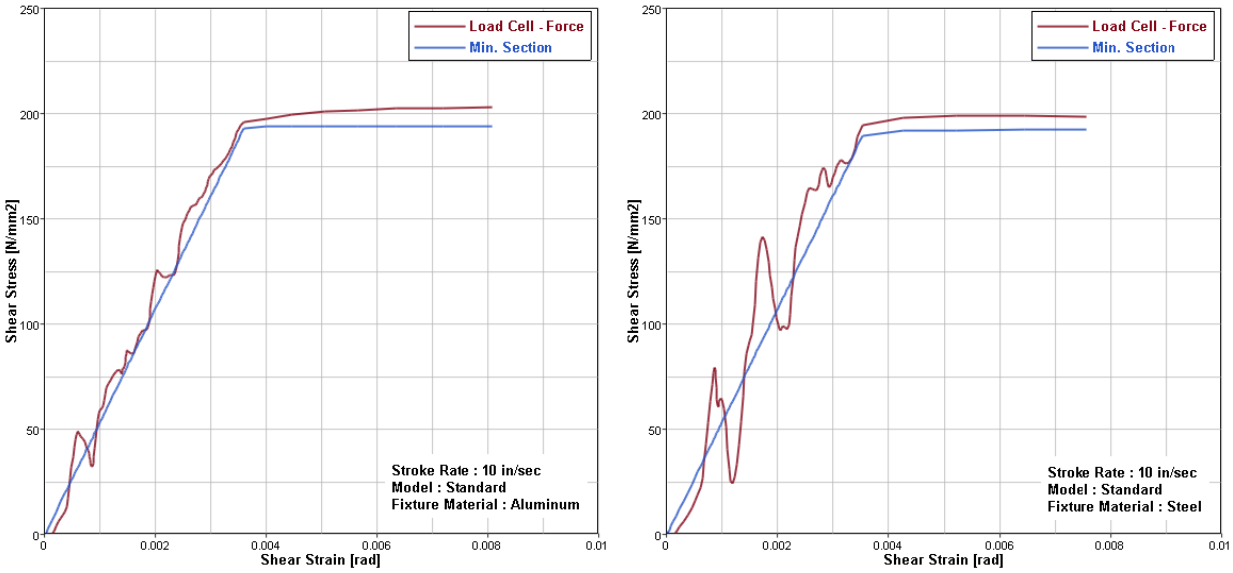

Figure 60. Shear stress vs. shear strain results for standard assembly with aluminum and steel fixtures at 10 in/sec

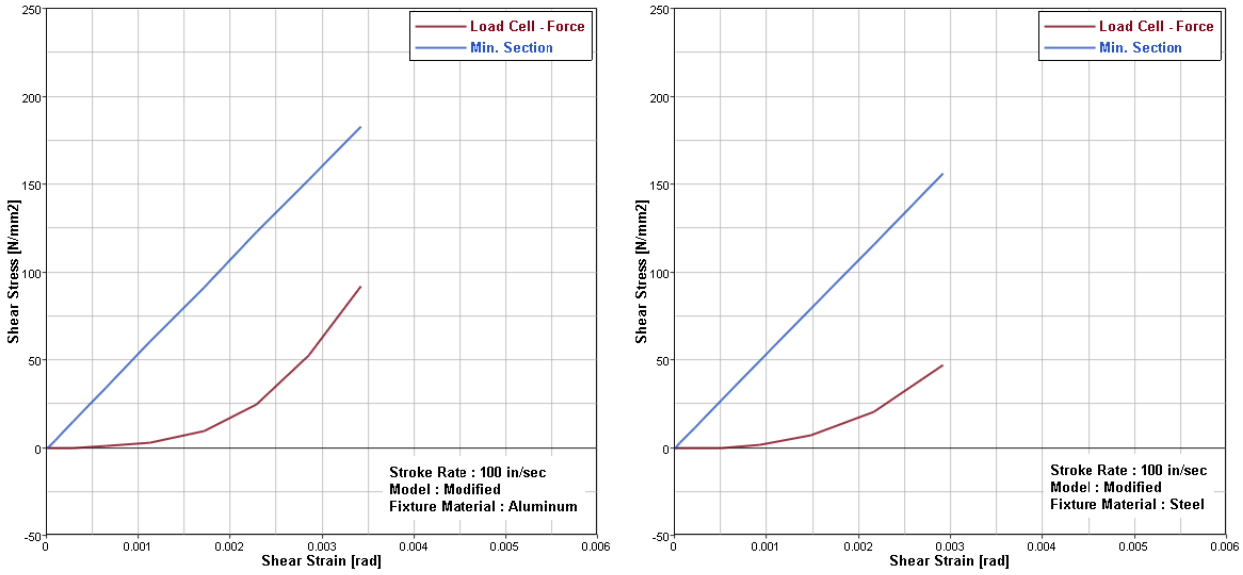

Figure 61. Shear stress vs. shear strain results for modified assembly with aluminum and steel fixtures at 100 in/sec

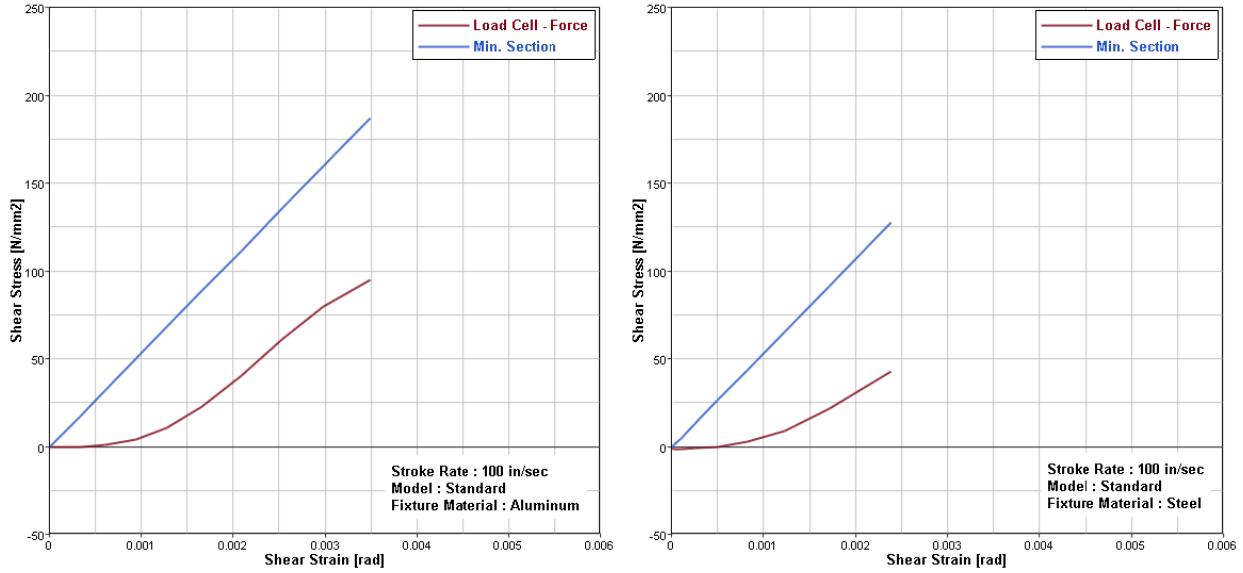

Figure 62. Shear stress vs. shear strain results for standard assembly with aluminum and steel fixtures at 100 in/sec

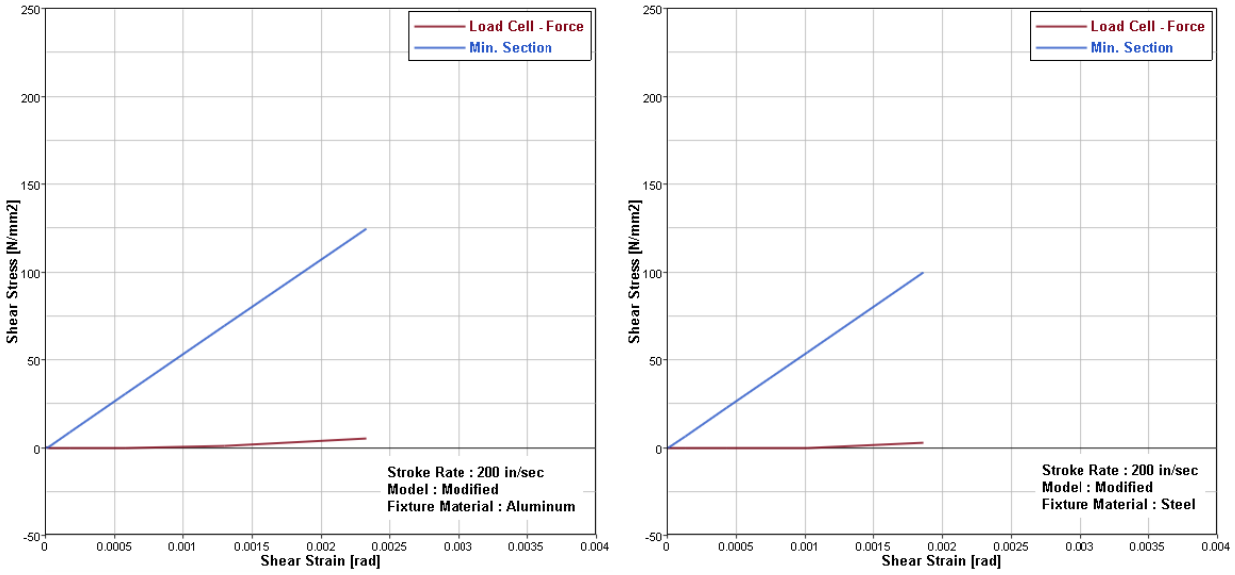

Figure 63. Shear stress vs. shear strain results for modified assembly with aluminum and steel fixtures at 200 in/sec

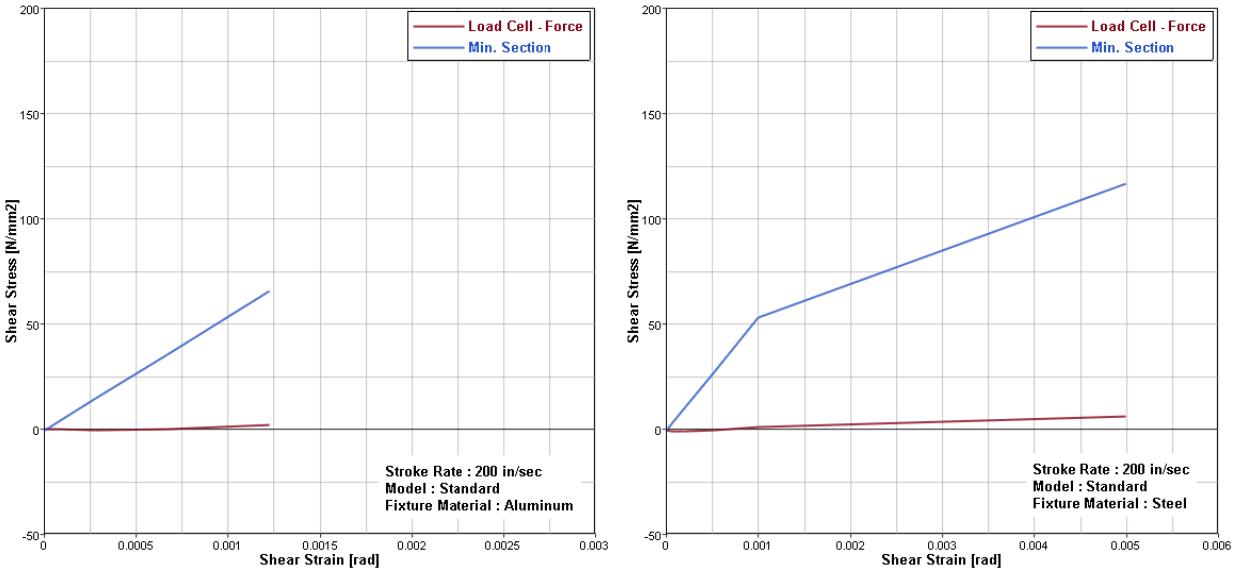

Figure 64. Shear stress vs. shear strain results for standard assembly with aluminum and steel fixtures at 200 in/sec

Since the primary focus of the present work is to increase the first band width so that the measured data is the data between the lowest frequency and the first high frequency, three other cases of modifications are presented below. Also, two more cases showing the analyses for

bending and plastic failure are presented. Case 1 to Case 3 presents various scenarios where the fixtures were modeled to have high stiffness but lower mass. Table 8 quantifies mass of the fixtures used in standard assembly, modified assembly and in the assemblies from cases 1 to 3. Cases presented from here on utilize modified fixtures for the analyses.

TABLE 8

MATERIAL OF THE FIXTURES & ESTIMATION OF MASS

FIXTURE	MATERIAL	VOLUME (mm^3)	DENSITY (tonne/mm^3)	MASS	
				(tonne)	(lb)
Standard	Steel	291719	7.860E-09	2.29E-03	5
Modified		285479		2.24E-03	4.93
Case 1	Steel (With Al Density)	285479	2.796E-09	7.98E-04	1.76
Case 2	Steel (With 10 Times Lower Steel Density)		7.860E-10	2.24E-04	0.493
Case 3	Steel	142740	7.860E-09	1.12E-03	2.46

- *Case 1: Modified assembly - stainless steel fixtures with the density of aluminum*

The assembly with the modified stainless steel fixtures was loaded at 10 in/sec. Here the density of steel fixture halves is replaced with the density of aluminum, keeping the stiffness unchanged which makes the fixtures to have reduced mass and increased stiffness. The results are analyzed in a similar way as before and compared. Figure 65 shows a comparison of the results in time and frequency domain. The results from this case are compared to the standard and modified models with steel fixtures at 10 in/sec and presented in Figure 66. A significant increment in the band width was observed indicating the influence of having reduced mass. This case is discussed to show that decreasing the mass has indeed increased the band width as well

the frequency at which the first maximum amplification was occurring. An observation with a further decrease in the mass has been discussed in the following case.

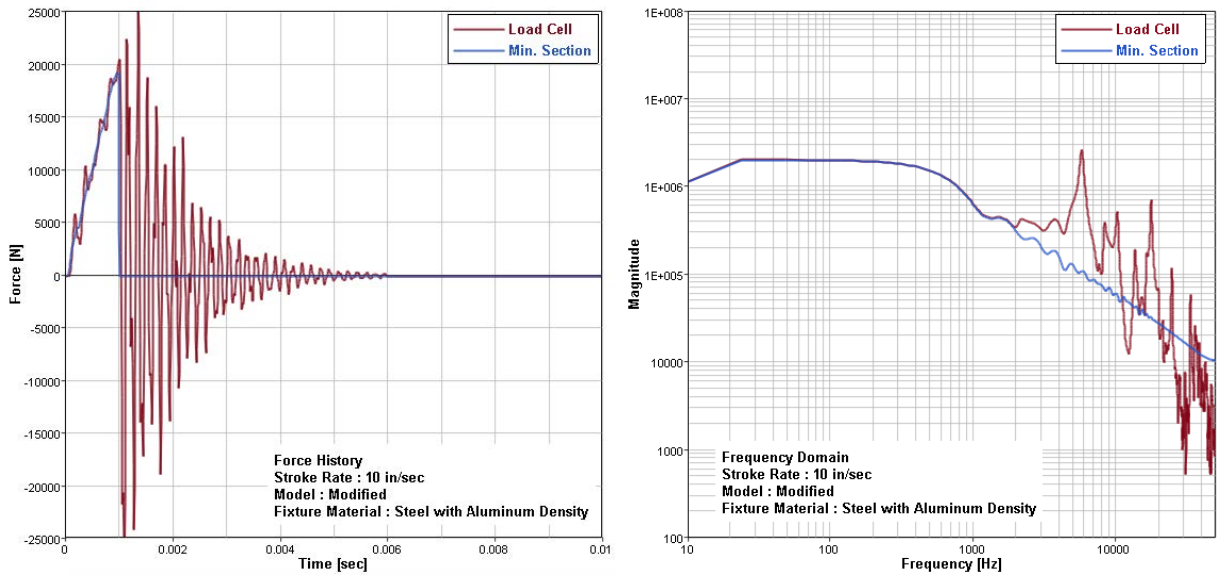

Figure 65. Modified model - Stainless steel fixtures with the density of aluminum

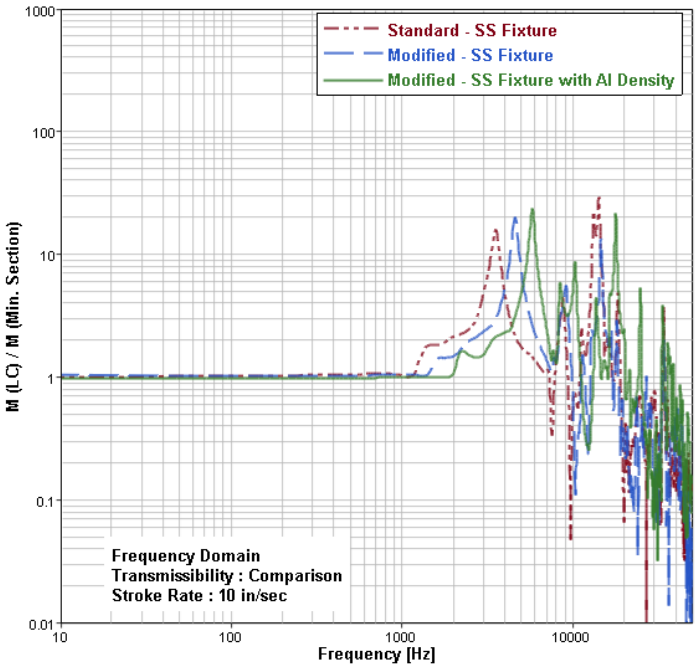

Figure 66. Case 1 – Transmissibility comparison showing an increment in the band width of the system at stroke rate 10 in/sec

- *Case 2: Modified assembly - stainless steel fixtures with ten times lower density*

In this case the mass of the fixtures are reduced further compared to Case 1. Here the density of the fixtures is reduced such that it is ten times lower than the density of steel. The assembly with theses fixtures is analyzed at 10 in/sec. Time domain and frequency domain results are compared and shown in Figure 67. Figure 68 presents the transmissibility comparison.

This simulation shows another 1 kHz increment in the frequency of peak amplification as compared to the previous case. As explained earlier, a fixture such as the one in this case is realistically difficult to manufacture with the materials available currently in the market, which has the stiffness of steel while having the density ten times lower. This case is another trial to observe the effect of mass on the band width.

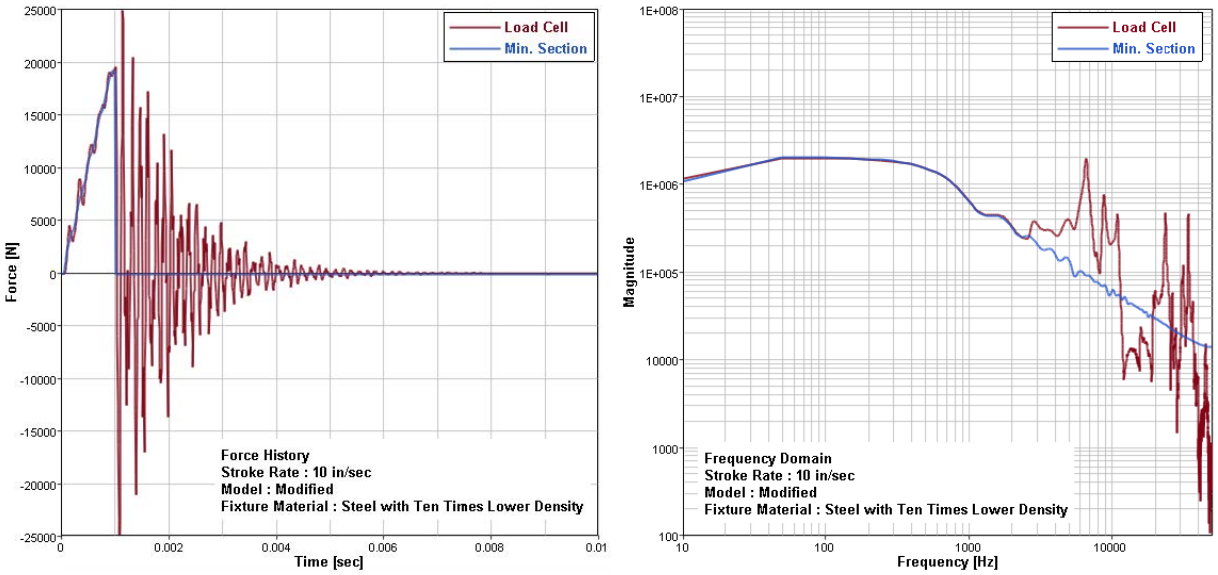

Figure 67. Modified model - Stainless steel fixtures with ten times lower density

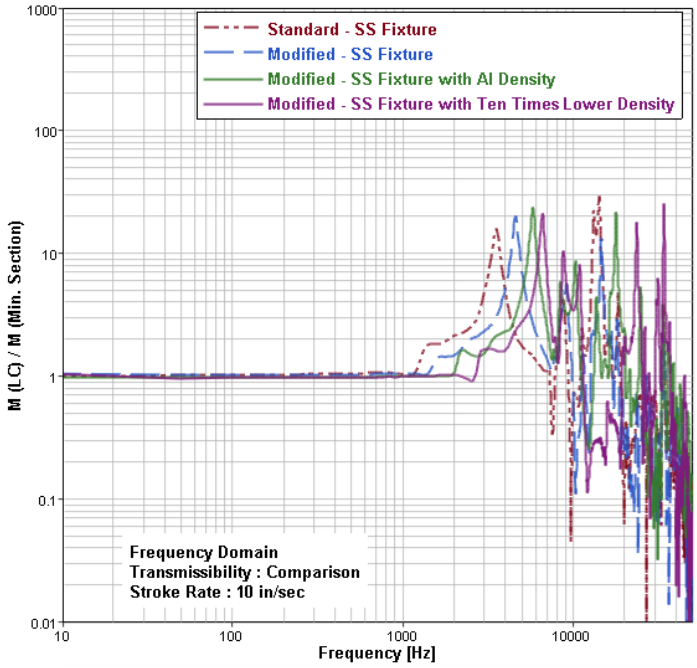

Figure 68. Case 2 – Transmissibility comparison showing an increment in the band width of the system at stroke rate 10 in/sec

- *Case 3: Modified assembly with stainless steel fixture halves – scaled down to 50%*

In this case the modified assembly with stainless steel fixtures has been scaled down to half of its size. This helps in reducing the mass by 50%. Though the size of the test apparatus is reduced by half, the frequencies of the system would still be in the same range as that of the previously analyzed models in this report. The assembly is loaded at 10 in/sec as before. The results are compared and shown in Figure 69. Figure 70 shows the transmissibility comparison of all models.

Comparing to the previous case i.e. Case 2, the model in the present case has shown an increment of nearly 3 kHz in the frequency of peak amplification whereas comparing the present model to the assembly with initially modified fixtures, there is an increment of 5 kHz. This suggests that the band width could be increased to a greater extent by scaling down the test

apparatus but a major limitation of this model would be the reduced size of the test specimen, which allows a reduced gage section.

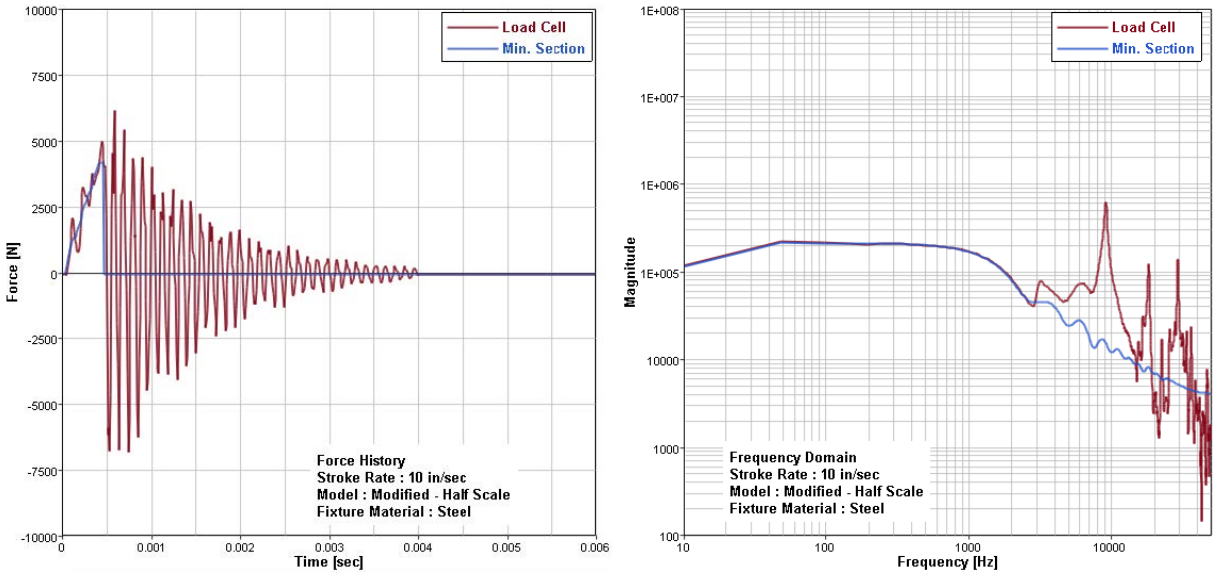

Figure 69. Modified model with stainless steel fixtures scaled down to half the size

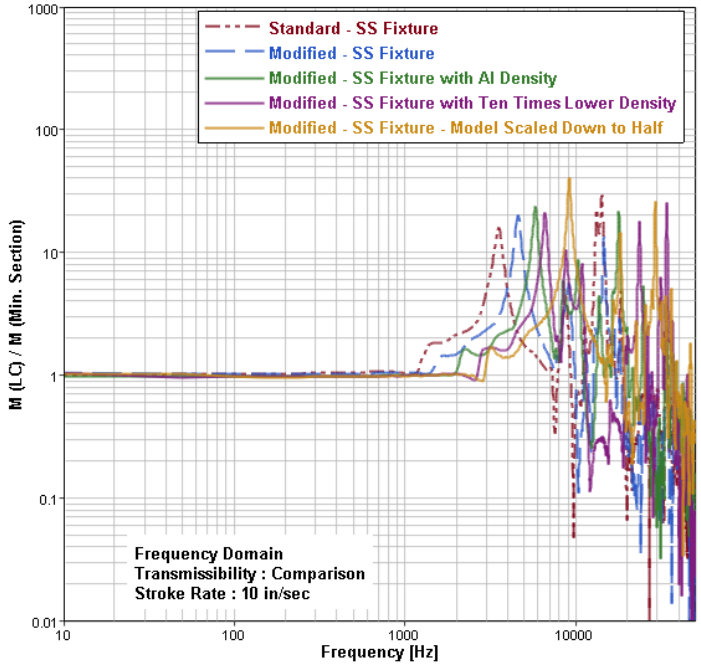

Figure 70. Case 3 – Transmissibility comparison showing an increment in the band width of the system at stroke rate 10 in/sec

- *Case 4: Bending analysis of the fixtures*

Bending at every stroke rate has been evaluated for the standard and modified test assemblies, using the results from the gage section of the specimen. Table 9 presents the ratio of normal force to the shear force extracted from the specimen. This comparison was made for both, standard and the modified assemblies with steel and aluminum fixtures. It was observed that bending increased as the rate increased, indicating a combined loading effect at higher rates. Figure 71 presents the direction of the lateral and the shear load in the minimum section of the specimen.

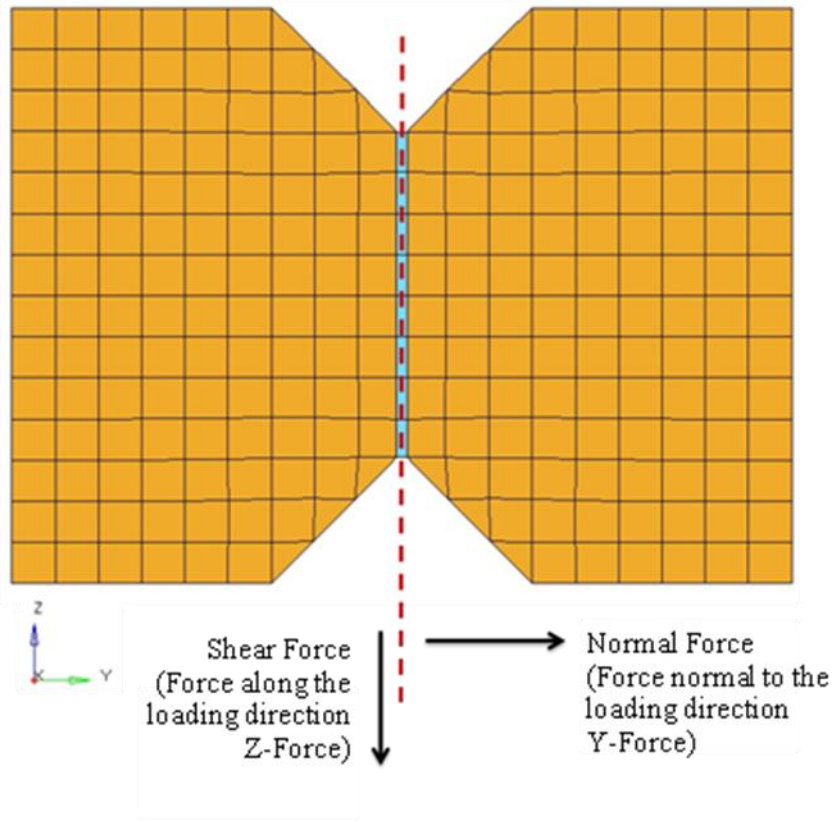

Figure 71. Direction of force results extracted from the minimum section

TABLE 9

BENDING OF THE FIXTURES

STROKE RATE (in/sec)	RATIO OF NORMAL FORCE TO SHEAR FORCE			
	STANDARD MODEL (Steel Fixtures)	MODIFIED MODEL (Steel Fixtures)	STANDARD MODEL (Aluminum Fixtures)	MODIFIED MODEL (Aluminum Fixtures)
1	0.013	0.0108	0.051	0.0105
10	0.122	0.106	0.084	0.097
100	1.096	0.793	0.582	0.608

From Table 9 it was observed that, with an increase in the stroke rate, bending of the fixtures increased drastically signifying combined loading effect at higher rates. Bending with the modified fixtures was observed to be lower compared to the standard fixtures; however a slight variation was observed among the aluminum fixtures at higher rates. A significant reduction in bending was seen with the modified steel fixtures compared to the standard steel fixtures though the overall bending increased as the stroke rate increased. However, due to the physical limitation of the assembly, bending could not be avoided considerably at higher rates.

The above analysis was followed by a case where the modified fixtures were constrained along the edges to avoid bending. The nodes shown in Figure 72 were constrained in all degrees of freedom except the z-translational so that the fixtures are free to move in the loading direction. The assembly was loaded at 10 in/sec and at 100 in/sec. Figure 73 and Figure 74 show a comparison of the results in time domain and frequency domain for 10 and 100 in/sec respectively. The transmissibility comparison for 10 in/sec is presented in Figure 75 while for 100 in/sec in Figure 76.

This analysis suggests that bending is indeed influencing the frequency content of the system, as highlighted in the transmissibility plots. The combined loading effect due to the bending of the fixtures has reduced considerably, as presented in Table 10.

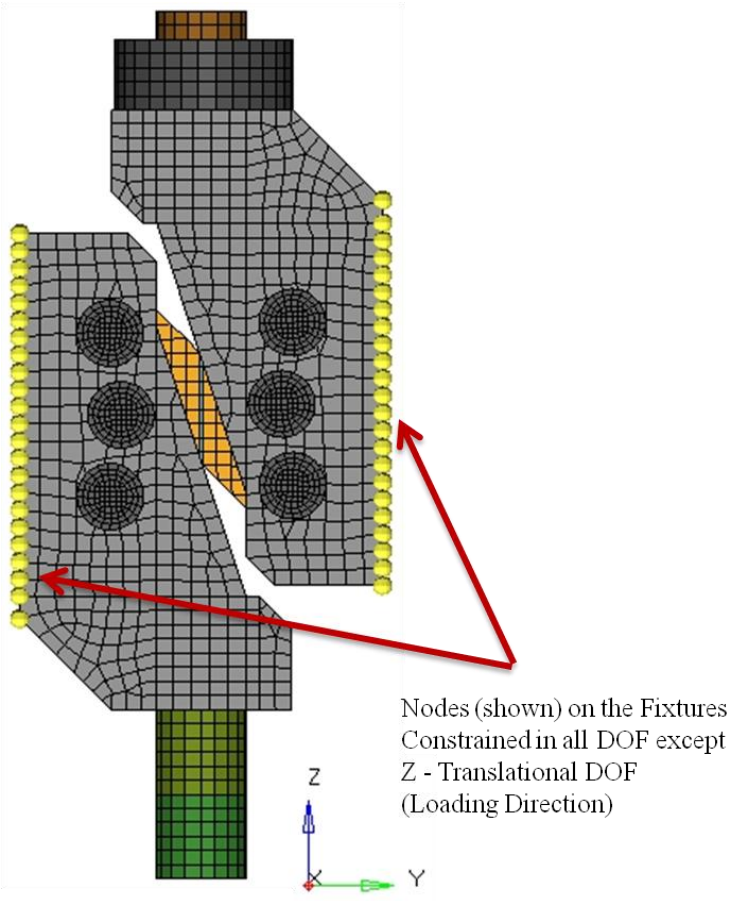

Figure 72. Nodes constrained on the assembly for bending analysis

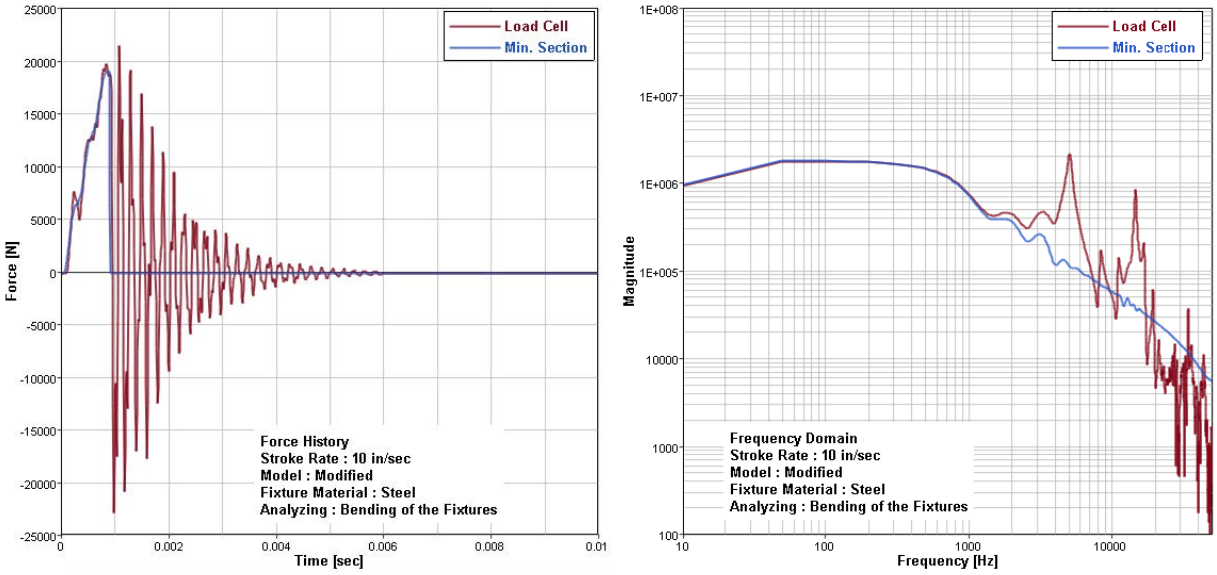

Figure 73. Bending analysis of the modified model with stainless steel fixtures at stroke rate 10 in/sec

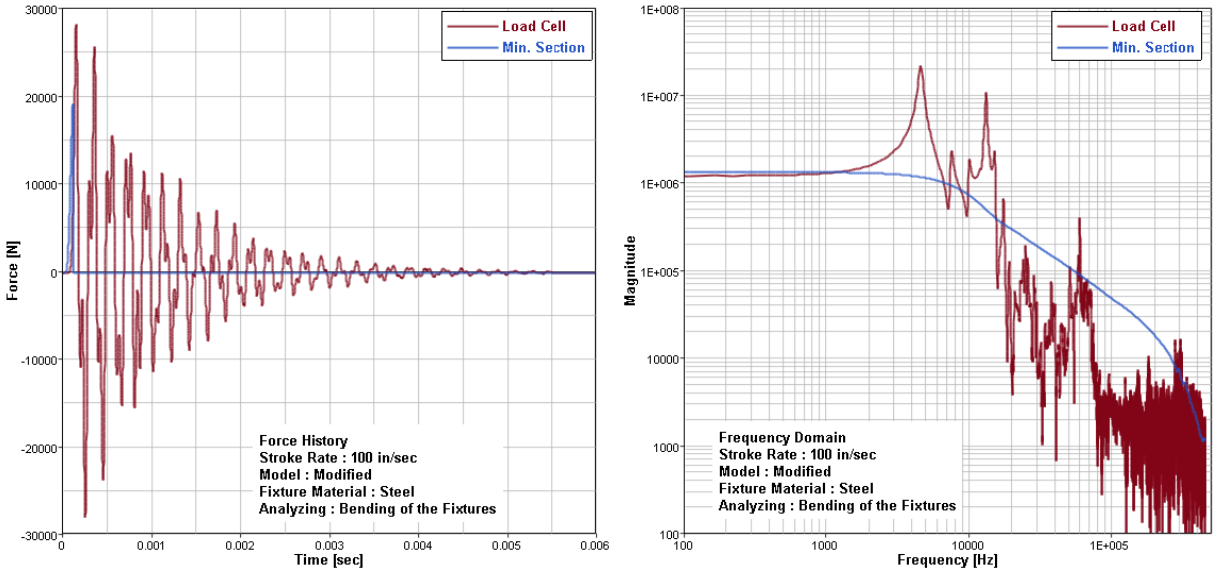

Figure 74. Bending analysis of the modified model with stainless steel fixtures stroke rate 100 in/sec

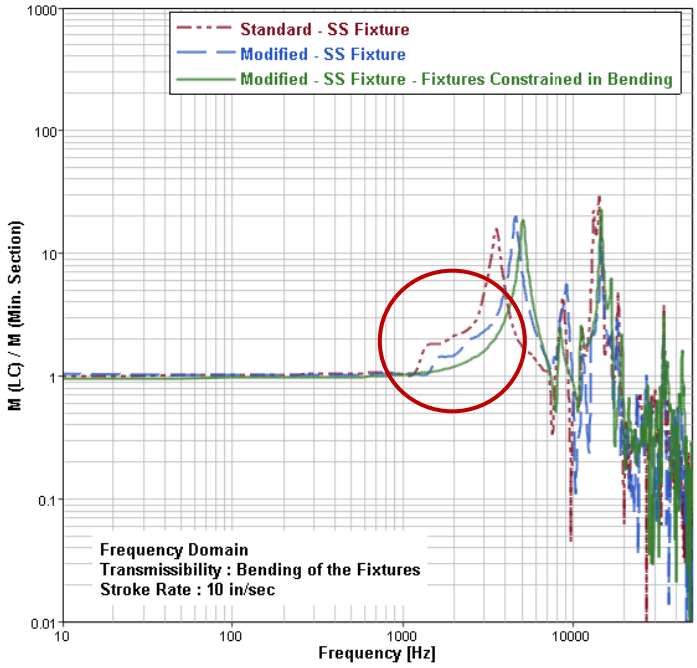

Figure 75. Transmissibility for bending analysis – Stroke rate 10 in/sec

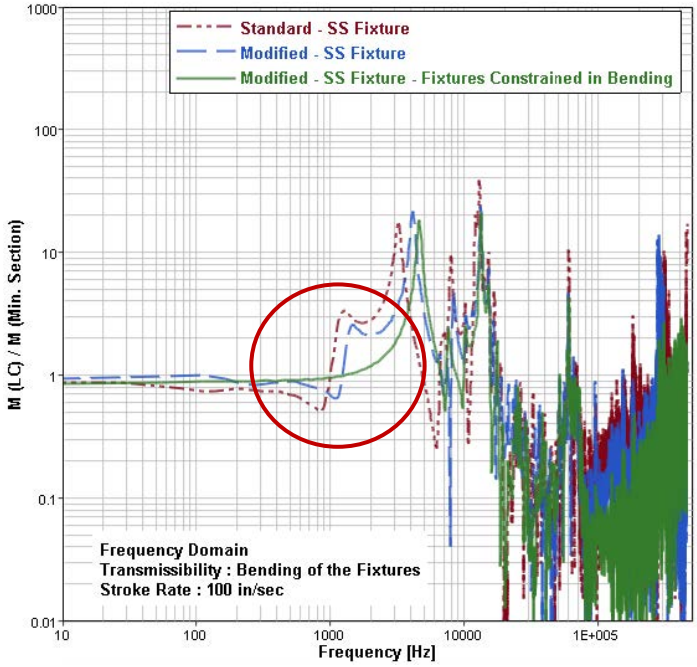

Figure 76. Transmissibility for bending analysis – Stroke rate 100 in/sec

TABLE 10

ANALYSIS OF THE FIXTURES WITH BENDING CONSTRAINT

STROKE RATE (in/sec)	RATIO OF NORMAL FORCE TO SHEAR FORCE		
	STANDARD MODEL (Steel Fixtures)	MODIFIED MODEL (Steel Fixtures)	MODIFIED MODEL (Steel Fixtures) (Bending Constraint)
10	0.122	0.106	0.021
100	1.096	0.793	0.033

- *Case 5: Other observations with the analyses of the numerical models*

In order to observe plastic failure in the gage section of the test coupon, a particular behavior encountered experimentally while testing reinforced composite materials [5], the modified assembly with steel fixtures was loaded at 10 in/sec with a higher failure strain defined for the minimum section elements. In this case the minimum section elements were modeled to fail at 15% strain. This analysis could be considered as a verification of the model compared to experimental. No possible change in the frequencies of the system was observed compared to earlier analyses. Figure 77 displays the load cell and the minimum section results in time and frequency domain with 15 % failure strain at 10 in/sec. Figure 78 show the shear stress versus shear strain results at 10 in/sec. Here the shear stress and shear strain results extracted from an element in the minimum section of the specimen (curve named as ‘Min. Section) is plotted against the shear stress estimated using the load cell force and the minimum section cross-section area (curve named as ‘Load Cell’) as explained earlier in this chapter.

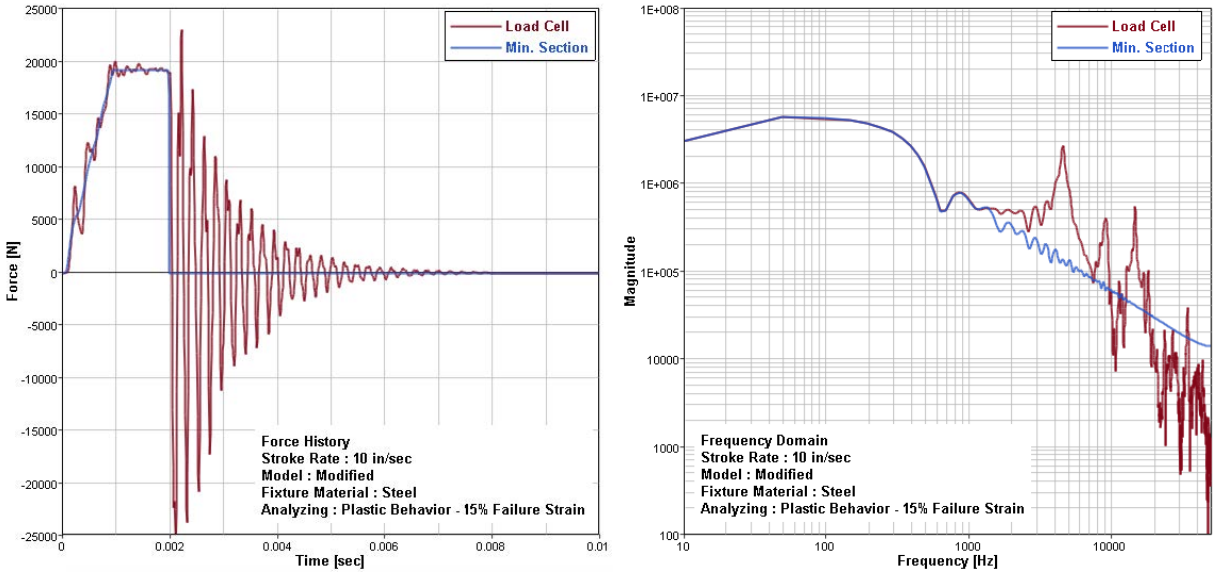

Figure 77. Specimen minimum section modeled to fail at 15% strain at 10 in/sec

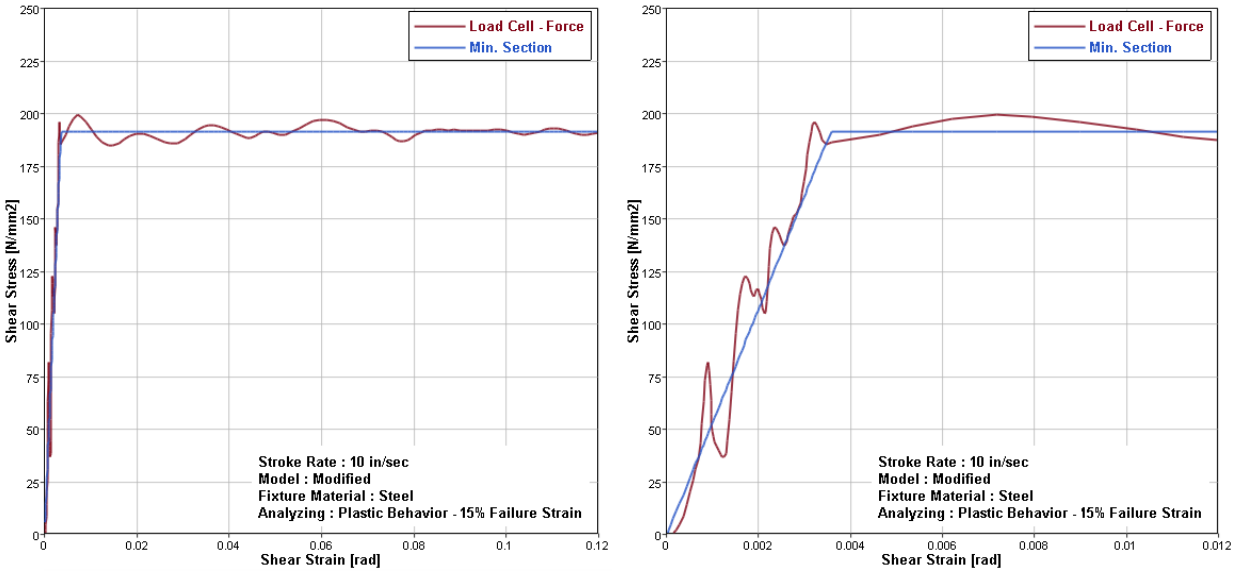

Figure 78. Shear stress vs. shear strain results at 10 in/sec with 15% failure strain

5.2 Data Filtering

A common practice of removing undesired frequency components from the data is by using filtering options available through various analytical tools. Filtering data is generally used to smooth out high frequency fluctuations or to remove periodic trends of a specific frequency. The analysis presented in this section shows that filtering eliminates useful frequencies and the

reproduced results vary compared to the original results as presented from Figure 79 through Figure 84. As shown, there is a huge difference in the force interpretation of the filtered curve compared to the actual data. Irrespective of the type of filter used or the loading rate, the re-plotted force history data implies discrepancy in understanding the material behavior when analyzing through the stress-strain plots.

In this analysis, HyperGraph was used to filter the original data. The results were compared between two types of filtering; low-pass filter and band-stop filter. Data from the standard model with steel fixtures at 1, 10 and 100 in/sec was compared, separately for two types of filters mentioned above. Since this section primarily concentrates on showing the discrepancy in the data obtained after using filtering, comparisons were only made for the assembly with standard steel fixtures. Moreover only the load cell data was filtered and compared. Therefore the filtered data shown in the following plots represents the filtered load cell data compared to the original data. Figure 79 through Figure 81 shows a comparison of curves obtained as a result of using low-pass filter with different cut-off frequencies. Each figure illustrates the complete curve as well as the initial pulse of the same curve for a more clear observation. As explained in Appendix, in low-pass filtering all frequencies above the cut-off frequencies are eliminated while only allowing the frequencies below the cut-off frequency to pass. Similarly, band-stop filter requires a range of frequencies to be defined. All frequencies within that range are eliminated while allowing the other frequencies to pass. Figure 82 through Figure 84 show a comparison of curves obtained as a result of using band-stop filter with a specified range of frequencies.

Since analytical filtering tools offer less control over the useful frequencies and the amplitudes, using an appropriate transfer function for filtering data could be a better solution. Depending on the objective, a transfer function helps in having more control over the frequencies

being eliminated. Also, it may alter both phase and amplitude of the variations in the data to obtain either a rougher or a smoother output. Detailed description or examples of a transfer function are not in the scope of this work but included in further research.

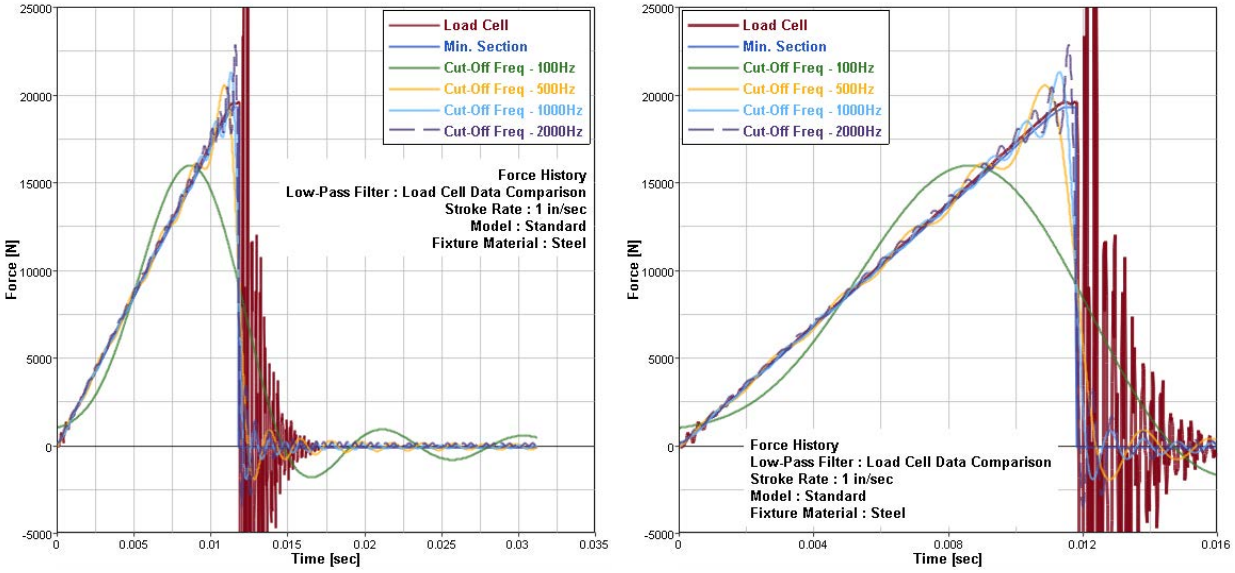

Figure 79. Standard model with steel fixtures at stroke rate 1 in/sec – Low-pass data filtering

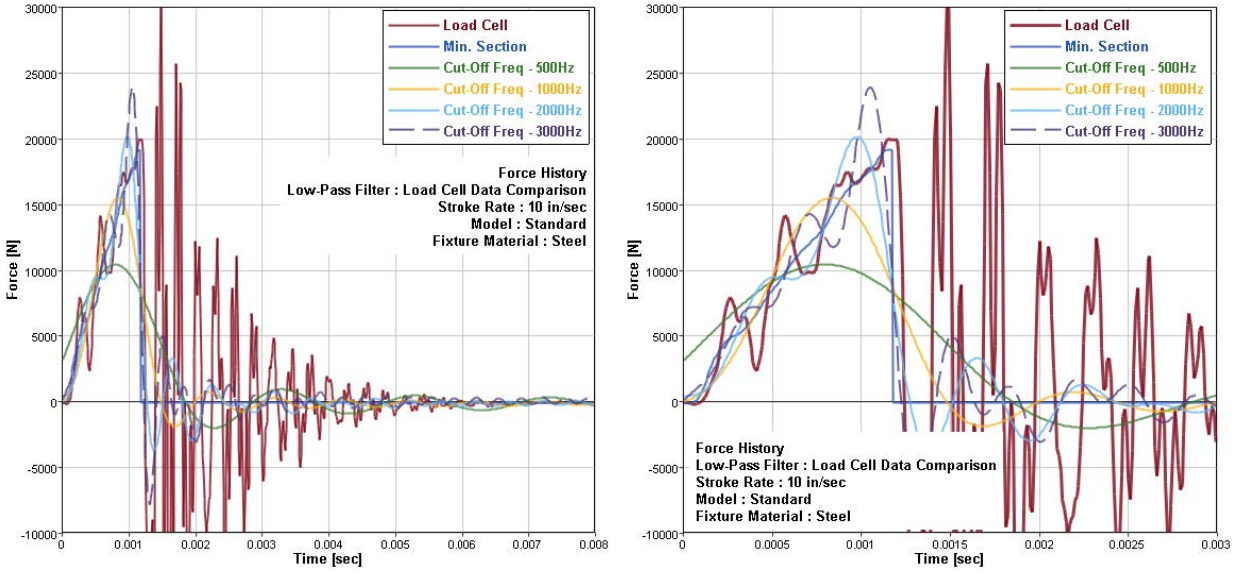

Figure 80. Standard model with steel fixtures at stroke rate 10 in/sec – Low-pass data filtering

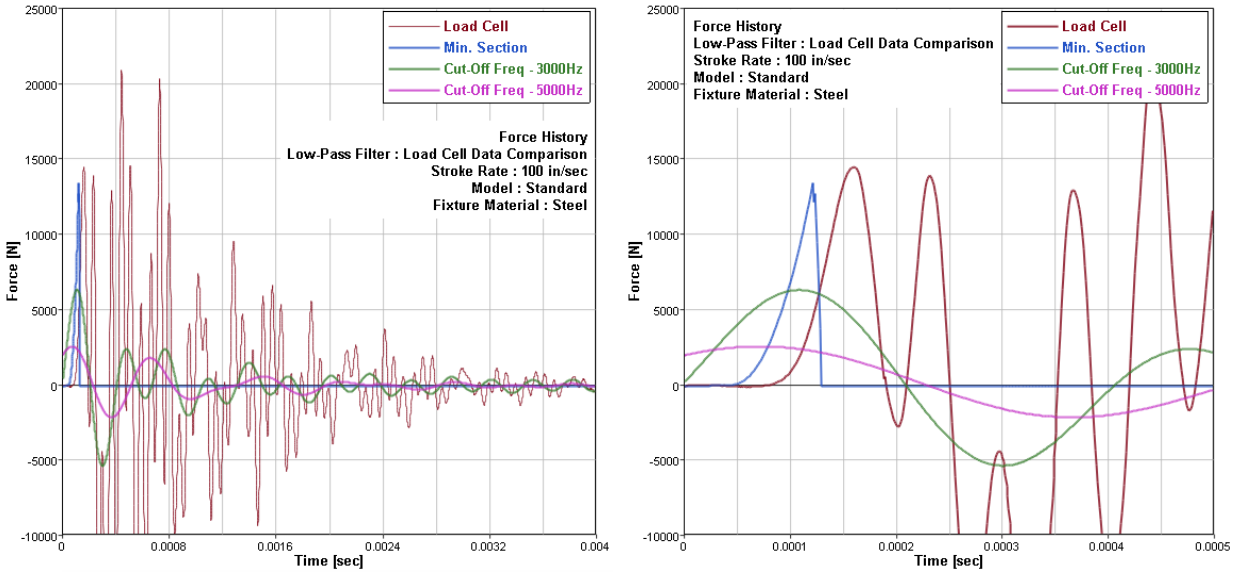

Figure 81. Standard model with steel fixtures at stroke rate 100 in/sec – Low-pass data filtering

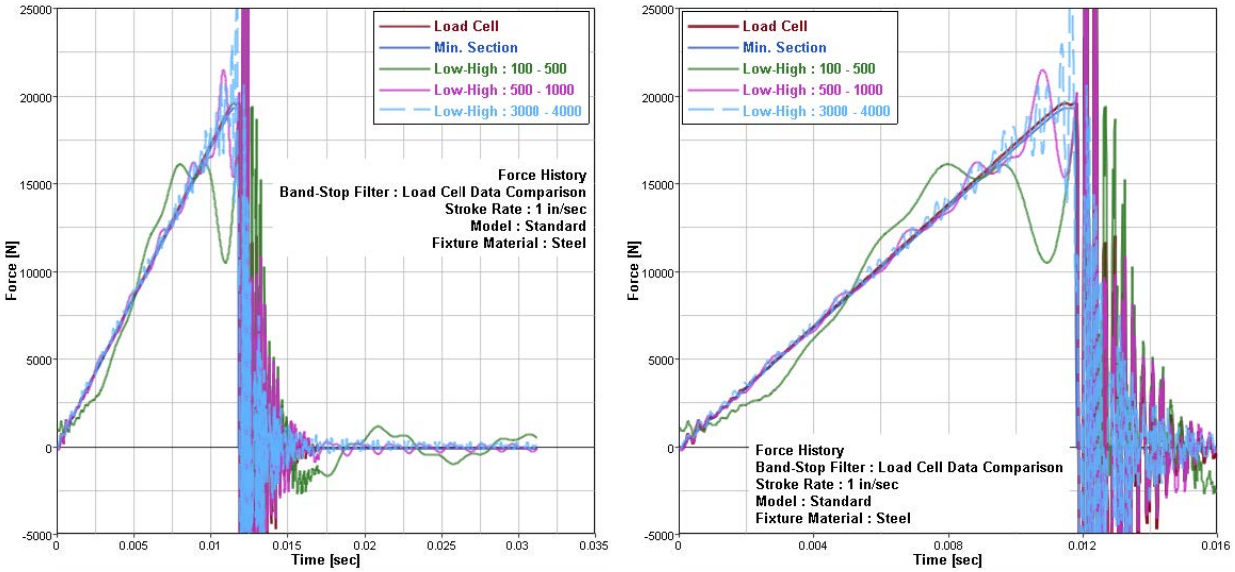

Figure 82. Standard model with steel fixtures at stroke rate 1 in/sec – Band-stop data filtering

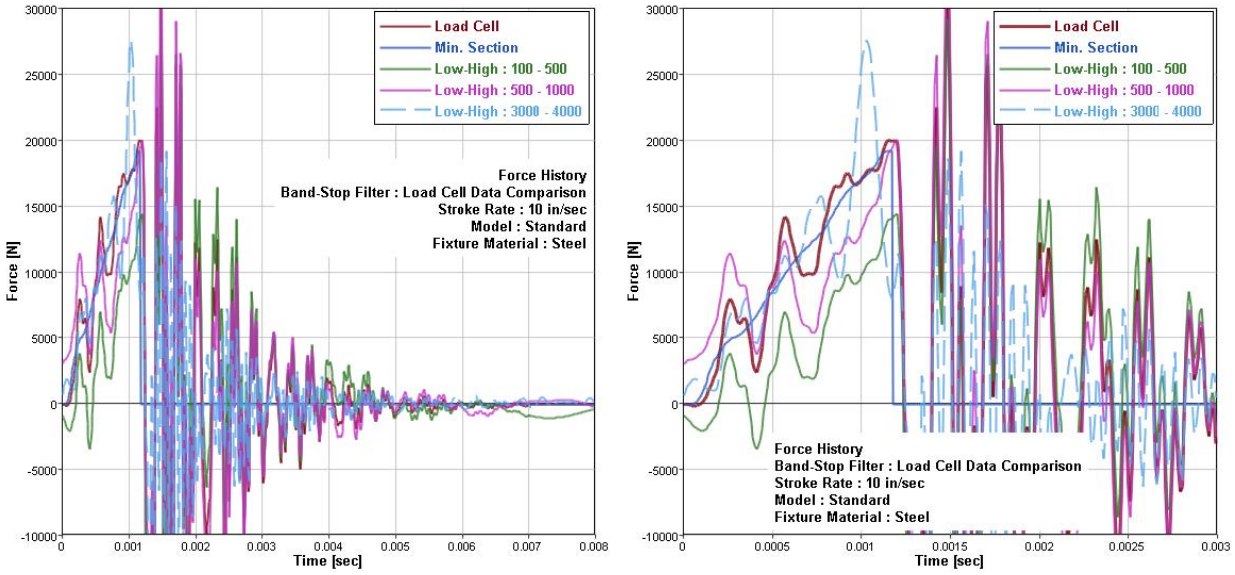

Figure 83. Standard model with steel fixtures at stroke rate 10 in/sec – Band-stop data filtering

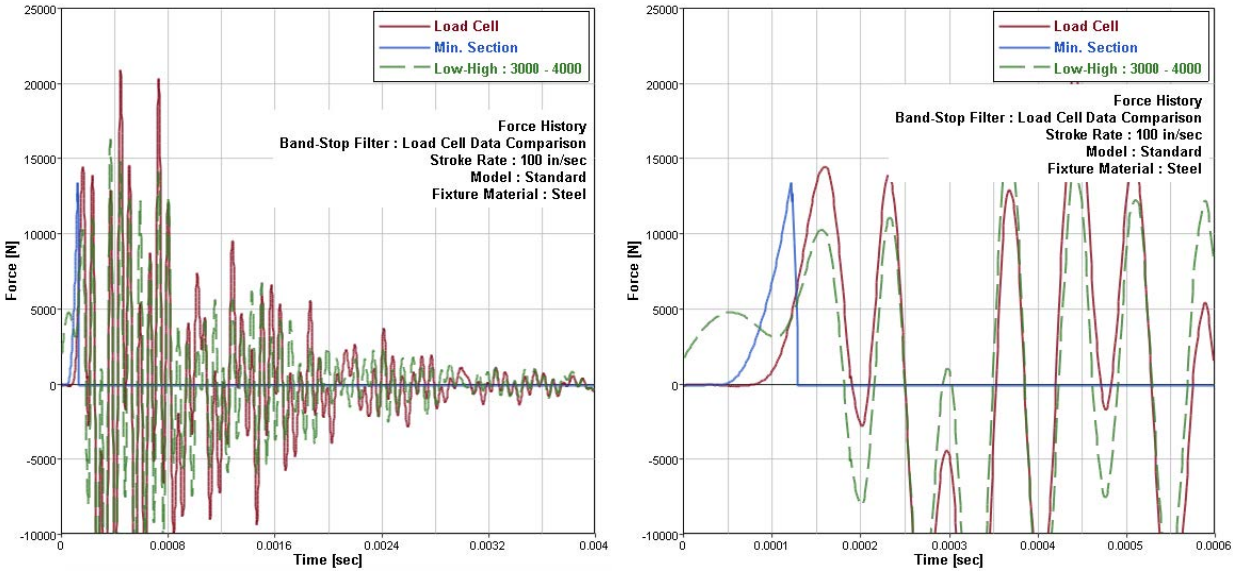

Figure 84. Standard model with steel fixtures at stroke rate 100 in/sec – Band-stop data filtering

CHAPTER 6

CONCLUSIONS AND FUTURE RESEARCH

6.1 Conclusions

The V-notch rail shear test apparatus was evaluated for use in dynamic tests to generate rate sensitive material shear properties. The evaluation was conducted using numerical models of the test apparatus using LS-DYNA explicit finite element code. The numerical model was used to identify the frequency response of the test apparatus measured in terms of the excitation force and the force transmitted to the load cell. Since the true force experienced by the test specimen during a physical test is not directly measurable, the load cell provides the only information about the same. However, the load cell measurement is affected by the vibrational characteristics of the test apparatus between the specimen and the load cell. The numerical models were used to systematically identify the effects of fixture mass, stiffness and loading speed on the force measurements captured by the load cell.

This was accomplished first by developing the numerical model of the standard V-notched rail shear test apparatus and analyzing at stroke rates ranging from 1 in/sec to 200 in/sec. The fixtures of the standard assembly were then modified by the addition of the webbings which increased its stiffness by 67% compared to the standard. Comparison of the results in the frequency domain had shown a considerable increment in the frequency at which the first peak amplification was encountered. The increment was about 1 kHz compared to the standard model.

Three other cases are presented in an attempt to increase the band width as mentioned above. In Case 1, the modified fixtures were modeled to have stiffness of steel but density of aluminum. This decreases the mass of the fixtures by three times while having same stiffness as that of steel. An increment of another 1 kHz was observed compared to the modified fixtures

(which is 2 kHz compared to the standard fixtures). In Case 2, the modified fixtures were modeled to have stiffness of steel but a ten times lower density as that of steel. This decreased the mass of the fixtures by ten times compared to the modified steel fixtures. This analysis presented an increment of another 1 kHz i.e. 2 kHz increment compared to the modified fixtures. While this decrease in density may be impractical, it gives an idea about the changes in the natural frequency of the fixture for an order of magnitude decrease in fixture mass. In Case 3, the modified test apparatus with steel fixtures was scaled down to half of its size reducing its mass by 50%. This analysis presented a significant increment of about 5 kHz, indicating an increment of about 6 kHz compared to that of standard assembly. However, fixtures discussed in Case 1 and Case 2 are difficult to achieve in reality because of the applied material properties though they present a significant change in the frequencies compared to the modified fixtures. But the modified fixtures and the assembly discussed in Case 3 are achievable in reality for an experimental validation. One of the major drawbacks of the assembly in Case 3 would be its reduced gage section of the coupon which may not be suitable for certain reinforced composites.

Effect of fixture bending on the specimen loading as well as the frequency content was observed in another analysis i.e. Case 4. It was noted that bending indeed affects the frequency content of the test apparatus. Also, bending of the fixtures tend to introduce a combined loading effect as the stroke rate increased, starting from 100 in/sec. Therefore, in order to have pure shear loading in the specimen, this analysis suggests the physical limitation of the test apparatus.

Test results from the standard assembly were filtered using HyperGraph, an analytical tool widely used for data processing and analysis. Low-pass filtering and band-stop filtering was used to filter data. The variation in the force data of the filtered curve, compared to the actual curve, implies filtering data eliminates useful frequencies included in the range of frequencies

defined as cut off values. There is very less or no control over the frequencies being eliminated when such filters are being used. The limited investigation indicated that using simple filters would distort the true material behavior. A frequency dependent *weighted* filtering scheme, i.e. a transfer function must be employed for correcting the load signals to obtain more accurate material behavior at higher test speeds.

6.2 Future Research

Recommendations for future work based on the observations from the present study are listed below.

1. A limited experimental validation of numerical model for V-notched rail shear test assembly under dynamic loading must be conducted.
2. Numerical analysis of the scaled down assembly of Case 3 should be carried out with a composite coupon.
3. Effects of damping and mesh sensitivity must be further explored.

REFERENCES

REFERENCES

[1] Iosipescu, N., "New Accurate Procedure for Single Shear Testing of Metals," *Journal of Materials, 1967.*

[2] Hussain, A. K., and Adams, D. F., "The Wyoming-Modified Two-Rail Shear Test Fixture for Composite Materials," *Journal of Composites Technology and Research, JCTRER, Vol 21, October 1999.*

[3] ASTM Designation D 7078/D 7078M, "Standard Test Method for Shear Properties of Composite Materials by V-Notched Rail Shear Method," ASTM International, 100 Barr Harbor Drive, West Conshohocken, PA, August 2005.

[4] Raju, K. S., Dandayudhapani, S., and Thorbole, C. K., "Characterization of In-Plane Shear Properties of Laminated Composites at Medium Strain Rates," *Journal of Aircraft, Vol. 45, No. 2, Wichita State University, Wichita, KS, March-April 2008.*

[5] Dandayudhapani, S. K., "Characterization of In-Plane Shear Properties of Laminated Composites at High Strain Rates," Master of Science Thesis, Department of Aerospace Engineering, Wichita State University, 2006.

[6] Daniel, O. A., Joseph, M. M., Adam, M. G., and Donald, F. A., "The V-Notched Rail Shear Test," *Journal of Composite Materials, Vol. 41, No. 3, University of Utah, Salt Lake City, UT, December 2005.*

[7] Lamancusa, J. S., "Noise Control; Vibration Isolation," Penn State, May 2002.

[8] ASTM Designation D 7078/D 7078M, "Standard Test Method for Shear Properties of Composite Materials by V-Notched Rail Shear Method," ASTM International, 100 Barr Harbor Drive, West Conshohocken, PA, August 2005.

[9] Adams, D. F., and Walrath, D. E., "Further Developments of the Iosipescu Shear Test Method," Experimental Mechanics, 1987.

[10] Hussain, A. K., and Adams, D. F., "An Analytical and Experimental Evaluation of the Two-Rail Shear Test for Composites Materials," University of Wyoming Composite Materials Research Group Report UW-CMRG-R-98-105, February 1998.

[11] Daniel, O. A., Joseph, M. M., Adam, M. G., and Donald, F. A., "Development and Evaluation of the V-Notched Rail Shear Test for Composite Laminates," FAA Report, Dept. of Mechanical Engineering, University of Utah, Salt Lake City, UT, September 2003.

[12] http://www.compositesworld.com, 2013.

[13] Leeuwen, D. A. van, Nijssen, R. P. L., Westphal, T., and Stammes, E., "Comparison of Static Shear Test Methodologies; Test Results and Analysis," Knowledge Center WMC, Wieringerwerf, The Netherlands, 2008.

[14] Jen, Y. L., Dwight, D. F., Robert, J. R., and Gary, J. L., "An Improved Shear Test Fixture using the Iosipescu Specimen," U.S. Department of Agriculture, Forest Products Laboratory, AMD-Vol. 231/MD-Vol. 85, Mechanics of Cellulosic Materials, ASME, 1999, Madison, Wisconsin.

[15] Hussain, A. K., and Adams, D. F., "Experimental Evaluation of the Wyoming-modified Two-rail Shear Test Method for Composite Materials," Society for Experimental Mechanics, Vol. 44, No. 4, August 2004.

[16] Garcia, R., Weisshaar, T. A., and McWithey, R. R., "An Experimental and Analytical Investigation of the Rail Shear-test Method as Applied to Composite Materials," Experimental Mechanics, August 1980.

[17] Lee, S., and Munro, M., "Evaluation of In-plane Shear Test Methods for Advanced Composite Materials by the Decision Analysis Technique," National Aeronautical Establishment, University of Ottawa, Vol. 17, Canada, January 1986.

[18] Andrew, K. C., and Michael, J. R., "Practical Methods for Vibration Control of Industrial Equipment," Bretech Engineering Ltd, 70 Crown Street, Saint John, NB Canada, 2003.

[19] LS-DYNA, "Keyword User's Manual," Volume I, Version 971, May 2007.

[20] http://www.altairhyperworks.com, 2013.

[21] CATIA v5, "Assembly Design," Revision 5.20, 2010.

[22] Metallic Materials Design Data, "Metallic Materials Properties Development and Standardization: MMPDS-05," Federal Aviation Administration, April 2010.

[23] Oskarsson, I., "A New H-Adaptive Method for Shell Elements in LS-Dyna," Division of Structural Mechanics, Lund Institute of Technology, Lund University, 2006.

APPENDIX

APPENDIX

THEORY – CONCEPTS UTILIZED

Element Types and Hourglassing [23]

Most frequently used shell and solid element types in LS-DYNA are Belytschko-Tsay (ELFORM 1) and Constant Stress Solid element (ELFORM 2) respectively which are the default element formulations. It is implemented that these element types are more efficient and accurate computationally compared to other element types. However, there are some disadvantages as these element types are classified as underintegrated. Since only single integration point is used in the plane, zero energy modes may occur. It is termed as hourglassing which is defined as a zero-energy deformation that occurs in an underintegrated element as the element tends to be excessively flexible. Strain is evaluated only at the integration point and it is possible that no strains occur in that point. As a result the strain energy of the element may be zero even though the element is considerably deformed. Therefore, this non-physical mode of deformation produces zero stresses and strains i.e. the normal and shear stress are zero at the integration point.

In a fully integrated element, the hourglass effect has no influence on the solution. It also behaves too stiff in many situations especially for poor aspect ratios. This numerical problem of being overly stiff in bending applications and modal analysis is known as Shear Locking. A comparison of an underintegrated and a fully integrated element is shown in Figure 85 and Figure 86 for shell and solid elements respectively.

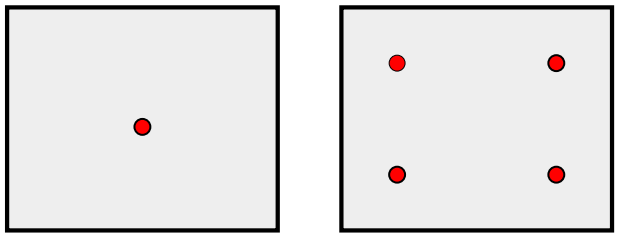

Figure 85. Underintegrated and fully integrated shell element [23]

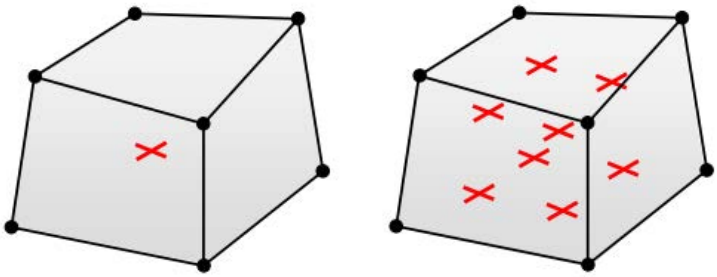

Figure 86. Underintegrated and fully integrated solid element [23]

For an analysis with underintegrated elements, LS-DYNA adds an hourglass force to the equation of motion. The main aim of this force is to control the formation of modes developed due to hourglassing. An example of such typical zero energy modes which can occur in an underintegrated shell are shown in Figure 87.

Six forms of hourglass control types are available in LS-DYNA. All six forms are applicable to solid elements whereas type six is applicable only to solid but not for shell elements. The parameter IHQ determines the hourglass type. These types are classified into stiffness-based and viscous-based. Usually viscosity-based controls are recommended for high velocity impacts of structural parts and stiffness-based controls for minimizing non-physical stiffening of the response. It is considered that viscosity-based control is less effective compared to stiffness-based for structural parts. Classification of these hourglass control types is shown in Table 11.

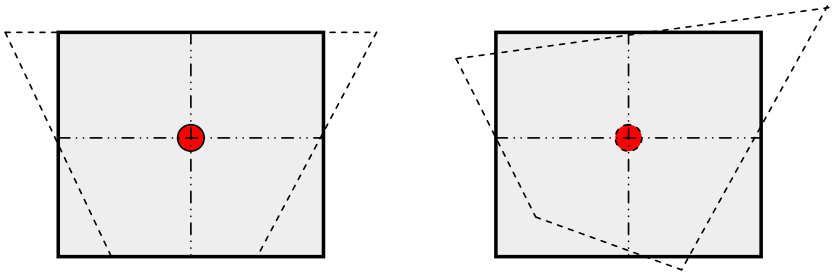

Figure 87. Two hourglass modes for an underintegrated shell element [23]

TABLE 11

HOURGLASS CONTROL TYPES

HOURGLASS FORMULATION	INTEGRATION METHOD	
	One-Point	Exact Volume
Standard LS-DYNA Viscous Form (Default)	IHQ=1	---
Flanagan-Belytschko Viscous Form	IHQ=2	IHQ=3
Flanagan-Belytschko Stiffness Form	IHQ=4	IHQ=5
Belytschko-Bindeman Assumed Strain Co-Rotational Stiffness Form	---	IHQ=6

Using default element formulations for solid and shell elements available in LS-DYNA, a comparison of various hourglass controls types is made. For the shear coupon with solid elements, using default element formulation (constant stress solid element - underintegrated), various hourglass control types are compared for the force history of the gage section (Figure 88) at a stroke rate of 0.1 in/sec. As shown, stiffness-based control types i.e. IHQ=4, 5, 6 predict better results compared to viscosity-based. Also, the above mentioned control types predict similar response. Therefore IHQ=6 is chosen for rest of the analytical work which uses solid elements in the specimen.

Similarly, an hourglass comparison for shell elements in the coupon is made among IHQ=1, 4, 6 where IHQ=1 is default and IHQ=6 is used only for solid elements (Figure 89). This

comparison is made at stroke rate 1 in/sec. Since IHQ=4 and 6 predict similar response, control type 4 is chosen for rest of the analysis of the coupon with shell elements.

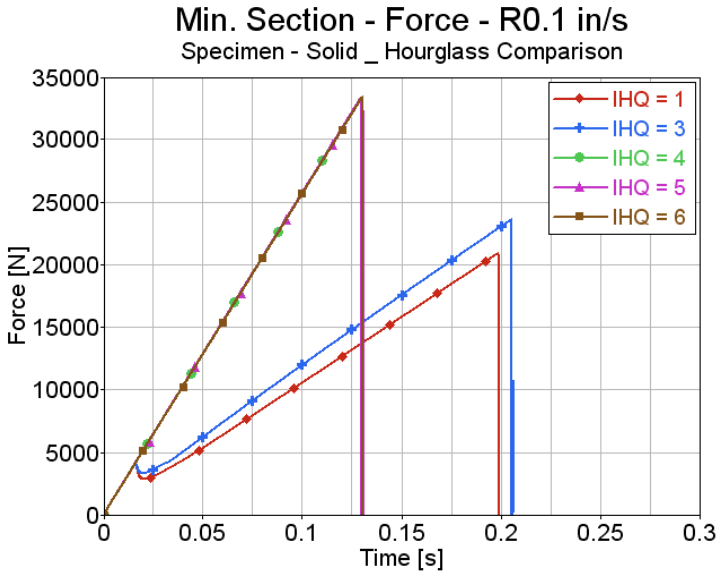

Figure 88. Hourglass control comparison – Specimen with solid elements

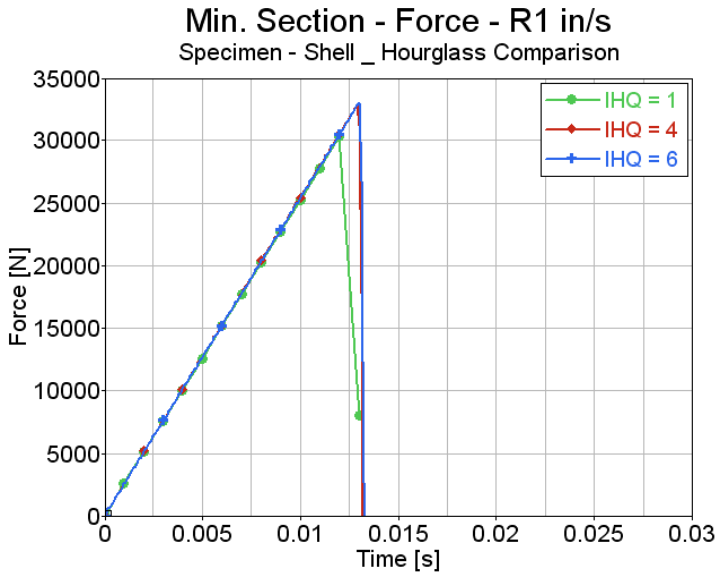

Figure 89. Hourglass control comparison – Specimen with shell elements

An underintegrated and fully integrated element formulation comparison is made for the specimen with solid elements. Element formulation 2 of solid elements is fully integrated which do not require hourglass stabilization. A comparison between element formulation 1 and 2 is

made at stroke rates 0.1 in/sec and 1 in/sec as shown in Figure 90. As no variation is seen among an underintegrated formulation with hourglass stabilization and a fully integrated formulation, it is decided that default element formulations will be used with hourglass control for further analysis.

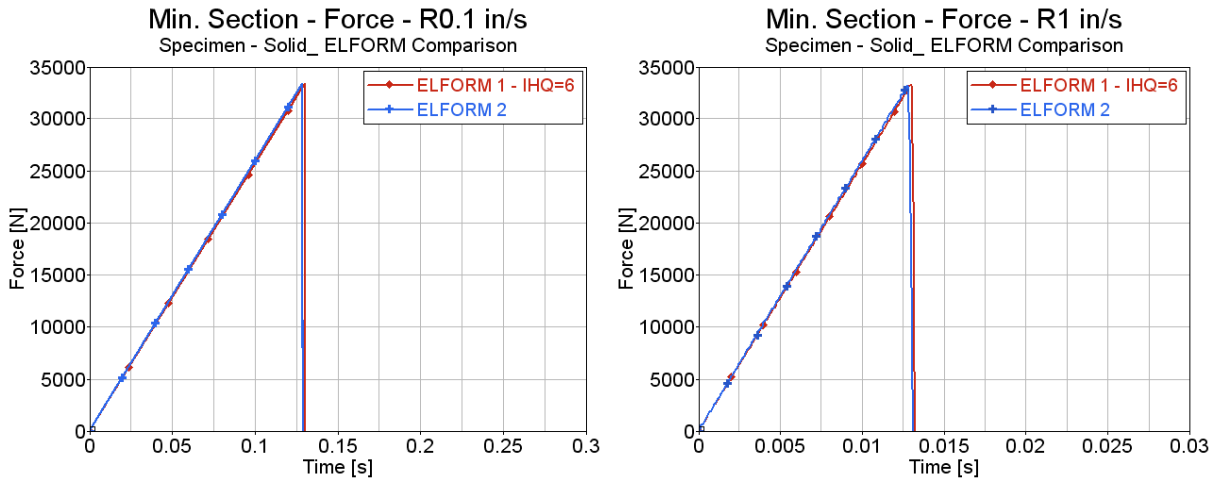

Figure 90. Element formulation comparison – Specimen with solid elements

Contact Definitions [19]

In LS-DYNA an interaction between various parts in a model are treated by the 'contact option'. These contact options are divided into constraint based or penalty based. Majority of them are based on the penalty method. Forces in different parts appear in the contact interface while they are interacting. Contacts are usually defined by a master and a slave side. Choice of assigning master and slave side to a component depends on the mesh density. A part with highest mesh density is chosen as a master side. Although in some of the contact types, the choice of master and slave side is arbitrary.

Zero Padding and Fast Fourier Transform (FFT) [20]

Fast Fourier Transform (FFT) is similar to Discrete Fourier Transform (DFT) but is much faster for calculations. It converts a signal in the time domain to the frequency domain. A plot of

frequency versus magnitude on an x-y graph is known as frequency spectrum or frequency domain. FFT of any signal produces a frequency spectrum which is a different form of the original wave. According to Fourier, a set of sine waves or cosine waves of different amplitudes and frequencies can be summed up to equal any wave form. That is, FFT is used to decompose a function into sine and cosine waves, projecting the energy in the signal as a function of frequency.

Depending on the number of points (N) and the number of periods of the signal, FFT can vary dramatically. Here, the number of points (N) refers to the sampling rate of the signal in the time domain. This implies that FFT contains information between 0 and f_s, where f_s is the sampling frequency. The sampling frequency must be at least twice the highest frequency component. If it is too low, the amplitude towards the lower frequencies may rise very high for a strong wave with larger period. Depending on the theory described, the signal's frequency spectrum should be entirely below $\frac{f_s}{2}$. In the frequency domain, each point represents a particular frequency contained in the spatial domain. Using an Inverse Fourier Transform, the converted signal can be restored back to original form.

A theorem known as Similarity or Reciprocity theorem states that: 'As the time domain function expands in time, the frequency domain function compresses in spectrum, and increases in amplitude'. This means if the spectrum of a function is compressed, its time domain will be expanded while simultaneously decreasing the amplitude. This is the fundamental relationship between time and frequency domains which can be put forward as: Faster transitions and shorter durations require higher frequencies, and slower transitions and longer durations require lower frequencies.

The results in the present work are analyzed in the frequency domain where a Fourier Transform is used to map a time domain result (or curve) into frequency domain. Data in frequency domain curve contains same information as time domain but in a different form. The equation for Fourier Transform is given below:

$$F(\omega) = \int_{-\infty}^{\infty} f(t) e^{-j\omega t} dt$$

A Fourier Transform option which is available in HyperGraph (post-processor) is used for the present work. The result of a Fourier Transform is a complex function represented by magnitude and phase instead of real and imaginary components, as they do not have a physical meaning. Also, the lower limit of the integral is considered as zero as time cannot be negative in physical sense. FFT is computationally efficient compared to Discrete Fourier Transform.

The input curve (or signal) for FFT requires having number of points equal to two raised to the power of some integral i.e. 2^7 (128), 2^8 (256) etc. Failure to meet this criterion would add zeros at the end of the curve until a valid number of points are reached. This phenomenon is called as zero-padding which allows one to use a longer FFT essentially giving a similar result as that of a non-zero padded FFT but a smoother looking result. This is because of having more number of closely spaced frequency bins in a longer FFT. In the present work, zero-padding is applied in order to analyze the results better in the frequency domain.

Filtering [20]

Filtering is a process of eliminating high-frequency components in order to smooth data. In this process, the time domain data is transformed into frequency domain using FFT and all unwanted frequencies are eliminated by multiplying the FFT values by zero. This modified data is then transformed back into time domain. Types of filters generally used are low-pass filter, high-pass filter, band-pass filter, band-stop filter etc.

In the present work a comparison of the original data is shown with the data obtained after using various filtering options. Low-pass filtering and band-stop filtering is primarily chosen for the comparisons. Low-pass filter requires a cut-off frequency to be defined. All frequencies above the cut-off frequencies are eliminated while allowing only the frequencies below the cut-off frequency to pass. Since it keeps the low-frequency components and eliminates the high-frequency components, it is termed as low-pass filter. Similarly, band-stop filter requires a range of frequencies to be defined. All frequencies within that range are eliminated while allowing the other frequencies to pass.